Aus dem: Institut für Schlaganfall-und Demenzforschung

Klinikum der Ludwig-Maximilians-Universität München, Großhadern

Dissertation

zum Erwerb des Doctor of Philosophy (Ph.D.)

an der Medizinischen Fakultät der

Ludwig-Maximilians-Universität zu München

The impact of post-stroke sterile inflammation in atherosclerotic plaque rupture and recurrent stroke

vorgelegt von:

.....Jiayu Cao.....

aus:

.....Linyi, China.....

Jahr:

.....2023.....

Mit Genehmigung der Medizinischen Fakultät der

Ludwig-Maximilians-Universität zu München

First evaluator (1. TAC member): Prof. Dr. med. Arthur Liesz

Second evaluator (2. TAC member): Prof. Dr. med. Martin Dichgans

Third evaluator: Prof. Dr. Christian Schulz

Fourth evaluator: Prof. Dr. Andreas Schober

Dean: **Prof. Dr. med. Thomas Gudermann**

Datum der Verteidigung:

_____01.06.2023_____

Table of content

Abstract (English):

Stroke is a major cause of mortality and permanent disability worldwide with high economic costs and health tolls. Currently established acute stroke therapies are limited to revascularization approaches of occluded cerebral artery. Despite improvements in neuroimaging diagnostics, acute stroke management and extensive use of secondary prevention, recurrent stroke remains a challenge. It is known that the risk of recurrent stroke is highest in the early phase after the primary ischemic event. It has been reported that more than 10% of patients experienced a recurrent stroke within 90 days of the initial ischemia, and approximately half of these secondary events occur within 2 days after the primary stroke. Moreover, the risk of recurrent stroke is highest among patients with large artery atherosclerosis. However, the underlying mechanism of how stroke leads to atherosclerotic plaque progression and subsequent rupture, causing secondary ischemia remains largely unknown.

Atherosclerosis is a disease defined as the development of chronic inflammatory response to lipid accumulation in medium and large arteries. Animal models play a pivotal role in exploring the pathological progression of the disease, diagnostic imaging modalities, as well as pre-clinical therapeutic testing. However, standard animal models utilized in atherosclerosis research do not adequately exhibit vulnerable plaques as observed in patients. Thus, posing great limitations to our understanding of unstable plaque pathology, as well as exploration of plaque rupture prevention.

In this study, we induced rupture-prone plaques by a tandem stenosis (TS) ligation of the right common carotid artery (RCCA) in high fat diet-fed *ApoE*$^{-/-}$ mice. Four weeks after TS surgery, transient left middle cerebral artery occlusion (MCAO) surgery of the *ApoE*$^{-/-}$ mice was conducted. The appearance of secondary brain lesions was systematically analyzed by MRI scan on day 2 and day 7 after stroke. Potential lesions were further confirmed by histology and immunofluorescence staining. Morphological features

of the plaques were analyzed in the RCCA 7 days after stroke. Vascular inflammatory response was studied by western blot, flow cytometry and immunofluorescence staining.

We observed that stroke leads to activation of the AIM2 inflammasome in advanced atherosclerotic plaques due to the increase of circulating cell-free DNA in the blood. Increased post-stroke plaque inflammation results in atherosclerotic destabilization and atherothrombosis, leading to arterio-arterial embolism and recurrent stroke within days after the initial brain ischemia. We also validated key observations of plaque destabilization in carotid artery plaque samples from stroke patients. Neutralization of cell-free DNA by DNase I treatment or pharmacological inhibition of inflammasome activation efficiently reduced recurrence rate after experimental stroke.

Taken together, we provide a mechanistic explanation for high recurrence rates of atherosclerotic stroke in a novel animal model of recurrent ischemic events. Our study reveals that stroke leads to exacerbated plaque inflammation and ultimately plaque rupture by cell-free DNA-mediated AIM2 inflammasome activation. Additionally, targeting DNA-mediated inflammasome activation after remote tissue injury implicates a plausible therapeutic approach for further clinical development in the prevention of early recurrent events.

List of figures

List of figures

List of abbreviations

ACA	Anterior cerebral artery
ACS	Acute coronary syndrome
AIM2	Absent in melanoma 2
ApoE	Apolipoprotein E
ASC	Apoptosis-associated speck-like protein containing a C-terminal caspase recruitment domain
BMDMs	Bone marrow-derived macrophages
BSA	Bovine Serum Album
CANTOS	Canakinumab Anti-inflammatory Thrombosis Outcomes Study
CARD	Caspase recruitment domain
CCA	Common carotid artery
CCL2	C-C motif chemokine 2
CCR2	C-C chemokine receptor 2
CE	Cardiogenic embolism
CE	Cholesteryl ester
CH	Clonal haematopoiesis
CSF-1	Colony stimulating growth factor 1
CVD	Cardiovascular disease
EDTA	Ethylenediamine tetraacetic acid
EDV	End diastolic velocity
FACS	Fluorescence-activated cell sorting

FC	Fibrous cap
FITC	Fluorescein isothiocyanate
FJC	Fluoro Jade C
FXII	Factor XII
FXIIa	Activated factor XII
GM-CSF	Granulocyte/ macrophage stimulating growth factor
H&E	Haematoxylin and eosin
HMGB1	High-mobility group box 1
LAA	Large artery atherosclerosis
LCCA	Left common carotid artery
LDL	Low-density lipoprotein
LDL	Low-density lipoprotein receptor
LOX-1	lectin-like oxidized low-density lipoprotein receptor-1
Ly6C	Lymphocyte antigen 6 complex
MCAO	Middle cerebral artery occlusion
MI	Myocardial infarction
MMPs	Matrix metalloproteinases
MRI	Magnetic resonance imaging
MV	Mean velocity
NC	Necrotic core
NETs	Neutrophil extracellular traps

NLRP3	NACHT, LRR and PYD domains-containing protein 3
oxLDL	Oxidized low-density lipoprotein
PAMPs	Pathogen associated patterns
PFA	Paraformaldehyde
PRR	Pattern recognition receptor
PSV	Peak systolic velocity
RCCA	Right common carotid artery
ROS	Reactive oxygen species
SMCs	Smooth muscle cells
SR	Scavenger receptor
SVD	Small vessel disease
TF	Tissue factor
TIA	Transient ischemic attack
TLR	Toll-like receptor
TNF	Tumor necrosis factor
TOAST	Trial of Org 10172 in Acute Stroke Treatment
TS	Tandem stenosis
TUNEL	Terminal deoxynuceotidyl transferase dUTP nick end labeling
UND	Undetermined
VCAM1	Vascular cell adhesion molecule 1
VLA4	Very late antigen 4

VPI	Vulnerability plaque index

1. Introduction

1.1 Stroke

A stroke occurs when the blood supply to the brain is interrupted, frequently due to a blood vessel that has burst (hemorrhagic) or is blocked by a clot (ischemic). It is estimated that 87% of all strokes are ischemic, while 13% are hemorrhagic. This event results in brain damage due to lack of blood and oxygen to the tissue and nutrient deprivation. One of the most common symptoms of a stroke is sudden weakness or numbness on one side of the body, especially on the face, arm or leg. Other common stroke symptoms include: confusion, difficulty speaking or understanding speech; vision impairment of one or both eyes; trouble walking, dizziness, loss of balance or coordination; and fainting or unconsciousness, among others. The effects of a stroke depend on which region of the brain is affected and the severity of the injury.

1.1.1 Epidemiology

Nearly 795,000 individuals worldwide suffer a new or recurrent stroke each year, nearly 610,000 of those are incident events, and 185,000 are recurrent events[1-3]. When considered independently of other cardiovascular disease (CVD), stroke ranks fifth in leading cause of death worldwide[4]. The incidence of stroke is unequivocally associated with aging[5]. Thus, with the acceleration of global aging population, the economic burden of stroke related patient care on the healthcare system and society in general is overwhelming. Stroke occurrences increased from 22.8% in 1990 to 24.9% in 2016, representing a relative increase of 8.9% after adjusting for any competing risk of death due to other causes[6]. Despite considerable improvements in neuroimaging diagnosis, advanced acute stroke management and extensive utilization of secondary prevention, recurrent stroke remains frequent. Posing an even greater risk for debilitation, mortality and economic burden than the initial stroke. Moreover, a retrospective study suggested that the

risk of having a secondary stroke is greater than the risk of having a cardiac event following an initial stroke[7]. Recurrent stroke is most likely to occur as soon as days or weeks follow a transient ischemic attack (TIA) or stroke. According to previous research, 10.5% of stroke and TIA survivors suffered recurrent stroke within 90 days of the primary event, more strikingly, with half of these secondary events occurring within 2 days of the original events[8]. The result of another study indicated that nearly 40% of recurrent stroke occurred within the first 24 hours of the primary event[9].

1.1.2 Etiology

Regarding the two main categories of stroke, ischemic stroke is the most common type, accounting for 87%, with the remaining 13% being hemorrhagic[2]. The Trial of Org 10172 in Acute Stroke Treatment (TOAST) criteria[10] categorizes ischemic stroke into four categories: large artery atherosclerosis (LAA), cardiogenic embolism (CE), small-vessel disease (SVD), stroke of other determined etiology, and stroke of undetermined etiology. The most common cause of stroke associated with LAA is an artery-to-artery embolism or, less common, a vessel stenosis that results in hemodynamic infarction. The onset of CE stroke occurs when a blood clot from heart blocks an artery in the brain. A SVD stroke is typically characterized by a small lacunar infarct, which is responsible for lacunar syndromes[11]. Stroke of other determined etiology incorporates, extracranial or intracranial arterial dissections, vasculitis, coagulation disorders, or hematological diseases[11]. Among all stroke subtypes, patients with LAA have the greatest occurrence of recurrence — about 4.0% at 7 days, 12.6% at 30 days and 19.2% at 3 months[12-14] (Table 1).

	At 7 days	At 30 days	At 3 months
SVD	0	2.0% (0-4.2)	3.4% (0.5-6.3)
CE	2.5% (0.1-4.9)	4.6% (1.3-7.9)	11.9% (6.4-17.4)
UND	2.3% (0.5-4.1)	6.5% (3.4-9.6)	9.3% (5.6-13.0)
LAA	4.0% (0.2-7.8)	12.6% (5.9-19.3)	19.2% (11.2-27.2)

Table 1. Three-month actual recurrent stroke by TOAST criteria (*modified from Lovett JK, et al. 2004[14]*)**.**

Although various studies have focused on the identification of treatments for ischemic stroke, thrombolysis with tissue plasminogen activator (tPA)[15] and mechanical vascular recanalization[16] are currently the only approved approaches in acute stroke management. However, limited by the short treatment time window, the high risk of intracranial hemorrhage and abnormal coagulation, only 3.4%-5.2% of ischemic stroke patients qualify for these therapeutic options[17, 18]. An endarterectomy of the carotid artery is a surgical procedure to remove the fatty deposits and atherosclerotic plaques within the carotid artery, which is typically performed for patients who have substantial carotid artery narrowing or symptoms due to carotid stenosis. It may reduce the risk of stroke, yet brings a risk of complications immediately before, after, and during the operation, such as, debilitating stroke or death[19]. To achieve the protection of brain tissue from both ischemia and reperfusion injury and, to extend the time window for thrombolytic strategies, a large number of neuroprotective agents and compounds are developed and tested in animal models[20]. However, translation of most neuroprotective treatments from animal models to humans has failed to generate positive results[21].

The second pillar of stroke therapy is secondary prevention by reduction of blood pressure, aspirin and statin treatment and life-style interventions. These strategies are effective in reducing long-term progression of stroke comorbidities, but unfortunately do not sufficiently target early recurrent ischemia[22]. In this regard, it has been reported in a previous large meta-analysis of secondary prevention studies for recurrent events, current secondary prevention by using antiplatelet therapy seldomly prevents the rate of recurrent events[21]. In addition, the robust residual stroke recurrence and the potential for major bleedings limit the effectiveness of antiplatelet strategies in reducing the early recurrent stroke in patients[23]. Conversely, carotid endarterectomy has been proven effective for reducing recurrent stroke[24]. However, apart from the risks of this procedure may cause, the benefit of carotid endarterectomy for secondary prevention is maximal if surgery is performed within 2 weeks after primary stroke event. Moreover, the benefit is reduced with the delay of surgery and eventually disappear if it is delayed more than 3

months[25]. No alternative therapeutic options are currently available to prevent or reduce the high rate of early recurrent events after stroke. The need for improved secondary prevention therapies becomes even more evident when considering the occurrence of in-hospital recurrent stroke was approximately 5.7% in acute ischemic stroke survivors, which predominantly occurred within the first five days of hospitalization[26]. These observations particularly emphasize the contribution of early CVD recurrence rate on secondary mortality and morbidity of atherosclerotic stroke patients and that the need for treating early CVD recurrence is currently unmet.

1.1.3 Systemic immune response after stroke

Solid evidence suggests that the immune system (both local and systemic inflammation) plays a pivotal role during the ischemic stroke pathology[27-29](Fig. 1.1). Due to the sudden reduction of blood flow, stroke impairs the cells for the acquisition of nutrients, causing instant cellular death and tissue damage. The brain infarct core is the region where blood supply is lost, leading to necrotic cell death[30]. Dying cells release damage-associate molecular patterns (DAMPs) such as double strand DNA (dsDNA), glutamate (Glu), reactive oxygen species (ROS) and, adenosine triphosphate (ATP). Through pattern recognition receptors (PRRs), these molecules are capable of activating effector cells such as microglia and astrocytes to initiate downstream inflammatory cascades. Consequently, pro-inflammatory mediators such as interleukin (IL)-1β, IL-6 and, tumor necrosis factor (TNF)-α can be released from these activated cells, thereby amplifying the local inflammation[31].

In addition to provoking local inflammatory responses, stroke also leads to severe systemic immune alterations[32]. Acutely after the ischemic event, within the first several hours, concentrations of pro-inflammatory cytokines such as IL-1β, IL-6 and TNF-α elevate in the circulation[33]. This acute inflammatory response involves an increased mobilization and egress of monocytes and neutrophils from the bone marrow[34]. Neutrophils play an essential role in the innate immune response after stroke. Due to their short half-

life and considerable heterogeneity, phenotype rather than quantity determines their involvement in the stroke pathogenesis. Under homeostatic conditions, neutrophils can be found mainly in circulation or within certain tissue such as in the lung, but not in the brain[35, 36]. Nevertheless, neutrophils instantly infiltrate into brain parenchyma after stroke onset[37, 38]. Activated neutrophils exacerbate tissue damage by releasing oxygen metabolites and proteases to surviving neurons[39]. Alternatively, they can expel neutrophil extracellular traps (NETs), which impairs post-stroke revascularization and vascular remodelling[40, 41]. Within the brain parenchyma, neutrophils exacerbate blood-brain barrier damage via activating DAMP-driven toll-like receptor (TLR) in resident cells, which consequently release cytokines and chemokines, as well as ROS[42].

Monocytes originate from myeloid progenitor cells in the bone marrow and systemically distribute in the body. Monocytes express a large range of differentiation clusters, including CD11b (Integrin α-M) and lymphocyte antigen 6 complex C1 (Ly6C) in rodents, and CD11c (Integrin α-X), CD14 (Glycoprotein) and CD16 (FcyRIII) in humans[43]. In mice, two subsets of monocytes exist and can be distinguished by the Ly6C expression. The population expressing high levels of Ly6C ($Ly6C^{hi}$ monocytes) is known as pro-inflammatory and antimicrobial subset. $Ly6C^{hi}$ monocytes express high level of C-C chemokine receptor 2 (CCR2) with low levels of CX3C chemokine receptor 1 (CX3CR1; $CCR2^{hi}CX3CR1^{low}$)[44]. They have the ability to accumulate at the site of inflammation, where they can further differentiate into macrophages or dendritic cells (DCs) depending on local tissue microenvironment[45, 46]. However, the $Ly6C^{low}$ subset act as patrolling monocytes and are involved in early phase of inflammation and tissue repair[46]. Shortly after a stroke, the number of pro-inflammatory monocytes rapidly rises in blood, and their recruitment to the injured lesion is highly reliant on CCR2/CCL2 interaction[47]. Absence of CCR2 or its ligand CCL2 results in better functional outcome and reduced inflammatory response in murine stroke[48].

The subacute stage after stroke is characterized by lymphopenia, lymphocyte dysfunction and atrophy of peripheral lymphoid organs such as thymus and spleen[49, 50]. In stroke

patients, peripheral lymphopenia has been described as reduced counts of T, B and NK cells within one day after ischemic stroke[51, 52]. In mice, the reduction in lymphocytes counts has been similarly shown in circulation, spleen and lymph nodes as early as 12 h after stroke[53]. During this phase, the functional status of the peripheral immune system transitions from immunocompetence to immunosuppression, which is caused by the injury and immune alterations in the brain[54, 55]. As a consequence of immunosuppression, stroke patients have an increased risk of life-threatening infection after stroke onset[56]. A recent concept for subacute infections is that T cell apoptosis is associated with inflammasome-dependent monocyte activation and FasL-Fas interaction after stroke[57].

It is noteworthy that circulating cell free DNA (cfDNA) is of great interest in the context of ischemic brain injuries. While, cfDNA is released by necrotic and apoptotic cells within the injured brain tissue, it can also arise from leukocytes such as neutrophils, which expel NETs. As a potential biomarker, the level of circulating cfDNA can be used for prediction of stroke severity and outcome[58]. Stroke induced neutrophils to release excessive NETs in the vasculature and parenchyma, which correlates with attenuated post-stroke vascular remodeling[41]. The increased levels of cfDNA may contribute to impaired cognitive functional recovery by damaging blood-brain barrier repair and vascularization[41].

In the chronic phase after ischemic stroke, the immune system is transformed to a state of persistent low-grade inflammation. This can be characterized by increased neutrophils counts and IgM^+ B cells in patients' peripheral blood[59]. Due to long-lasting levels of HMGB1 and proinflammatory cytokines such as IL-1β and IL-6, severe stroke also induces prolonged immune alterations[33, 60].

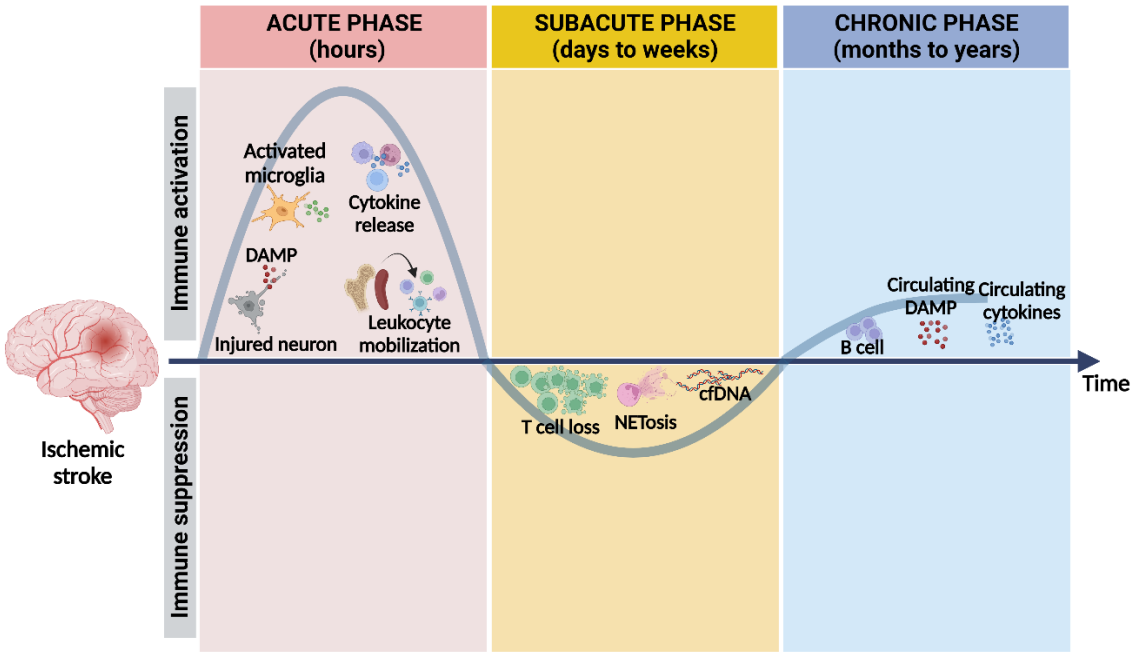

Figure 1.1 Systemic immunomodulation after stroke (*Adapted from Simats, et al. 2022*[61])**.** Systemic immune response is triggered by stroke in a multiphasic manner. Shortly after the onset of the ischemic stroke, DMAP released from dying or stressed cells in the ischemic tissue activates both microglia and peripheral immune cells, leading to the release of pro-inflammatory cytokines to the bloodstream. In addition, stroke triggers leukocytes mobilization from bone marrow and spleen. A state of immunosuppression is triggered during the subacute stage. Acutely released DAMP and other pro-inflammatory mediators results in lymphopenia as a result of massive cell death after stroke. Furthermore, NETs expelled from activated neutrophils may contribute to the increased level of cfDNA, which correlates with stroke outcome and plays a key role in T cell death. During the chronic phase, immune system is characterized by chronic and sustained levels of DAMP and pro-inflammatory cytokines.

1.2 Atherosclerosis

Atherosclerosis, defined as a slow progression of atheromatous plaques formation in the inner layer and luminal narrowing of the large arteries, is one of the most common cause of death and disability worldwide[2]. Atherosclerosis is considered as the most outstanding contributor to the growing burden of cardiovascular disease (CVD). It is characterized as a chronic inflammatory process mostly occurring at predilection sites with disturbed laminar blood flow such as artery bifurcation[62]. Pathologically, atherosclerosis begins with endothelial dysfunction and structural alteration, causing the disruption of the coherent luminal elastin layer and proteoglycans exposure[63], and allowing low-density lipoprotein

(LDL) accumulates under the endothelium. Advanced atherosclerotic plaques can rupture and cause thrombosis, which is the most common reason of acute coronary syndrome (ACS), myocardial infarction (MI) and stroke.

1.2.1 Epidemiology

CVDs – comprising coronary heart disease, hypertension and stroke – are the primary causes of mortality globally[2]. Approximately 18.6 million people died from CVDs in 2019, which amounted to an increase of 17.1% from 2010, representing 32% of all global deaths[2]. Among these deaths, 85% were due to myocardial infarction (most frequently caused by atherosclerotic disease of the coronary arteries) and stroke. Globally, over 75% of CVD deaths occurs in low- and middle-income countries[2]. With the contribution of public awareness and prevention, CVDs led to a significant decline in mortality in high-income countries since 1950s[64]. However, as it is reported in the Global Burden of Disease study, this decrease has not taken place consistently in low- and middle-income countries, putting a heavy burden on their economic costs[65].

1.2.2 Pathology

Under healthy conditions, the artery has a tri-laminar structure. The inner layer, the intima, is composed of a monolayer of endothelial cells which is in direct contact with blood flow. The middle layer, called the media, contains resident smooth muscle cells as well as extracellular matrix containing elastin, collagen and other macromolecules. The outer layer, the adventitia, consists of microvessels, nerve endings and mast cells.

Atherosclerosis progression starts from the innermost layer–the intima (Fig. 1.2). In the early stage, LDL accumulates within the intima, where it undergoes oxidative modifications due to ROS, referred to as oxidized LDL (oxLDL). By activating multiple receptors, including the lectin-like oxidized low-density lipoprotein receptor-1 (LOX-1), oxLDL triggers the expression of adhesion molecules and chemokines in endothelial cells[66]. Inflammatory monocytes circulating in the bloodstream are attracted by chemokines bound

to adhesion molecules expressed by activated endothelial cells and migrate into the artery walls. After migration into the intima, monocytes can differentiate and mature into macrophages obtaining traits associated with pro-inflammatory macrophages. Accumulated lipoproteins are taken up by both monocyte-differentiated macrophages and tissue resident macrophages via micropinocytosis, phagocytosis, and scavenger receptors (SRs), such as SR-A, CD36, SR-Bl, and LOX-1[67]. Once macrophage uptake is saturated, free cholesterol is converted into cholesteryl ester (CE), which further accumulates in macrophages, differentiating them into foam cells[68]. Although not as numerous as myeloid cells, T lymphocytes are also able to migrate into atherosclerotic lesion and regulate innate immunity while affecting endothelial cells as well as smooth muscle cells (SMCs)[69-71]. The accumulating leukocytes can also secrete mediators that cause SMCs in the media to migrate into the intima.

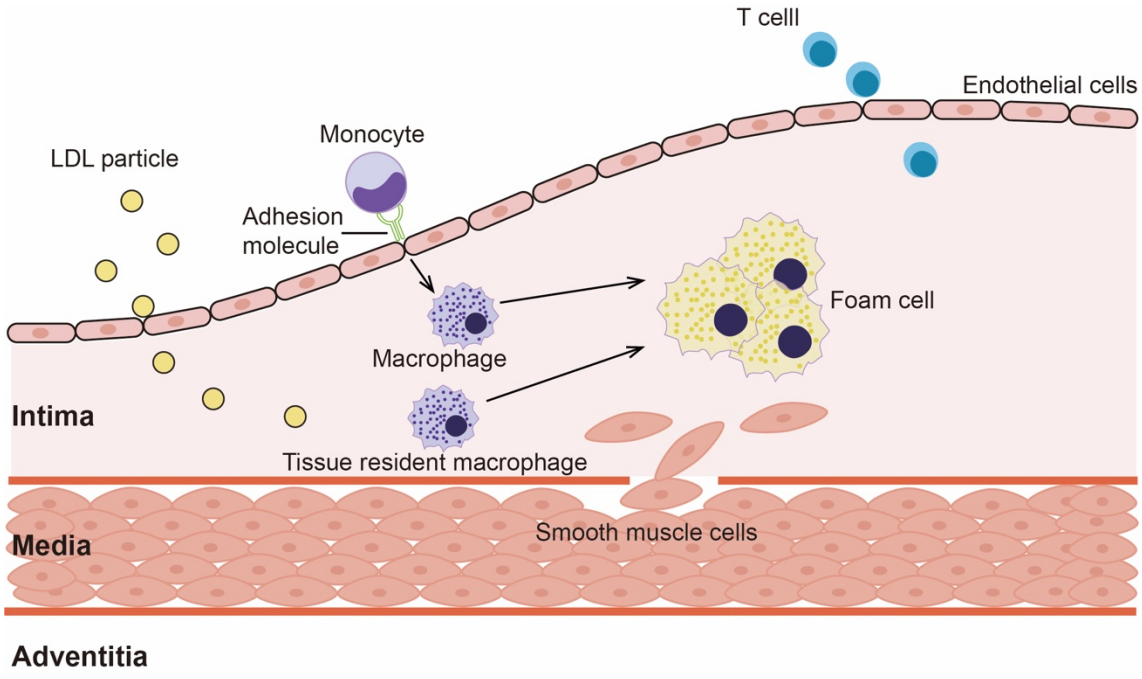

Figure 1.2 The initiation of atherosclerosis (*Adapted from Oliver Soehnlein, et al. 2021*[72])**.** Atherosclerosis is initiated by the accumulation of low-density lipoproteins in the subendothelial space. After oxidation, oxLDL activates endothelial cells, which induces endothelial cells to up-regulate adhesion molecules, which facilitate circulating monocyte adhesion and migration into arteries. The intima is the place where monocytes differentiate and mature into macrophages. Both differentiated and resident macrophages engulf lipoprotein-derived cholesterol, leading to

foam cell formation. T lymphocytes also enter the intima playing a role in innate immune regulation. At the same time, SMCs also migrate towards atherosclerotic lesions and undergo clonal expansion.

During the progression of atherosclerotic lesions, monocyte infiltration and foam cell retention continue, making the atherosclerotic plaque vulnerable, featured by large necrotic cores and fibrous cap thinning (Fig. 1.3). Both resident and migrating smooth muscle cells (SMCs) are the main source to elaborate extracellular matrix proteins containing interstitial collagen, elastin, proteoglycans, as well as glycosaminoglycans. Thus, further promoting lipid accumulation within the intima, which plays a role in the thickening of the intimal layer[73]. However, mediated by T cell mediators such as Interferon-γ (IFN-γ), the SMC function to synthesize collagen can be impaired. As a consequence, these cells will have a diminished ability to repair and update themselves[74]. As the most numerous leukocytes within atherosclerotic plaque, macrophages also play a key role in plaque progression and evolution. On one hand, activated macrophages produced higher levels of matrix metalloproteinases (MMPs), such as MMP2 and MMP9 that digest the collagen and further weaken the fibrous cap. On the other hand, macrophages can undergo programmed cell death called apoptosis, forming the lipid-rich core in the advancing atheroma[75, 76]. Moreover, defective efferocytosis, the dampened process of clearing dead cells, contributes to the formation of necrotic cores[77, 78].

Eventually, with the remodeling of the arterial wall and expansion of the plaques, the growing atherosclerotic plaque starts to erode upon the arterial lumen. Atherosclerosis causes myocardial infarction or stroke due to an acute thrombosis when the plaque ruptures, which is one of the most common outcomes and serious complications[79, 80]. The fragment of the fibrous cap of the atherosclerotic plaque allows coagulation components from blood to reach the core of the plaque. Subsequently, both intrinsic (factor XIIa – factor XIa) and extrinsic (tissue factor – factor VIIa) coagulation pathways play essential roles in thrombus formation on atherosclerotic plaques[81, 82].

The intrinsic and extrinsic pathways of coagulation are both capable of triggering coagulation processes. The extrinsic pathway is initiated by the transmembrane protein tissue factor (TF) exposed at the site of injured subendothelial tissues. On the contrary, the intrinsic contact system is triggered by factor XII (F.XII). F.XII is produced and regulated by the liver and is activated by the serine protease factor XIIa (F.XIIa) after binding to its negatively charged surface[83]. Numerous substances are capable of activating F.XII via contact-activation, including collagen, mast cell-derived heparin, misfolded protein aggregates and, neutrophil extracellular traps (NETs)[84]. F.XIIa initiates the intrinsic coagulation cascade via its downstream coagulation factor F.XI[85]. It has been shown that F.XII-driven coagulation specifically contributes to pathological thrombosis instead of physiological hemostasis and therapeutically targeting F.XIIa in *vivo* provides protection from thrombosis[84, 86, 87]. Given that F.XIIa contributes to thrombosis but does not cause severe side-effects, its pharmacological inhibition has emerged as a potent target for thrombosis prevention without hemorrhagic risk[88, 89].

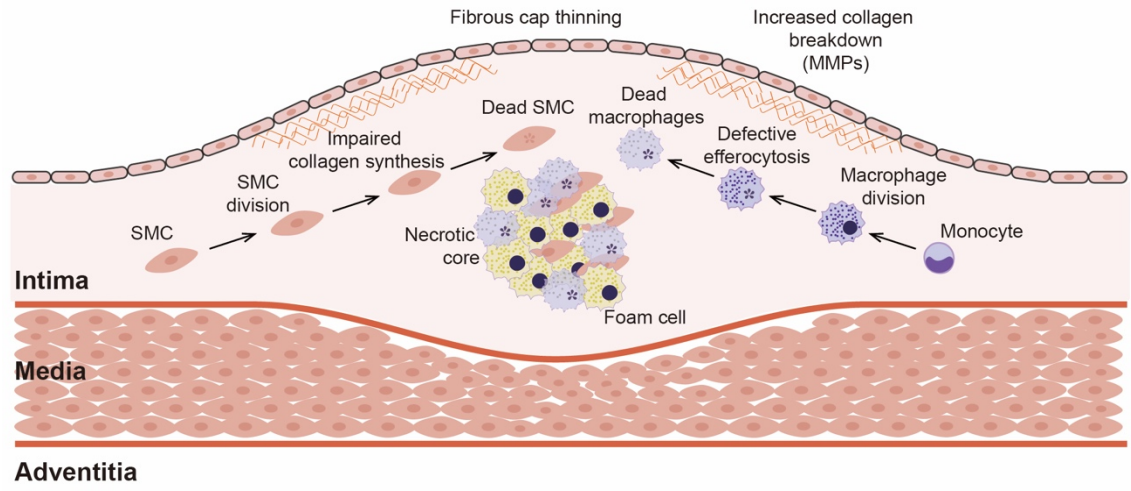

Figure 1.3 The progression of atherosclerosis (*Adapted from Gemma L. Basatemur, et al. 2019[90]*)**.** Once initiated, atherosclerotic plaques develop by continuous lipid accumulation and cell expansion. Migration of SMCs contribute to the retention of SMCs in the growing atherosclerotic plaque. Infiltrated T lymphocytes release INF-gema that impairs collagen synthesis of SMCs and promote atherosclerosis. Monocyte-derived macrophages secrete elevated amounts of enzymes of the matrix metalloproteinase (MMPs) family which degrade the collagen subsequently thinning the fibrous cap. Macrophages and SMCs undergo programmed cell death forming necrotic cores in the advanced plaque. Dampened efferocytosis additionally facilitate the necrotic core formation.

1.2.3 Inflammatory processes in atherosclerosis

1.2.3.1 Innate immunity involved during atherosclerosis development

Once accumulated within the subendothelial layer, LDL particles activate endothelial cells, resulting in elevated expression of adhesion molecules such as C-C motif chemokine 2 (CCL2)[91]. In response to endothelial activation, inflammatory monocytes and neutrophils in the bloodstream are attracted to the endothelium at the lesion site through the expression of chemokine receptors, including C-C chemokine receptor type 2 (CCR2)[92]. Additionally, activated endothelial cells express membrane-bound adhesion proteins including vascular cell adhesion molecule 1 (VCAM1) and selectins[93, 94]. VCAM1 has high affinity with very late antigen-4 (VLA4) which is expressed on immune cells[95]. This VLA4-VCAM1 interaction plays a pivotal role in orchestrating immune cells adhesion and migration within the initiation processes of atherosclerosis. When monocytes migrate into the intima, they differentiate into macrophages and undergo a variety of procedures dependent upon the signals given from the local microenvironment [96] (Fig. 1.4).

Scavenger receptors (SRs) such as CD36 and SR class A (SR-A), expressed on macrophages, are known to facilitate cholesterol uptake by macrophages[97]. However, others, such as ATP-binding cassette (ABC) transporter A1 (ABCA1), ABCG1 and scavenger receptor-BI (SR-BI), take principle responsibility to export cholesterol from macrophages[98]. Unfortunately, once the lipid metabolic pathway is imbalanced, large quantities of lipid droplets accumulate within macrophages and result in foam cells, a term referred to their foam-like morphology. Recent transcriptomic analyses in human atherosclerotic plaques suggested that foam cell formation by itself is not pro-inflammatory as showing absence of pro-inflammatory markers[99]. However, the cycle of continual hydrolysis and re-esterification of cholesterol droplet wastes cell energy and consequently induces foam cell death in the hypoxic area within the atherosclerotic lesion[100]. Components of dead cells are released into the extracellular space and phagocytosed by neighbouring macrophages, as a result, exacerbating the pro-inflammatory status[101].

Furthermore, both resident arterial macrophages and monocyte-derived macrophages can undergo local proliferation depending on several proatherogenic signals. Cytokines, growth factors as well as oxLDL play key roles in regulating macrophages proliferation[102]. Growth factors such as macrophage colony stimulating growth factor 1 (CSF-1) and granulocyte/ macrophage stimulating growth factor (GM-CSF) take primary responsibilities in atherosclerotic plaque development and macrophage proliferation[103, 104]. A previous study identified the outcome of SMC specific deletion of CSF-1 in the progression of atherosclerosis and discovered that macrophage proliferation highly correlates with local CSF-1 production[105]. Not only are cell extrinsic regulators vital players in atherosclerosis development, but intrinsic pathways play a role in macrophage expansion within the atherosclerotic plaque as well. One of the most recently reported examples is clonal haematopoiesis (CH), a phenomenon which hematopoietic stem cell (HSC) clones begin generating disproportionate fraction of blood leukocytes[106]. A current meta-analysis reported increased incidence of atherosclerotic disease in patients with CH, suggesting that CH is an independent risk factor for an atherosclerosis[107, 108]. One potent underlying explanation has been reported that the common somatic mutation $Jak2^{VF}$ led to increased macrophage turnover in atherosclerotic plaques and resulted in enlarged necrotic core formation[109]. In addition, this phenomenon is mediated via the activation of noncanonical absent in melanoma 2 (AIM2) inflammasome due to elevated DNA replication stress[109].

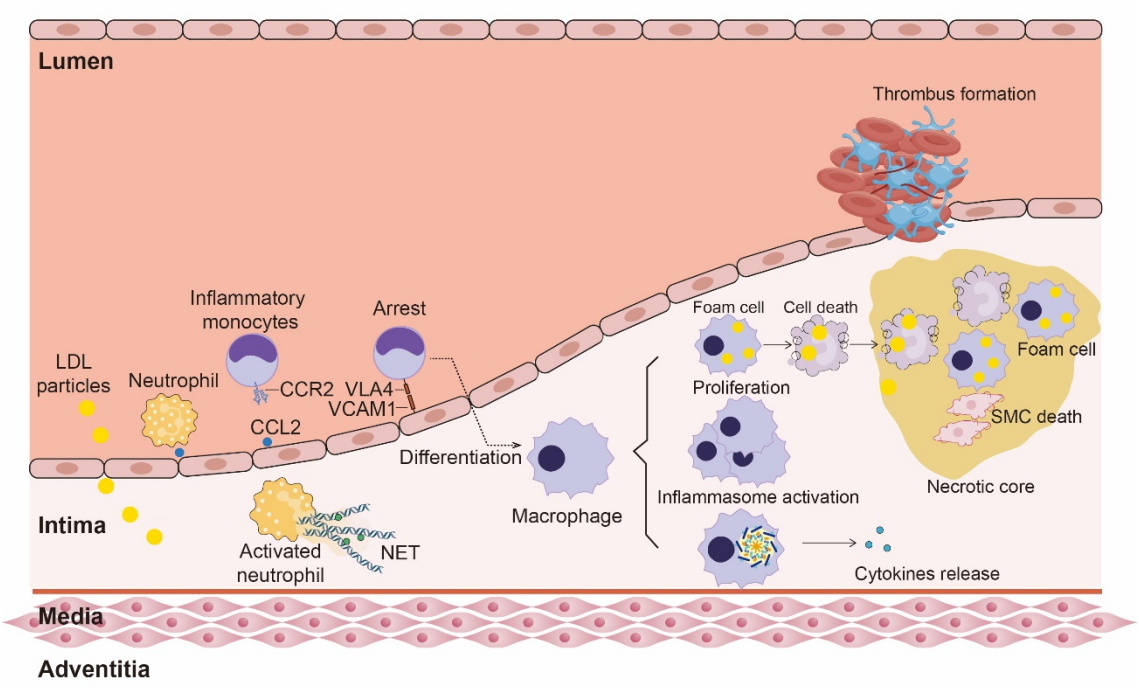

Figure 1.4 Inflammatory processes during atherosclerosis development (*Adapted from Oliver Soehnlein, et al. 2021*[72])**.** Circulating monocytes as well as neutrophils were adhered to the atherosclerotic lesion via chemokines (CCL2) and adhesion molecule (VCAM1) secreted by activated platelets at early stage. Activated neutrophils within artery lumen expel neutrophil extracellular traps (NETs) which can further promote monocytes adhesion. Monocyte-derived macrophages can engulf oxidized lipid droplets and turn into foam cells, and excessive lipid uptake promotes macrophage local proliferation. Not only NETs accelerate monocytes adhesion, histones released by activated neutrophils prime macrophages to produce pro-inflammatory cytokines by activating the NLRP3 inflammasome. Macrophages may recognize NETs via absent in melanoma 2 (AIM2), a cytoplasmic sensor that can bind to DNA hence activates inflammasome to produce IL-1β. With the necrotic core growing and fibrous cap thinning, atherosclerotic plaque may rupture and a thrombus occurs at the site of ruptured plaque, which may further cause ischemic events such as ischemic stroke or myocardial infarction.

1.2.3.2 Inflammasome activation during atheroprogression

Accumulation of lipoprotein-derived cholesterol crystals activate NACHT, LRR and PYD domains-containing protein 3 (NLRP3) – containing inflammasome, which is well described in the context of atherosclerosis[110]. The NLRP3 inflammasome is a multimeric protein complex, mainly expressed in myeloid lineage cells, which contains the sensor NLRP3, the adaptor apoptosis-associated speck-like protein containing a C-terminal caspase recruitment domain (ASC) and caspase-1[111]. After being activated by pathogen-

associated molecular patterns (PAMPs), DAMPs and other signals, NLPR3 monomers form oligomers and interact with ASC through homophilic ineractions[112, 113]. Hence, ASC recruits pro-caspase-1 through a caspase recruitment domain (CARD), which results in cleavage-derived caspase-1 activation and further leads to the secretion of pro-inflammatory cytokines interleukin-1β (IL-1β) and interleukin 18 (IL-18)[114]. In the context of atherosclerosis, cholesterol crystals directly activate the NLRP3 inflammasome by inducing lysosomal damage[112]. NLRP3 inflammasome expression has been linked to the severity of coronary artery disease and clinical risk of cardiovascular disease[115]. Moreover, as an atherogenic factor, IL-1β plays a crucial role in initiation, formation, development, and rupture of the plaque[116]. The Canakinumab (monoclonal IL-1β antibody) Anti-inflammatory Thrombosis Outcomes Study (CANTOS) strongly supports the importance of inflammation contributing to the pathogenesis of atherosclerosis. Neutralization of IL-1β by canakinumab significantly reduced the risk of recurrent cardiovascular events[117]. The underlying mechanism of these beneficial effects might be attributed to the reduction of blood inflammatory leukocyte supply, thereby reducing the inflammatory leukocyte accumulation in atherosclerotic plaque[118].

The development of atherosclerotic lesions is characterized by the aggregation of dead cells. Cell death, such as necrosis or NETs release, allows cells to release nuclear or mitochondrial dsDNA. It has been shown that the elevated levels of cell-free DNA correlate with the incidence of severe cardiovascular diseases[119]. Cytoplasmic DNA can be recognized by the inflammasome-forming sensor (AIM2)[120]. AIM2 is a PRR, which is constitutively expressed in intima and media of carotid arteries as well as aorta, and specifically detects cytosolic dsDNA. After binding to dsDNA, AIM2 activates the assembly of inflammasome with recruitment and catalytic cleavage of pro-caspase-1, leading to the secretion of inflammatory cytokines IL-1β and IL-18[121]. Growing evidence suggests the contribution of AIM2 in the context of atherosclerosis. Overexpression of AIM2 delivered by lentivirus increased atherosclerotic plaque loading in *ApoE*$^{-/-}$ mice, while silencing of AIM2 by RNA interference reduced lesion area after 12 weeks on a high-fat diet[122].

These results indicate that AIM2 plays a pro-atherogenic role in the early stage of atherosclerosis[122]. Moreover, at later stages of atherosclerosis, abundant AIM2 expression can be identified within the plaque, which is restricted to macrophages and colocalizes to dsDNA[123]. Genetic deletion or therapeutic inhibition of AIM2 strikingly increased plaque stability, suggesting that AIM2 exacerbates plaque vulnerability and could be a potent therapeutic target in atherosclerosis[123].

1.2.4 Atherosclerosis mouse model

A clinical retrospective study of 800 patients who died of acute coronary syndromes observed that 60% of deaths were attributed to atherosclerotic plaque rupture[124]. Despite the clear etiology, the mechanisms leading to plaque rupture are challenging to study in mice. A reason for this is the difficulty of the animal models to mimic unstable plaques with large necrotic cores and thin fibrous caps, such as in humans.

Animal models are essential tools for the understanding of pathological mechanisms in atherosclerosis, diagnostic imaging technologies, as well as the pre-clinical screening and testing of therapeutics. By far the most utilized animal models for investigating atherosclerosis are the Apolipoprotein E and Low-Density Lipoprotein Receptor deficient strains of mice (*ApoE*$^{-/-}$ and *LDLR*$^{-/-}$, respectively)[125]. These mouse models provided the platform on which we built the pathological knowledge of atherosclerosis. However, there is still a huge gap in understanding how plaques develop from stable to unstable, or even ruptured stages. Unfortunately, the dynamic evolution of plaque destabilization and pathology underlying plaque instability and rupture are hardly investigated in mouse models. Unlike what is observed in human post-mortem analysis and carotid endarterectomy samples, none of the atherosclerotic plaques found in *ApoE*$^{-/-}$ or *LDL*$^{-/-}$ mice show spontaneous rupture.

Many factors have been shown as potential contributors in regulating plaque vulnerability, including alterations of vessel hemodynamics, lipid profiles and inflammation[126].

Blood flow hemodynamic changes play an important role in the initiation and development of atherosclerotic plaque. It has been reported that atherosclerotic plaque preferentially develops at the site of artery bifurcation experiencing non-laminal blood flow and low shear stress[127]. Furthermore, tensile stress has been found as an essential factor in vulnerable plaque formation[128]. Based on this knowledge, a model of unstable and rupture-prone atherosclerotic plaques called tandem stenosis (TS) was developed in mice, which combines low shear stress and high tensile stress in common carotid artery[129]. This model is generated by surgically applied ligations on common carotid artery (CCA) leading to tandem stenosis, thereby inducing blood flow turbulence between ligations. With the dual ligation on the common carotid artery of *ApoE*$^{-/-}$ mice, the TS model can replicate the unstable plaques observed in humans, including massive lipid accumulation, large necrotic cores, thin or even discontinued fibrous caps. Therefore, this model shows highly translational relevance and provides the possibility to investigate advanced atherosclerotic lesions and potential therapeutic approaches for plaque ruptures.

2. Aim of the study

Stroke patients with large-artery atherosclerosis have the highest risk of recurrent cardiovascular events owing to atherosclerotic plaque rupture and thromboembolic infarctions[14]. In a previous study, it has been reported that stroke accelerates atheroprogression via alarmin-mediated propagation of vascular inflammation[33]. In addition, profound systemic immune activation has been identified both in mice and stroke patients characterized by substantially increased level of cell-free double-strand DNA (dsDNA) in the blood circulation after acute tissue injury[57]. However, the mechanism of by which systemic inflammatory response following the acute brain ischemia contributes to atherosclerotic plaque rupture is largely unknown. In addition, new therapeutic targets to prevent early recurrent cardiovascular events after ischemic stroke are currently unmet.

Therefore, the overall goal of this study was to clarify the underlying impact of the systemic inflammatory response induced by acute stroke on atherosclerotic plaque rupture and, more importantly, to identify potential novel therapeutic options for early secondary prevention. In order to achieve this goal, the following specific aims were addressed:

1. To investigate the impact of stroke on atherosclerotic plaque destabilization by histological parameters and immunological tools;
2. To explore the potential mechanism of post-stroke plaque destabilization and thrombus formation, which contribute to recurrent ischemic events;
3. To identify a novel therapeutic approach to prevent post-stroke early recurrent events by targeting soluble mediators.

3. Material and Methods

3.1 Materials

3.1.1 Equipment and software

Cytek Northern lights	Cytek Biosciences (US)
Centrifuge 5424	Eppendorf (Germany)
Cytostat NX70	Thermo Fisher Scientific (US)
Mini-protein electrophoresis cell	BIO-RAD (Germany)
PowerPac HC power supply	BIO-RAD (Germany)
LSM 980 confocal microscope	Zeiss (Germany)
Axio Observer Z1 microscope	Zeiss (Germany)
iMark Microplate reader	BIO-RAD (Germany)
Ultrasound imaging system Vevo 3100LT	VisualSonics (Cananda)
3T nanoScan® PET/MR	Mediso (Germany)
Nanodrop Spectrophotometer	Peqlab (US)
Excel	Microsoft Corporation (US)
FlowJo v. 10.6	Treestar Inc. (Ashland)
Image J	National Institute of Health (US)
GraphPad Prism 6	Graphpad Software Inc. (US)
VevoLab v3.2.0	VisualSonics (Cananda)

3.1.2 Reagents and consumables

7-0 fine MCAO suture Re L12 PK5	Doccol (US)
Aspirin	Sigma Aldrich (Germany)
Bovine serum albumin (BSA)	Sigma Aldrich (Germany)
Caspase-1 inhibitor (VX-765, Belnacasan)	Invivogen (US)

Cell lysis buffer 2	R&D systems (US)
Collagenase type I	Sigma (Japan)
Collagenase type XI	Sigma (Japan)
DMEM+GlutaMAX (4.5g/l D-Gluc. / Pyruvate)	Gibco (US)
DNase I	Roche (Switzerland)
DNase I	Sigma (Japan)
DQ-gelatin	Thermo Fisher Scientific (US)
Ethanol absolut	Merk Group (Germany)
Ethylenediamine tetraacetic acid (EDTA)	Carl Roth (Germany)
Fetal calf serum (FCS)	Gibco (US)
Flow cytometry staining buffer	Thermo Fisher Scientific (US)
Gentamycin (50mg/ml)	Gibco (US)
Histopaque solution	Sigma (Japan)
Hyaluronidase type 1-s	Sigma (Japan)
Isoflurane	CP-Pharma (Germany)
Isopentane	Sigma (Japan)
LPS from E.coli	Adipogen (US)
Methanol	Carl Roth (Germany)
NaCl isotonic solution 0.9%	Fresenius Kab (Germany)
NLRP3 inflammasome inhibitor (MCC950)	Invivogen (US)
Normal goat serum	Abcam (US)
NuPAGE™ LDS sample buffer (4X)	Thermo Fisher Scientific (US)
NuPAGE™ transfer buffer (20X)	Thermo Fisher Scientific (US)
Penicilin / Streptomycin	Gibco (US)
Phorbol 12-myristate 13-acetate (PMA)	Adipogen (US)
RIPA lysis buffer (+protease/phosphatase inhibitor)	Thermo Fisher Scientific (US)

Rosuvastatin	Sigma Aldrich (Germany)
RPMI 1640 (L-Glutamine / 25 mM HEPES)	Gibco (US)
Tween-20	Sigma (Japan)
Zymogram Developing Buffer	Thermo Fisher Scientific (US)
Zymogram Renaturing Buffer	Thermo Fisher Scientific (US)

3.1.3 Commercial assays

Name	Company	Reference No.
Click-iT™ Plus TUNEL Assay for In Situ Apoptosis Detection, Alexa Fluor™ 647 dye	Thermo Fisher Scientific (US)	C10619
Colloidal blue staining kit	Thermo Fisher Scientific (US)	LC6025
Duoset ELISA murine IL-1beta	R&D systems (US)	MLB00C
Fluoro-Jade C Ready-to-Dilute Staining Kit	Biosensis (Australia)	TR-100-FJ
HS dsDNA Assay Kit	Thermo Fisher Scientific (US)	Q32851
Neutrophil isolation kit	Miltenyi Biotec (Germany)	130-097-658
Picro-Sirius Red Stain Kit (Cardiac Muscle)	Abcam (US)	Ab245887
Plasma / Serum Cell-Free Circulating DNA Purification Mini Kit	NORGEN Biotek (Canada)	55100

3.1.4 Antibodies

3.1.4.1 Flow cytometry antibodies

Name	Company	Reference No.
Anti-human CD11b (PE; ICRF44)	Invitrogen (US)	12-0118-42

Anti-human CD14 (PerCP-Cy5.5; 61D3)	Invitrogen (US)	45-0149-42
Anti-human CD16 (FITC; CB16)	Invitrogen (US)	11-0168-42
Anti-human CD19 (APC; HIB19)	Invitrogen (US)	17-0199-42
Anti-human CD3 (FITC; HIT3a)	Invitrogen (US)	11-0039-42
Anti-human CD45 (eFluor 450; 2D1)	Invitrogen (US)	48-9459-42
Anti-human CD8a (PE; SK1)	Invitrogen (US)	12-0087-42
Anti-mouse CD11b (PerCP-Cy5.5; M/70)	Invitrogen (US)	45-0112-82
Anti-mouse CD192 (APC; SA203G11)	Biolegend (US)	150628
Anti-mouse CD45 (APC-Cy7; 30-F11)	Biolegend (US)	103116
Anti-mouse CD45 (eFluor450; 30-F11)	Invitrogen (US)	48-0451-82
Anti-mouse F4/80 (PE-Cy-anie7; BM8)	Invitrogen (US)	25-4801-82
Anti-mouse Ly6C (BV570; HK1.4)	Biolegend (US)	128030
Anti-mouse Ly6G (PE-Fluor610; 1A8-Ly6g)	Invitrogen (US)	61-9668-82
Anti-mouse MHC II (PE; NIMR-4)	Invitrogen (US)	12-5322-81

3.1.4.2 Antibodies for histology and immunoblotting

Name	Company	Reference No.
Anti Iba-1, Rabbit	Wako (Japan)	019-19741
Anti-alpha smooth muscle Actin antibody[1A4], Mouse	Abcam (US)	ab7817
Anti-CD31 Antibody, Rat	OriGene (Germany)	BM4086

Anti-CD41 [MWReg30] Antibody, Rat	Abcam (US)	ab33661
Anti-CD68 antibody [FA-11], Rat	Abcam (US)	ab53444
Anti-Factor XII Polyclonal Antibody, Rabbit	Invitrogen (US)	PA5-116703
Anti-Fibrinogen Antibody, Rabbit	Abcam (US)	ab34269
Anti-human caspase-1 (p20, BALLY-1; mouse)	Adipogen (US)	AG-20B-004
Anti-Ki-67 (D3B5) mAb, Rabbit	Cell Signaling (US)	9129S
Anti-MMP9 antibody	Abcam (US)	ab38898
Anti-mouse actin, Rabbit	Sigma (Japan)	A2066-.2ml
Anti-mouse caspase-1 (p20; CASPER1; mouse)	Adipogen (US)	AG-20B-0042-C100
Anti-mouse IgG (goat, HRP-conjugated)	Dako (Denmark)	P0447
Anti-rabbit IgG (goat, HRP-conjugated)	Dako (Denmark)	PI-1000
Anti-Von Willebrand Factor Antibody, Sheep	Abcam (US)	ab11713
Donkey anti-Sheep IgG (H+L) Cross-Adsorbed Secondary Antibody, Alexa Fluor 594	Invitrogen (US)	A-11016
Goat anti-Mouse IgG (H+L) Highly Cross-Adsorbed Secondary Antibody, Alexa Fluor 488	Invitrogen (US)	A-32723
Goat anti-Rabbit IgG (H+L) Crossed-Adsorbed Secondary Antibody, Alexa Fluor 594	Invitrogen (US)	A-11005

Goat anti-Rat IgG (H+L) Cross-Adsorbed Secondary Antibody, Alexa Fluor 647	Invitrogen (US)	A-21247
Recombinant Anti-MMP2 antibody	Abcam (US)	ab92536

3.2 Methods

3.2.1 Animal Experiments

All animal experiments were performed in accordance with the guidelines for the use of experimental animals and were approved by the government committee of Upper Bavaria (Regierungspraesidium Oberbayern; #02-2018-12). *ApoE*$^{-/-}$ mice (B6.129P2-Apoetm1Unc/J; JAX strain: 002052) were bred and housed at the animal core facility of the Centre for Stroke and Dementia Research (Munich, Germany). *ApoE*$^{-/-}$ mice were fed an HFD (#88137, ssniff) from 8 weeks on.

A transient ischemia-reperfusion stroke model that depicts the extent and variability of atheroprogression after stroke was used to estimate the number of animals for this exploratory study. Data were excluded from all mice that died during surgery. Detailed exclusion criteria are described below. Animals were randomly assigned to treatment groups, and all analyses were conducted by investigators blinded to group assignment. All animal experiments were performed and reported in accordance with the Animal Research: Reporting of In Vivo Experiments (ARRIVE) guidelines[130].

3.2.2 Drug Administration

3.2.2.1 Oral gavage with Aspirin and Rosuvastatin

Mice received a daily bolus of Aspirin (20mg kg^{-1}, Sigma Aldrich, Germany) and Rosuvastatin (5mg kg^{-1}, Sigma Aldrich, Germany) via oral gavage. Aspirin and Rosuvastatin were solved in water (sterile ddH_2O) and mixed with powdered chow diet (ssniff). A single daily bolus was 500 µl.

3.2.2.2 Recombinant DNase I (DNase I)

ApoE$^{-/-}$ mice received DNase I injections as we previously described[57]. 1000 U of recombinant DNase I (Roche, Switzerland) dissolved in incubation 1x buffer (40 mM Tris-HCl, 10 mM NaCl, 6 mM $MgCl_2$, 1 mM $CaCl_2$, pH 7.9, diluted in PBS, Roche) was injected *i.v.* via tail vein right before surgery in a final volume of 100 µl. The control group was administered saline injections at the same volume, routine, and timing as experimental animals.

3.2.2.3 Caspase-1 inhibitor (VX-765)

The caspase-1 inhibitor VX-765 (stock in DMSO) dissolved in PBS (Belnacasan, Invivogen, US) was injected *i.p.* 1 h prior to surgery at a dose of 100 mg kg^{-1} body weight at a final volume of 300 µl[57]. The control group was administrated saline injections at the same volume, routine, and timing as experimental animals.

3.2.2.4 NLRP3 inflammasome inhibitor (MCC-950)

Mice received two injections (1 h prior to and 1 h after surgery) of NLRP3 inflammasome inhibitor MCC-950 dissolved in sterile saline at a dose of 50mg kg^{-1} body weight (Invivogen, US). MCC-950 or the control was injected *i.p.* in a final volume of 200 µl.

3.2.2.5 AIM2 inhibitor (4-sulfonic calix[6]arene)

The AIM2 inhibitor 4-sulfonic calix[6]arene[131] (stock in DMSO) was dissolved in PBS and injected *i.p*. 1 h prior to surgery at a dose of 50 mg kg^{-1} body weight at a final volume of 200 µl. The control group was administered saline injections at the same volume, routine, and timing as experimental.

3.2.2.6 DNA challenge

DNA derived from stimulated neutrophils (see below for stimulation and isolation of NET DNA) was injected *i.v.* at a dose of 5 µg at a final volume of 200 µl (sterile saline). The control group was administrated injections (sterile saline) at the same volume, routine, and timing.

3.2.3 Patient Cohort for Carotid Endarterectomy Sample Analysis

Human samples involved in this project were provide in collaboration by Dr. Gerrit Große at the Department of Neurology, Medical University Hannover. In detail, patients scheduled for carotid endarterectomy due to symptomatic or asymptomatic carotid stenosis were prospectively recruited at the Departments of Neurology and Cardiothoracic-, Transplantation- and Vascular Surgery at Hannover Medical School between June 2018 and December 2020. Carotid stenosis was defined as symptomatic if cerebral ischemia occurred in the territory of the affected artery and concurrent stroke etiologies were excluded following standardized stroke diagnostics including cranial computed tomography (CT) and/or magnetic resonance (MR) imaging, CT or MR-angiography, transthoracic or transesophageal echocardiography, cardiac rhythm monitoring and Doppler/duplex ultrasound. Peripheral venous blood was drawn immediately prior to surgery and EDTA whole blood samples were used for flow cytometric analyses. Carotid plaque samples were obtained during carotid endarterectomy and immediately preserved in phosphate-buffered saline. Both blood and tissue samples were sent for further analysis on the same day of collection. All patients provided written informed consent and the ethics committee at Hannover Medical School approved the study.

Thirteen patients with symptomatic and seven patients with asymptomatic, high-grade carotid stenosis were recruited. Median age was 73 years (25th-75th percentile: 62-80 years). See Table 2 for clinical and demographic patient details.

	Symptomatic carotid stenosis (n=13)	Asymptomatic carotid stenosis (n=7)
Age (median (a); 25^{th}-75^{th} percentile)	64 (61-75)	78 (76-82)
Sex (male, n)	12 (92%)	6 (86%)
Arterial hypertension (n)	11 (84%)	7 (100%)

Diabetes mellitus (n)	4 (31%)	3 (43%)
BMI (median (kg/m²); 25th-75th percentile)	25.5 (23.2-29.3)	26.8 (24.5-31.6)
Current nicotine consumption (n)	5 (38%)	0 (0%)
Dyslipidemia (n)	9 (69%)	6 (85%)
Coronary artery disease	3 (23%)	3 (43%)
Peripheral artery disease	1 (8%)	2 (29%)
History of myocardial infarction	1 (8%)	1 (14%)
History of stroke	2 (15%)	0 (0%)

Table 2 Demographic and clinical details of patients undergoing carotid endarterectomy.

3.2.4 Carotid Tandem Stenosis Model

Tandem stenosis (TS) surgery was performed as previously described[129]. At 12 weeks of age, 4 weeks after commencement of HFD, *ApoE*$^{-/-}$ mice (C57BL/6J background) were anesthetized with isoflurane delivered in a mixture of 30% O_2 and 70% N_2O. An incision was made in the neck and the right common carotid artery was dissected from circumferential connective tissues. To control the stenosis diameter, a 150 µm or 450 µm pin was placed on top of the exposed right common carotid artery, with the distal point 1 mm away from the bifurcation and proximal point 3 mm from the distal stenosis, subsequently, a 6-0 blue braided polyester fibre suture was tied around both the artery and needle, and then the pin was removed (Fig. 3.1). Animals were fed with HFD for additional 4 weeks after TS surgery.

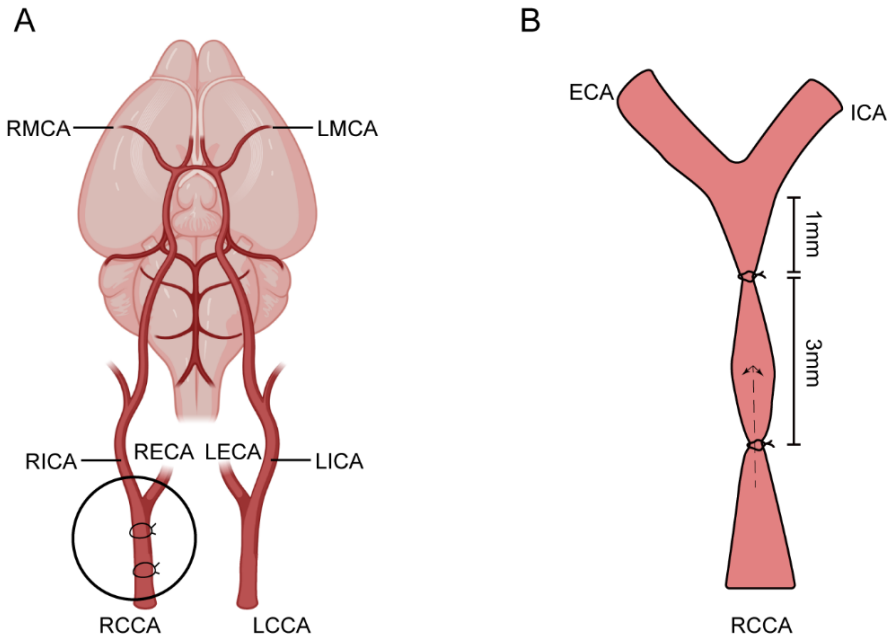

Figure 3.1 Schematic illustration of tandem stenosis surgery. Scheme of a murine CCA tandem stenosis (A) and magnified for the region highlighted on right common carotid artery (B). Legend: RCCA = right common carotid artery; LCCA = left common carotid artery; RICA = right internal carotid artery; LICA = left internal artery; RECA = right external carotid artery; LECA = left external carotid artery; RMCA = right middle cerebral artery; LMCA = left middle cerebral artery. Dotted arrow in (B) represents blood turbulence.

3.2.5 Translational Ischemia-Reperfusion Stroke Model

4 weeks after TS, *ApoE*$^{-/-}$ mice were anaesthetized with 2% isoflurane delivered in a mixture of 30% O_2 and 70% N_2O[33]. The temporal bone was exposed by making an incision between the ear and the eye. In supine position, the mice were implanted with a laser Doppler probe that attached to the skull above the middle cerebral artery (MCA) territory. By performing a middle incision, the common carotid artery and left external carotid artery were exposed and further isolated and ligated. A 2-mm silicon-coated filament (Doccol) was inserted into the internal carotid artery, advanced gently to the MCA until resistance was felt, and occlusion was confirmed by a corresponding decrease in blood flow (i.e., a decrease in the laser Doppler flow signal by ≥ 80%). Following 60 minutes of occlusion, the animals were re-anesthetized, and the filament was removed (Fig. 3.2). Once the mice recovered, they were kept in their home cage with ad libitum access to water and food. Sham-operated mice received the same surgical procedure,

but the filament was removed in lieu of being advanced to the MCA. In all mice, a feedback-controlled heating pad maintained the body temperature of 37 °C during surgery. Exclusion criteria: 1. Insufficient MCA occlusion (a decrease in blood flow to > 20% of the baseline value). 2. Death during the surgery. 3. Post-mortem histological analysis revealed no brain ischemia.

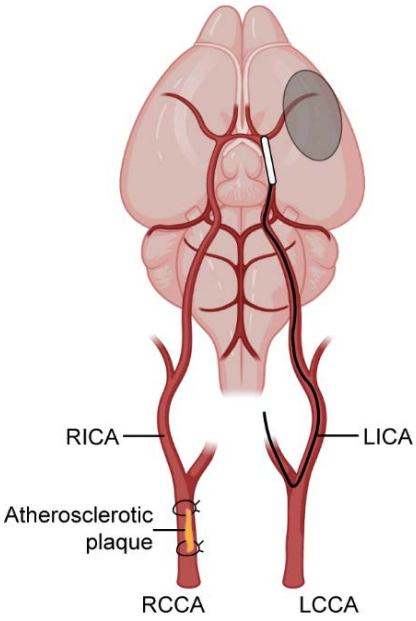

Figure 3.2 Schematic description of translational ischemia-reperfusion stroke model in mice. Brain ischemia was induced by inserting a filament into ICA to occlude MCA. Gray circle represents the ischemic lesion in MCA territory.

3.2.6 Ultrasound Imaging

Carotid artery blood flow in *ApoE*$^{-/-}$ mice were measured with a high-frequency ultrasound imaging system (Vevo 3100LT, VisualSonics, Toronto, ON, Canada) with a 40 MHz linear array transducer (MX550D, VisualSonics, Canada) before and right after TS surgery, and weekly for 4 weeks afterwards. Mice were anesthetized with isoflurane delivered in a mixture of 30% O_2 and 70% N_2O. B-mode, Color-Doppler mode and pulsed Doppler velocity spectrum were recorded from both sides of CCA. For the right common carotid artery (RCCA), five locations were examined: before proximal ligation, near proximal ligation, between two ligations, near distal ligation and above the distal ligations. For the left common carotid artery (LCCA), since it was not ligated, only three locations were measured: proximal, middle and distal part of LCCA. Pulsed Doppler velocity was determined with the sample volume calibrated to cover the entire vascular lumen and the smallest possible angle of interception (< 60°) between the flow direction and the ultrasound beam. The peak systolic velocity (PSV), end diastolic velocity (EDV) were recorded from CCAs of both sides. VevoLab v3.2.0 software was used for ultrasound imaging analysis. The mean velocity (MV) was calculated as: MV = (PSV+2*EDV)/3.

3.2.7 Magnetic Resonance Imaging (MRI)

MRI was performed in a small animal scanner (3T nanoScan® PET/MR, Mediso, Münster Germany with 25 mm internal diameter quadrature mouse head coil) at 2 and 7 days after sham or stroke surgery. For scanning, mice were anesthetized with 1.2% isoflurane in 30% oxygen/ 70% air applied via face mask[132]. Respiratory rate and body temperature (37 +/- 0,5 °C) were continuously monitored via an abdominal pressure sensitive pad and rectal probe and anaesthesia adjusted to keep them in a physiological range. The following sequences were obtained: coronal T2-weighted imaging (2D fast-spin echo (FSE), TR/TE = 3000/57.1 ms, averages 14, resolution 167 x 100 x 500 um^3), coronal T1-weighted imaging (2D fast-spin echo (FSE), TR/TE = 610/28,6 ms, averages 14, resolution 167 x 100 x 500 um^3), and DWI (2D spin echo (SE), TR/TE = 1439/50 ms , averages 4, resolution 167 x 100 x 700 um^3). MEI images were then post-processed using Image J.

3.2.8 Organ and Tissue Processing

Mice were deeply anaesthetized with ketamine (120 mg kg^{-1}) and xylazine (16 mg kg^{-1}) and venous blood was drawn via cardiac puncture of the right ventricle in 50 mM EDTA (Sigma-Aldrich, Germany); the plasma was isolated by centrifugation at 3,000 g for 15 min and stored at -80 °C until further use. Immediately following cardiac puncture, mice were transcardially perfused with ice cold saline. Subsequently, the common carotid arteries (CCA) from both sides as well as the aortic arches and hearts were carefully isolated and embedded in compound (O.C.T., Tissue-tek, Japan), frozen over dry ice and stored at -80 °C until sectioning.

Heads were cut just above the shoulders. Skin was removed from the head and the muscle was stripped from the bone. After removal of the mandibles and the skull rostral to maxillae, whole brain with skull was post-fixed by 4% paraformaldehyde (PFA) overnight at 4 °C. Subsequently, samples were transferred to a decalcification solution of 0.3 M EDTA (C. Roth, 292.94 g/mol) at pH 7.4 and stored at 4 °C. EDTA solution was

changed after 3 days. Samples were immersed with 30% sucrose in PBS and then frozen down in -20 °C isopentane (Sigma Aldrich, Germany). 15 µm thick coronal sections were obtained at the level of anterior commissure for immunohistochemical analysis (Fig. 3.3). Sections were mounted on SuperfrostPlus Slides (Thermo Scientific, US) and stored in -80 °C.

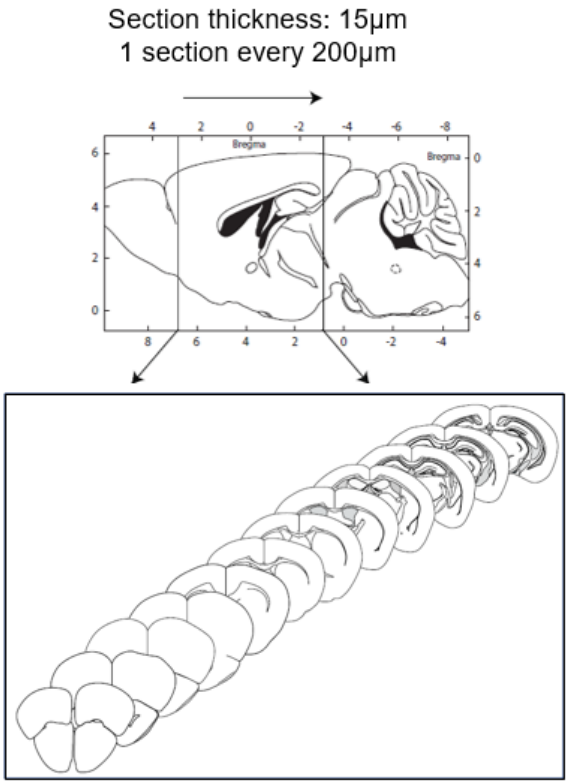

Figure 3.3 Brain sample processing scheme. In order to further confirm recurrent ischemic lesion, brain samples were started to collect at 3 mm anterior the bregma and stopped at 3 mm posterior the bregma.

3.2.9 Histology and Immunofluorescence

3.2.9.1 Hematoxylin and Eosin Staining

The purpose of H&E staining is to identify tissue types as well as morphological changes. Hematoxylin stains basophilic substances, such as DNA, while Eosin stains acidophilic substances including positively charged amino acids of proteins. To begin with, carotid cryosections (5 µm) were washed rinsed by dipping them three times into distilled water. Subsequently, sections were stained with a hematoxylin solution (Merck, Germany) for

5 min. Then, sections were washed in tap water for 5 min and immersed with eosin solution (Carl Roth, Germany) for additional 5 min. Afterwards, sections were washed again in tap water for 5 min. Then sections were dehydrated according to the following protocol:

Solution	Procedure
70% ethonal	5 s
80% ethonal	5 s
90% ethonal	5 s
100% ethonal	5 min
100% ethonal	5 min
Xylene 1	2 min
Xylene 2	2 min

Finally, sections were mounted with Roti Histokki medium (Carl Roth, Germany) and stored at RT before imaging.

3.2.9.2 Picrosirius red staining

In order to evaluate the collagen content within the atherosclerotic lesion, carotid cryo-sections were stained with Picrosirius red solution. Picosirius red is used as a strong anionic dye that can associate along cationic collagen fibers[133]. In the beginning of the staining, sections were covered with phosphomolybdic acid solution (0.2%, Abcam, US) for 2 min. Afterwards, sections were wash by tap water for 1 min. Then, sections were stained with picrosirius red solution (Abcam, US) for 90 min at RT. Subsequently, sections were quickly rinsed in acertic acid solution (0.5%, Abcam, US) for 2 min. Then, sections were rinsed in 100% ethonal for 1 min and dehydrated in 100% ethonal for additional 2 min. Finally, sections were mounted with Roti Histokki medium (Carl Roth, Germany). Sections were stored at RT until imaging.

3.2.9.3 Immunofluorescence staining

For immunofluorescence staining, cryosections were fixed with 4% PFA followed by antigen blockade using 2% goat serum blocking buffer containing 1% Bovine Serum Album (BSA, Sigma), 0.1% cold fish skin gelatin (Sigma Aldrich, Germany), 0.1% Triton X-100 (Sigma) and 0.05% Tween 20 (Sigma). Next, sections were incubated overnight at 4 °C with the following primary antibodies: Rat anti-mouse CD68 (1:200, ab53444, Abcam), mouse anti-mouse smooth muscle actin (1:200, ab7817, Abcam, US), rabbit anti-mouse Ki67 (1:200, 9129S, Cell Signaling, US), mouse anti-mouse caspase-1 (1:200, AG-20B-0042-C100, Adipogen), sheep anti- Von Willebrand Factor (1:100, ab11713, Abcam, US), rat anti-CD31 (1:200, BM4086, OriGene, US). After extensive washing, sections were incubated with secondary antibodies as following: AF647 goat anti-rat (1:200, Invitrogen, US), Cy3 goat anti-mouse IgG H&L (1:200, Abcam, US), AF594 goat anti-rabbit (1:200, Invitrogen, US), AF488 goat anti-mouse (1:200, invitrogen, US), AF594 donkey anti-sheep (1:200, invitrogen, US). Counterstain to visualize nuclei was performed by incubating with DAPI (1:5000, invitrogen, US). Finally, sections were mounted with fluoromount medium (Sigma Aldrich, Germany). Microphotographs of Immunofluorescent samples were taken with confocal microscope (LSM 880, LSM 980; Carl Zeiss, Germany). Sections were imaged with an epifluorescent microscope (Axio Imager M2; Carl Zeiss, Germany) and quantified by using ImageJ software (National Institutes of Health, US).

3.2.9.4 Fluoro Jade C and TUNEL staining

For the visualization of suspected secondary infarct lesions in the contralateral hemisphere, brain sections (15 µm) were first stained for Fluoro Jade C (FJC) to identify the degenerative neurons. FJC staining was performed using the “Fluoro-Jade C Ready-to-Dilute” Staining Kit (Biosensis, TR-100-FJ, US) according to the manufacturer’s instructions. To confirm the secondary lesion, double staining of microglia marker Iba-1 (1:200, FUJIFILM Wako Pure Chemical Corporation, US) and terminal deoxynuceotidyl transferase dUTP nick end labeling (TUNEL) staining was performed using Click-iT™ Plus

TUNEL Assay for In Situ Apoptosis Detection (Alexa Fluor™ 647 dye, Thermo Scientific, C10619) according to the manufacturer's instructions. Brain samples were photographed on an epifluorescence microscope (Zeiss Axiovert 200M, C. Zeiss, Germany) and a confocal microscope (LSM980, C. Zeiss, Germany).

3.2.10 Murine Plaque Analysis

Plaque vulnerability was assessed as previously described before[134]. Intima, media and necrotic core area was analyzed in H&E-stained sections. The necrotic core (NC) was defined as the area devoid of nuclei underneath a formed fibrous cap. NC area was quantified as the percentage of necrotic core area over the intima area (Fig. 3.4 A). Collagen content was quantified on Picrosirius Red-stained sections. Binary images were created by converting picrosirius red images into 8-bit images and segmenting them by thresholding. Collagen area was quantified as the percentage of collagen area over the intima area (Fig. 3.4 B). Images of CD68 staining were segmented by thresholding in order to generate binary images based on florescence signals. $CD68^+$ macrophage area was quantified as the percentage of CD68 area over the intima (Fig. 3.4 C). Smooth muscle actin (SMA) staining pictures were processed the same as for CD68 staining. SMA area was measured as the percentage of SMA area against the intima (Fig. 3.4 D). Vulnerability Plaque Index (VPI) was calculated as VPI = (% NC area + % CD68 area) / (% SMA area + % collagen area). This study excluded mice whose carotid samples showed no sign of lesion formation.

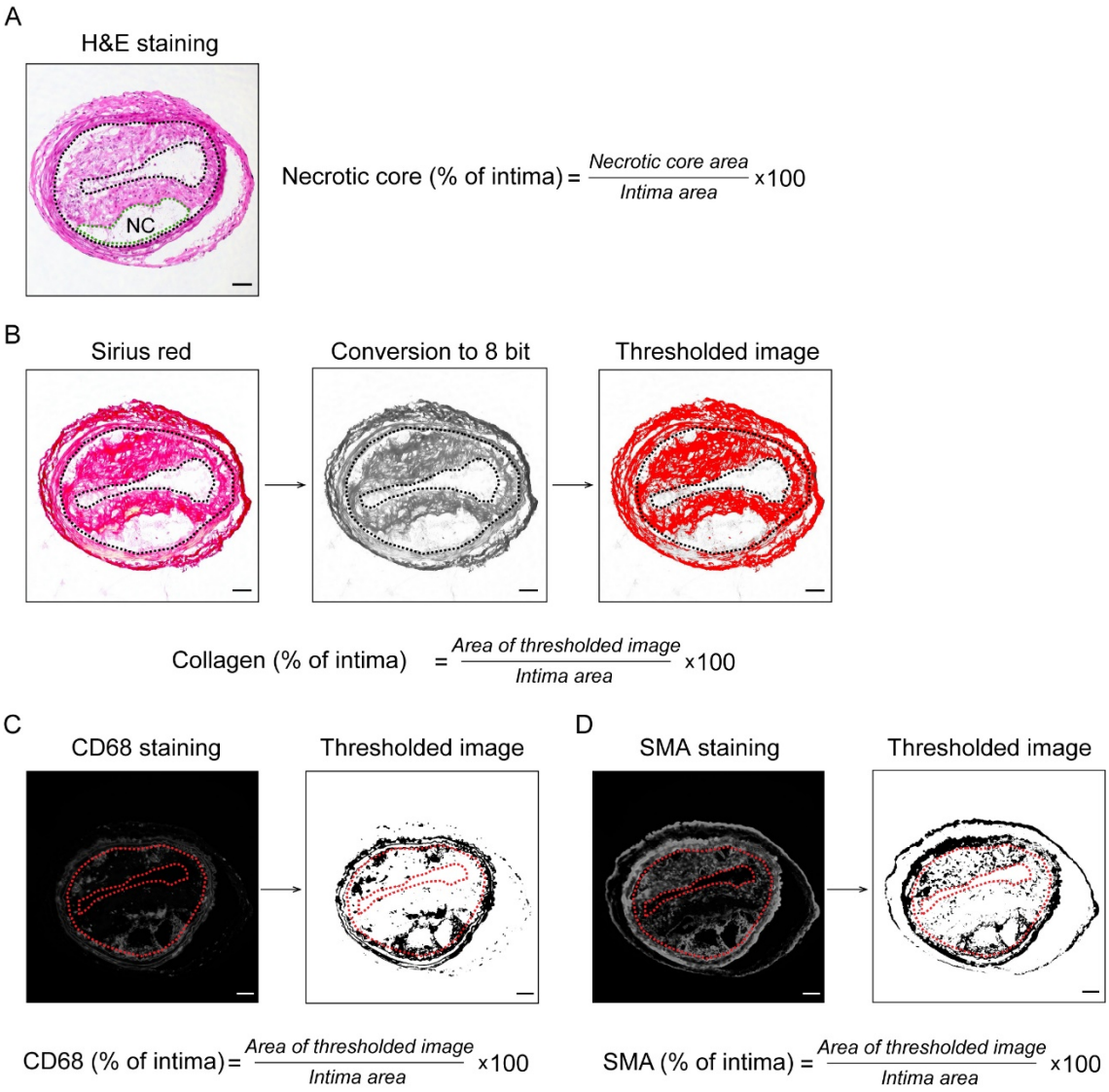

Figure 3.4 Illustration for murine histological analysis. The area between two black dotted lines represents the intima area; the area of green dotted line represents necrotic core. Scale bar = 50µm

3.2.11 Flow Cytometry Analysis

CCA materials were mixed with digestion buffer, consisting of collagenase type XI (125 U/ml, C7657), hyaluronidase type 1-s (60 U/ml, H3506), DNase I (60 U/ml, D5319), collagenase type I (450 U/ml, C0130; all enzymes from Sigma Aldrich, Germany) in 1x PBS[135], and were digested at 750 rpm for 30 min at 37 °C. After digestion, CCA materials were homogenized through a 40 µm cell strainer, washed at 500 g for 7 min at 4 °C and re-suspended in flow cytometry staining buffer (00-4222-26, Thermo Fisher) to generate single cell suspensions. Cell suspension were the incubated 30 min at 4 °C with flow

cytometry antibodies containing anti-CD45, CD11b, CD192, Ly6C, Ly6G, F4/80 and MCH II (detailed information of flow cytometry antibodies is provided in –'section'– 3.1.4.1). After staining, non-bound antibodies were washed away by adding 1 ml flow cytometry staining buffer and spinning down for 7 min at 500 g. Supernatant was discarded and cell pellet was re-suspended in 200 µl staining buffer. Samples were kept on ice until analysed using a spectral flow cytometer (Northern Light, CYTEK, US).

3.2.12 Tracking of Blood-Derived Infiltrating Leukocytes in the CCA Plaque

Leukocytes infiltration in the CCA was assessed by intravenous injection of a specific antibody to label circulating leukocytes[136]. Initially, 3 µg of anti-CD45 antibody was intravenously injected into *ApoE*$^{-/-}$ mice right after sham or stroke surgery. 24 hours later, in order to exclude the blood contamination, additional 3 µg anti-CD45 antibody conjugated to APC-Cy7 (clone: 30-F11, Biolegend, US) was injected intravenously 3 min before sacrifice (Fig. 3.5 A). Sample preparation was performed the same as described in –'section'– 3.11. Visualization of infiltrated intravascular-derived leukocytes (pre-labelled with anti-CD45 eF450 antibody) in atherosclerotic lesion of CCA was shown as CD45 eFluor450 positive but APC-Cy7 negative population in the spectral flow cytometer (Northern Light, CYTEK, US) (Fig. 3.5 B).

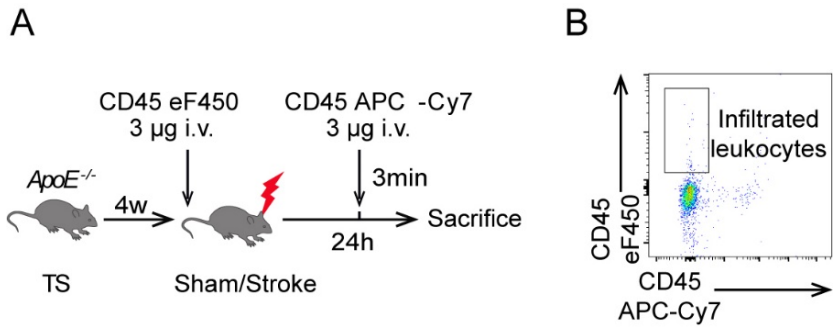

Figure 3.5 Schematic description of experimental design for tracking infiltrated blood-derived leukocytes in CCA plaque after stroke.

3.2.13 Western Blotting

Ipsi- and contralateral CCA materials were carefully isolated and snap frozen on dry ice. Whole frozen CCA was lysed with RIPA lysis/extraction buffer with added protease/phosphatase inhibitor (Thermo Fisher Scientific, US). Total protein quantified using the Pierce BCA protein assay kit according to the manufacturer's instructions (Thermo Fisher Scientific). Whole tissue lysates were fractionated by SDS-PAGE and transferred onto a polyvinylidene difluoride membrane (BioRad, Germany). After blocking for 1 hour in TBS-T (TBS with 0.1% Tween 20, pH 8.0) containing 4% skin mile powder (Sigma, Germany), the membrane was washed with TBS-T and incubated with the primary antibodies against following antibodies: mouse anti-caspase-1 (1:1000; AdipoGen, US), rabbit anti-actin (1:1000; Sigma, Germany) and rabbit anti-Factor XII (1:1000, Invitrogen, US). Membranes were washed three times with TBS-T and incubated for 1 hour with HRP-conjugated anti-rabbit or anti-mouse secondary antibodies (1:5000, Dako, Denmark) at room temperature. Membranes were washed three times with TBS-T, developed using ECL substrate (Millipore, US) and acquired via the Vilber Fusion Fx7 imaging system. After densitometry analysis by using Image J, the expression of target proteins is normalized to β-actin expression.

3.2.14 Enzyme Linked Immunosorbent Assay (ELISA)

The concentration of IL-1β in CCA plaque was quantified via ELISA. CCA tissue samples were isolated and snap frozen on dry ice. Whole frozen CCA was lysed with 200 µl cell lysis buffer (#895347, R&D system, US). The concentration of IL-1β in total CCA lysates was measured by ELISA according to the manufacturer's instructions (MLB00C, R&D system). Absorbance at 450 nm was measured by iMark Microplate Reader (BIO-RAD, Germany). IL-1β sample concentrations were quantified by interpolation of the standard curve, obtained by plotting absorbance values relative to corresponding standard concentrations using nonlinear regression for curve adjustment.

3.2.15 MMP2 and MMP9 *in situ* Zymography of CCA Sections

MMP2 and MMP9 *in situ* zymography on CCA sections was performed as previously described with slight modifications[33]. DQ-gelatin (D12054, Invitrogen) was dissolved in reaction buffer (50 mM Tris-HCl, 150 mM NaCl, 5 mM $CaCl_2$, 200 mM sodium azide, pH 7.6). 5 µm cryosections were incubated for 2 h at 37 °C with the gelatin-containing reaction buffer. Negative control sections were pre-incubated for 1 h with the MMP-inhibitor 1,10-Phenatheroline (Sigma). Nuclei were stained with DAPI. MMP activity was detected with an Axio Observer Z1 microscope with 20 x magnification (Carl Zeiss, Germany). MMP 2/9 area was quantified as the percentage of MMP 2/9 area over the intima area.

3.2.16 Neutrophil Isolation and Stimulation

Neutrophils were generated from tibia and femur of transcardially perfused wild type mice (Fig. 3.6). After isolation and dissection of tibia and femur, bone marrow was flushed out of the bones through a 40 µm strainer using a plunger and 1 ml syringe filled with sterile 1 x PBS. Strained bone marrows cells were washed with PBS, and resuspended in 1 x sterile PBS with 5% BSA. Afterwards, neutrophils were isolated by using neutrophil isolation kit (130-097-658, Miltenyi Biotec) according to the manufacturer's instructions. 1 x 10^7 cells were plated onto 150 mm culture dishes in 10 ml RIPA 1640 (Gibco, US), supplemented with 10% FBS and 1% penicillin/streptomycin. Cells were incubated under 37 °C with 5% CO_2 for 30 min. Afterwards, cells were stimulated with 100 nM phorbol 12-myristate 13-acetate (PMA) overnight at the same condition.

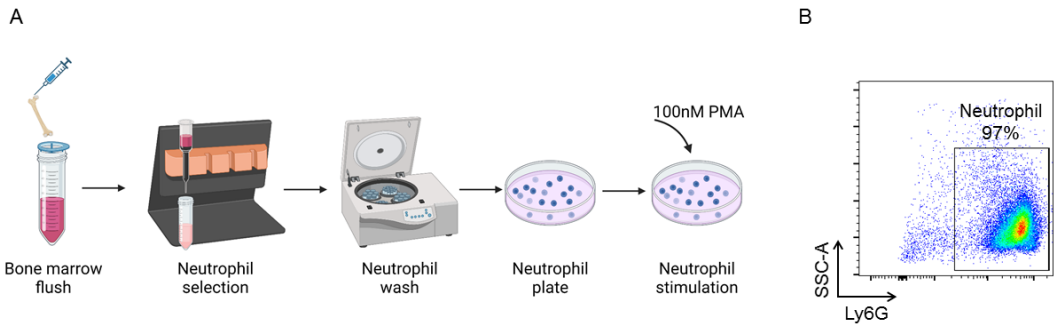

Figure 3.6 Schematic illustration of neutrophil isolation and stimulation. (**A**) Scheme of neutrophil isolation and stimulation. (**B**) Neutrophil purity check after isolated from tibia and femur of mouse. SSC-A: Side Scatter parameter.

3.2.17 Free Nucleic Acid Quantification

Total circulating cell-free (cf) DNA, single strand (ss) DNA and double strand (ds) DNA) levels in the plasma of mice and human patients were first purified with Plasma/serum Cell-free circulating DNA purification mini kit (#55100, NORGEN Biotek, Canada), according to the manufacturer's instructions. Afterwards, cfDNA and ssDNA were measured with Nanodrop Spectrophotometer (1000ND, Peqlab, US). dsDNA was measured with a Qubit 2.0 fluorophotometer (Invitrogen, US) using a specific fluorescent dye binding dsDNA (HS dsDNA Assay kit, Thermo Fisher Scientific). Dilutions and standards were generated following the manufacturer's instructions.

3.2.18 Bone Marrow-Derived Macrophages (BMDM) Isolation and Cell Culture

BMDMs were isolated and cultured as previously described[57]. BMDMs were generated from tibia and femur of transcardially perfused wild type mice. After isolation and dissection of tibia and femur, bone marrow was flushed out of the bones through a 40 µm strainer using a plunger and 1 ml syringe filled with sterile 1x PBS. Strained bone marrow cells were washed with PBS, and resuspended in DMEM + GlutaMAX-1 (Gibco, US), supplemented with 10% fetal bovine serum (FBS) and 1% Gentamycin (Thermo Scientific, US) and counted. 5×10^7 cells were plated onto 150 mm culture dishes. Cells were differentiated into BMDMs over the course of 8-10 days. For the first days after isolation, cells were supplemented with 20% L929 cell-conditioned medium (LCM), as a source of M-CSF. Cultures were then maintained at 37 °C with 5% CO_2 until they reached ≥ 90% confluence.

3.2.19 BMDM Stimulation with Sham or Stroke Serum

BMDMs were cultured for 8-10 d for full differentiation. Cells were then harvested, washed, counted, and seeded in flat-bottom tissue culture-treated 24-well plates at a density of 2 x 10^5 cells per well in a total volume of 500 µl, and then cultured overnight for at least 16 h (Fig. 3.7). BMDMs were then stimulated with LPS (100 ng/ml) for 4 h. Afterwards, the cells were incubated with serum from either stroke or sham operated wild type mice (4 h post-surgery) at a concentration of 25% total volume for 1 h. Control treated BMDMs received only FBS-containing culture medium. After stimulation, the supernatant was discarded and the cells were washed with sterile PBS to ensure no leftover serum on the cells. Afterwards, 500 µl serum-free DMEM was added to the BMDMs, which were then incubated overnight for 16 h at 37 °C and 5% CO_2. The culture medium was then collected for further analysis.

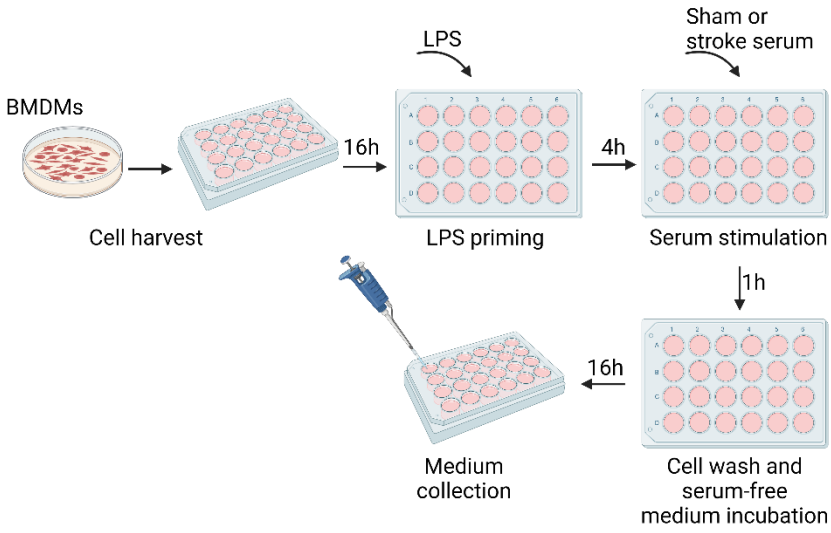

Figure 3.7 Schematic description of BMDMs conditional stimulation.

3.2.20 Gelatin Zymography of Mouse CCA Extracts, BMDMs Culture Medium and Patient Plaque Lysates

MMPs CCA tissue extracts were analysed using gelatin zymography (Novex TM 10% zymography plus protein; ZY00100BOX, Thermo Scientific, US) according to the manufacturer's instructions. CCA tissue was lysed with cell lysis buffer (#895347, R&D system,

US). Total protein was quantified using Pierce BCA protein assay kit (Thermo Fisher Scientific, US). Aliquots of appropriately diluted tissue extracts were loaded on gels at total volume of 20 µl. After electrophoresis, gels were incubated in 1 x Zymogram Renaturing Buffer (LC2670, Invitrogen, US) for 30 min at room temperature with gentle agitation. Afterwards Zymogram Renaturing Buffer was decanted and 1 x Zymogram Developing Buffer (LC2671, Invitrogen) was added to the gel. The gel was then equilibrated for 30 minutes at room temperature with gentle agitation. After an additional wash with 1x Zymogram developing buffer the gels were incubated at 37 °C overnight. Gels were stained with colloidal blue staining kit (LC6025, Invitrogen, US) and acquired on a gel scanner. MMPs activity reflected as clear bands against a dark blue background where the gelatin has been digested by MMPs. The MMPs activity was further quantified by Image J. BMDM culture medium was collected and loaded on gelatin zymography gels at total volume of 25 µl. MMP activity in BMDM culture medium was analysed using the same protocol as for the tissue samples.

3.2.21 *En face* Immunofluorescence Staining

Both, ipsi- and contralateral CCA were dissected and adventitial fat and ligation nodes were thoroughly trimmed away. CCAs were then cut open, unfolded, and pinned out on a silicon-elastomer for fixation in 4% PFA at room temperature for 2 h. The CCAs then were washed for 1 h at room temperature in 5% BSA with 0.3% Triton-100X (Sigma Aldrich, Germany). Afterwards, CCAs were incubated with rabbit anti-Factor XII (1:100, PA5-116703, Invitrogen, US) at 4 °C overnight. After washing in 5% BSA with 0.3% Triton-100X for 1 h at room temperature, CCAs were incubated with AF647 goat anti-rabbit (1:100, Invitrogen, US) and DAPI for 2 h at room temperature. Finally, CCAs were mounted with fluoromount medium (Sigma Aldrich, Germany). Microphotographs were taken with a confocal microscope (LSM 980; C. Zeiss, Germany).

3.3 Statistical analysis

Data analysis was performed using GraphPad version 6.0. All summary data are presented as the mean ± standard deviation (s.d.) unless indicated otherwise. A Shapiro-Wilk normality test was used to determine the normality of all datasets. The groups containing normally distributed independent data were analysed using a two-way Student's t test (= 2 groups) or ANOVA (for > 2 groups). Normally distributed dependent data were analysed using a 2-way ANOVA. Mann-Whitney U test (= 2 groups) or Kruskal-Wallis Test (H test, for > 2 groups) were used to analyse the remaining data. The P value was adjusted for comparison of multiple comparisons using Bonferroni correction or Dunn's multiple comparison tests. P values < 0.05 was considered to be statistically significant.

4. Results

4.1 Post-stroke vascular inflammation and atheroprogression cannot be rescued by established secondary prevention

To test the efficacy of established secondary prevention on atheroprogression early after stroke, 8-week-old apolipoprotein E–deficient (*ApoE*$^{-/-}$) mice[126] were assigned to three groups: sham, stroke and stroke treated with anti-platelet (aspirin) and cholesterol-lowering treatment (rosuvastatin), a currently established secondary prevention treatments[137] (Fig. 4.1 A). Aspirin and statin treatment did not improve post-stroke mortality (Fig. 4.1 B). To evaluate vascular inflammation after secondary prevention treatment, flow cytometry analysis was performed for whole-aorta cell suspensions. Monocyte counts per aorta were increased both in stroke control and treated stroke mice compared to sham (Fig. 4.1 C). Overall plaque load in aortic valve was significantly increased both in stroke control and treatment group compared to sham operated mice, quantified by Oil Red O staining (Fig. 4.1 D, E). Taken together, these findings suggest that currently established anti-platelet and cholesterol-lowering therapies fail to attenuate atheroprogression and vascular inflammation early after experimental stroke.

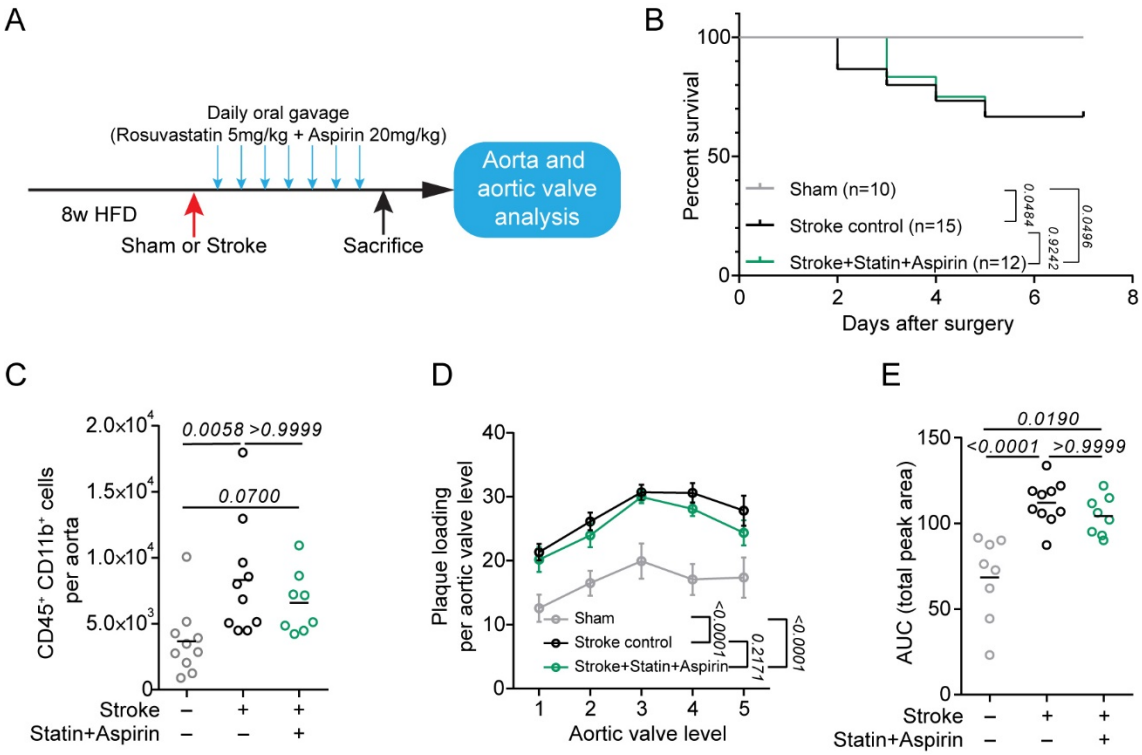

Figure 4.1 Established secondary prevention fails to attenuate early post-stroke vascular inflammation and atheroprogression. (A) Experimental design: 8w-old HFD fed *ApoE*$^{-/-}$ mice underwent sham or stroke surgery. Mice were treated orally with either control or a combination of Rosuvastatin (5 mg/kg) and Aspirin (20 mg/kg) for 7 consecutive days after stroke. **(B)** Kaplan-Meier survival curves of stroke control, statin and aspirin treated, or sham operated mice. Mantel-Cox test; n = 10 (sham), n = 15 (control), n = 12 (statin + aspirin treatment). **(C)** Flow cytometry analysis of whole aorta cell suspensions revealed no difference in total monocyte (CD45^{+}CD11b^{+}) cell counts between control or treated mice after stroke in contrast to sham-operated mice (ANOVA, n = 8-10 per group). **(D, E)** Quantification of aortic valve plaque load displayed no differences between stroke control and statin + aspirin-treated mice. Data is shown as (D) percentage of plaque area per aortic valve level and (E) area under the curve (ANOVA, n = 8-10 per group).

4.2 Advanced atherosclerotic plaque model establishment

Atherosclerotic plaques in human and animals preferentially develop at the site of vessel bifurcations or arteries branches where shear stress is low in magnitude[127]. Moreover, tensile stress has also been considered as a responsible factor contributing to plaque rupture[128]. To unravel the mechanisms leading to increased risk of recurrent events and stroke in atherosclerotic patients with an ischemic event, a mouse model that combines both low shear stress and high tensile stress[129] was adapted (Fig. 4.2 A). In this mouse

model, tandem ligations were introduced with 150 µm stenotic diameter with the distal point 1 mm away from the CCA bifurcation and the proximal one 3 mm from the distal ligation. 4 w after TS induction, *in vivo* MRI TOF sequences of CCA further confirmed that TS ligation was successfully induced (Fig. 4.2 B).

Dynamic change of blood flow plays a key role in development and progression of atherosclerosis. In order to clarify the hemodynamically change after TS, Doppler ultrasound was performed before and weekly after TS surgery on CCA for 4 weeks (Fig. 4.2 C). As it shown in Pulse-wave mode, both peak systolic velocity (PSV) and end diastolic velocity (EDV) decreased in the middle of the ligation after TS when compared with before, where caused blood turbulence and low wall shear stress between the two ligations[128] (Fig. 4.2 D, E). Lowered shear stress and disturbed blood flow have been related to endothelial dysfunction, leukocytes infiltration, macrophage accumulation in the intima and the initiation of aroma[138, 139]. Additionally, TS results in robustly increase of both PSV as well as EDV at the site close to ligation where high tensile stress is induced (Fig. 4.2 F). Higher tensile stress is an essential factor for vulnerable plaques due to it has been correlated with the prevalence of plaque rupture in proximal coronary arteries compared with the periphery coronary arteries[140]. Furthermore, systemically examining the blood flow on CCA after TS surgery, TS ligation leads to persistent hemodynamically change on ipsilateral CCA while the contralateral remains unaffected (Fig. 4.2 G, H).

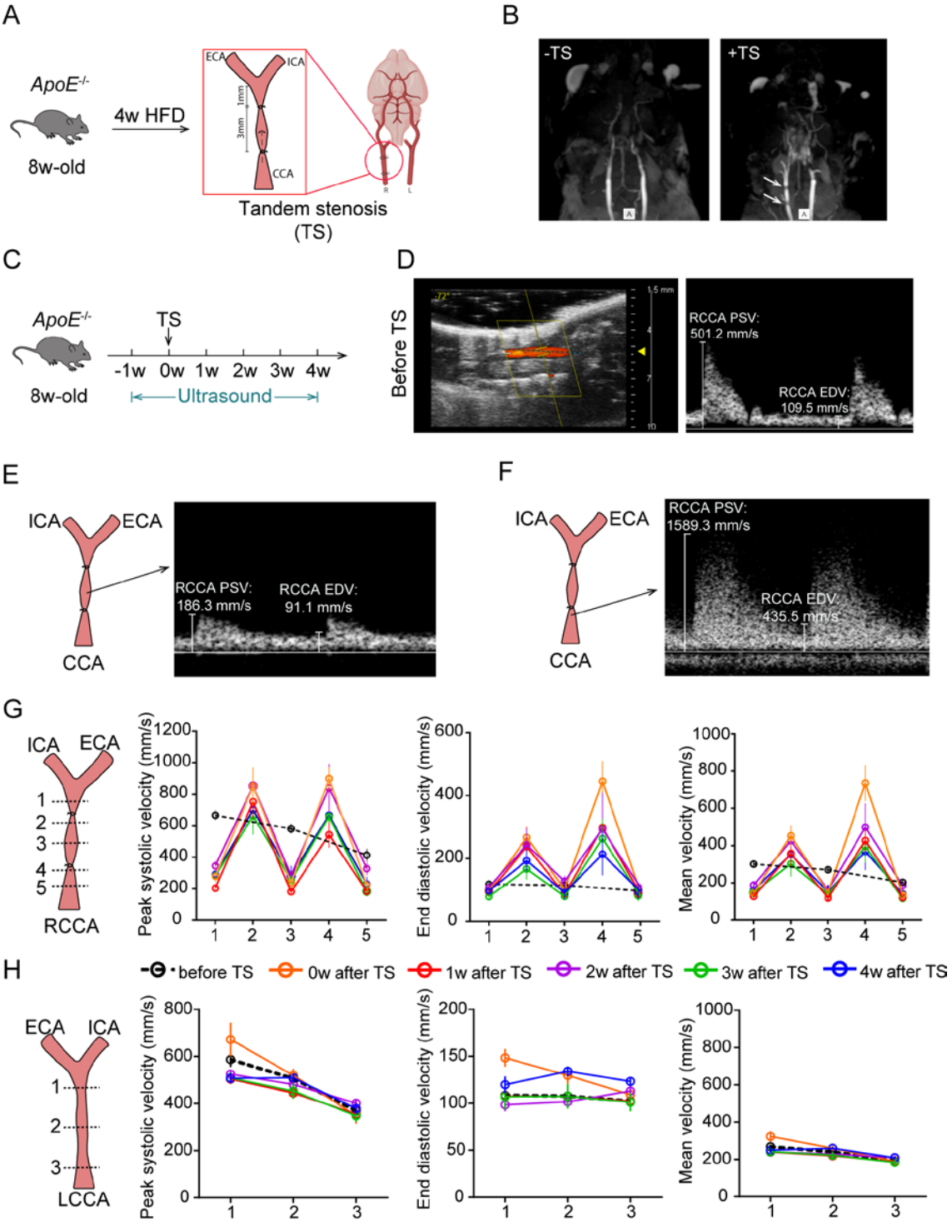

Figure 4.2 Characterization of the tandem stenosis model. (A) Schematic illustration of the tandem stenosis (TS) model for induction of vulnerable atherosclerotic plaques: 8w-old HFD fed *ApoE*$^{-/-}$ mice received TS surgery on the right common carotid artery (RCCA). Mice are then fed with high fat diet for an additional 4 w. **(B)** Representative images of CCA MRI TOF sequence 4 w after mice receiving control or TS surgery. White arrows highlight the two ligations on the RCCA. **(C)** Schematic description of the experimental design for Doppler ultrasound performance. **(D)** Representative color mode (left) and pulse-wave mode (right) image of RCCA in the mouse before TS, imaged at proximal ligation at 40 MHz (left panel). Corresponding CCA velocity waveform

measured at proximal ligation location 4 w after TS surgery (right panel). PSV: peak systolic velocity, EDV: end diastolic velocity. **(E)** Schematic description of location for blood flow measurement on the right CCA (ICA: internal carotid artery; ECA: external carotid artery; RCCA: right common carotid artery, left panel). Arrow indicates the site between the two ligations. Corresponding CCA velocity waveform measured at the site between two ligations (right panel). **(F)** Schematic description of location for blood flow measurement on the right CCA. Arrow indicates the site close to proximal ligation. Corresponding CCA velocity waveform measured at the site close to the proximal ligation (right panel). **(G)** Schematic illustration of locations for blood flow measurement on RCCA (left panel). 1 represents the site above the distal ligation; 2 indicates the area close to the distal ligation; 3 indicates the area between the two ligations; 4 represents the site close to the proximal ligation; 5 indicate the area below the proximal ligation. Corresponding quantification for PSV, EDV and mean velocity (MV, MV= (PSV+2*EDV) / 3) at RCCA before and 4 w after TS surgery (right). Data were shown as mean ± standard error of the mean (SEM). **(H)** Schematic illustration of locations for blood flow measurement on LCCA (left panel). 1 indicates the site close to CCA bifurcation; 2 represents the area in the middle of CCA; 3 indicates the area at the beginning of CCA. Corresponding quantification for PSV, EDV and MV at LCCA before and 4 w after TS surgery (right). Data were shown as mean ± standard error of the mean (SEM).

4.3 Plaques morphological phenotype on CCA in TS model

In order to evaluate the impact of TS on CCA in a morphological level, *ApoE*$^{-/-}$ mice were sacrificed 4 w after TS surgery, and both CCAs were isolated and collected for histological analysis. H&E staining showed that 4 w after TS surgery, complex plaque formation with the typical indicators for instability —necrotic cores and fibrous cap thinning —are found in ipsilateral CCA (+TS) but not on the contralateral side (-TS) (Fig. 4.3 A). To better characterize plaques morphological phenotype, key parameters including necrotic core area, collagen content, smooth muscle cell actin (SMA) and macrophage content of plaques were quantified in histological analysis. Larger necrotic core and higher macrophage content were related to more vulnerable plaque, while higher content of SMA and collagen suggest the plaque is more stable[134]. Whole CCA were processed and divided into 5 parts for histological quantification based on two ligations as introduced in –‘section’– 4.2. Detailed measurements of necrotic core, collagen content, SMA and macrophage content of plaques are described in –‘section’– 3.2.10.

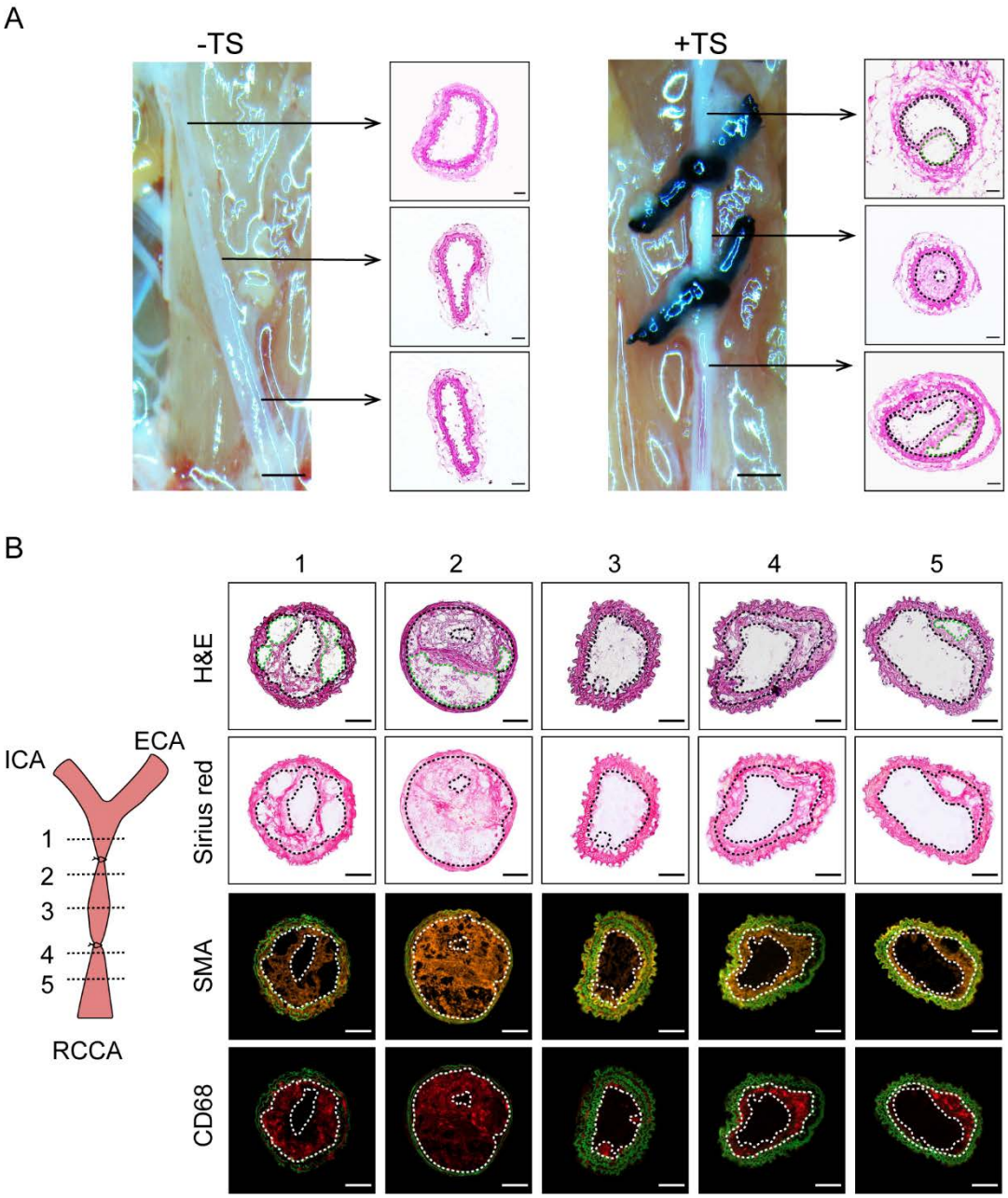

Figure 4.3 Histological characterization of atherosclerotic plaques. (A) Representative photograph of the CCA anatomy and corresponding H&E staining for each vessel segment 4 w after TS surgery of both CCAs (-TS represents contralateral (left) CCA without TS ligation; +TS represents ipsilateral (right) CCA with TS ligation, scale bar = 100 µm; H&E staining, scale bar = 50µm). **(B)** Schematic illustration of CCA with TS. Dotted lines indicate the location of sections analyzed in the study. (The area between two dash lines represents the intima area; the area of green dotted line represents the necrotic area; Scale bar = 50 µm).

4.4 Ischemic events induce recurrent ischemia as well as atherosclerotic plaque rupture

4.4.1 Ischemic stroke induces early recurrent events

Next, the TS model was used to test the effect of acute ischemic stroke, induced in the brain hemisphere contralateral to the CCA TS on atherosclerotic plaque morphology and potential rupture (Fig. 4.4 A). The occurrence of secondary ischemic events in the contralateral brain hemisphere (supplied by the stenotic atherosclerotic CCA) was screened by MRI and histological analysis of cell loss (Fluoro Jade C and TUNEL staining) and microgliosis (Fig. 4.4 B). A recurrent ischemia in the contralateral brain hemisphere, supplied by the atherosclerotic CCA, was defined through an MRI scan; with the histological analysis further verifying cell death and microgliosis in this area. Indeed, it showed that experimental stroke resulted in secondary brain ischemia in 30% of the animals, while no recurrent events were observed in any of the animals with CCA plaques but only sham surgery (Fig. 4.4 C). This observation suggests that stroke leads to rupture of the remote CCA plaque, leading to secondary recurrent stroke events. One of the most common causes inducing ischemic lesion is thrombi that originates from a ruptured atherosclerotic plaque[141]. To detect the possible thrombi to support this hypothesis, the intracerebral arteries stained with smooth muscle actin (SMA) was screened. An intravascular thrombus formation shown as platelet (CD41) and fibrinogen enrichment in the supplying anterior cerebral artery (ACA) was observed, corresponding to the contralateral secondary stroke territory (Fig. 4.4 D) — no thrombi were found in any of the sham-operated animals.

4.4.2 Ischemic stroke exacerbates atherosclerotic plaque vulnerability

In order to assess the atherosclerotic plaque vulnerability after ischemic stroke, the plaque vulnerability index was calculated by using the histological analysis from necrotic

core, SMA, collagen and macrophage staining (detailed calculation of plaque vulnerability index can be found in –'section'– 3.2.10). It suggested that necrotic core area shown by H&E staining was significantly increased in mice after experimental stroke (Fig. 4.5 A). As markers indicating plaque stability, the content of both SMA and collagen were found significantly decreased in stroke mice when compared to sham group (Fig. 4.5 B-C). Interestingly, macrophage content labeled by CD68 was observed significantly increased after primary stroke and even further elevated in the mice with recurrent ischemic lesion (Fig. 4.5 D). Plaque vulnerability index was found significantly increased in mice after experimental stroke and was even further exacerbated in mice with secondary ischemic events after the primary stroke (Fig. 4.5 E).

Plaque rupture is one of the most important pathological factors leading to ischemic stroke and myocardial infarction[141]. A ruptured plaque is characterized with discontinuous endothelial or disrupted fibrous cap[142]. With the aim of analyzing atherosclerotic fibrous cap continuity, CCA sections from sham or stroke-operated mice were stained by H&E and systemically screened. In order to evaluate the endothelial continuity, CCA sections of both sham or stroke-operated mice were further confirmed by endothelium marker (CD31) and von Willebrand factor immunofluorescence labeling. The disruption of endothelial in both H&E as well as immunofluorescence staining was defined as a ''ruptured plaque''. Direct morphological indication of plaque rupture was observed in 40% of mice after stroke but only 10% of mice undergoing sham surgery (Fig. 4.5 F).

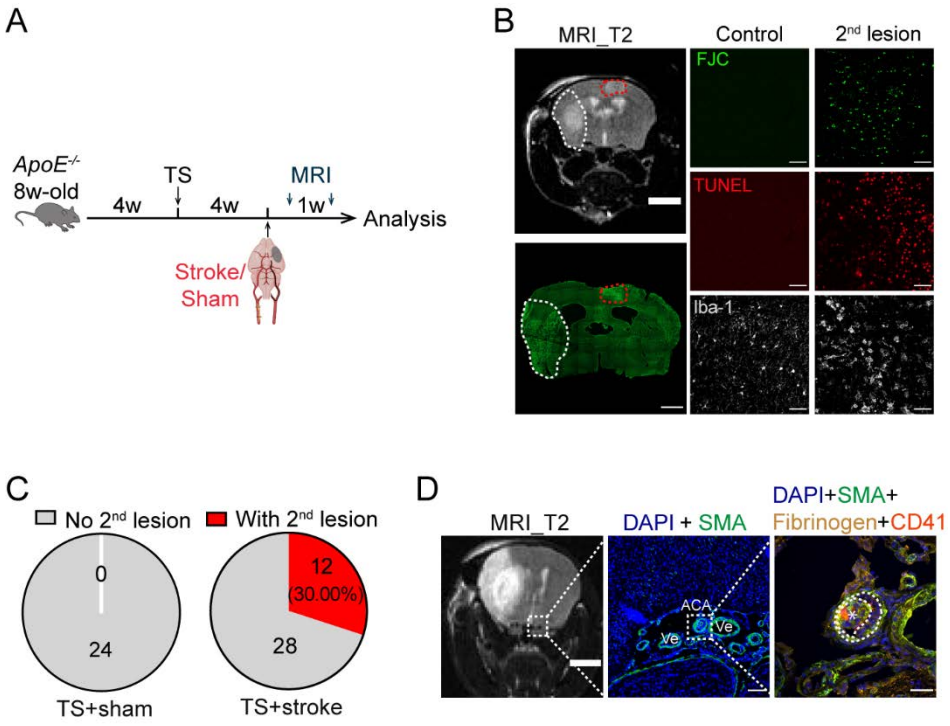

Figure 4.4 Stroke induces early atherosclerotic ischemia. (A) Experimental design: 8-week-old Apolipoprotein E-deficient mice fed a high cholesterol diet (HCD-fed *ApoE*$^{-/-}$) underwent tandem stenosis (TS) surgery. Subsequently, these mice undergo an experimental ischemic stroke or sham surgery 4 weeks after TS. The recurrence of secondary ischemia in the contralateral hemisphere was examined by MRI on days 2 and 7 after stroke. Mice were sacrificed 1 w after sham or stroke surgery. **(B)** Representative images of recurrent stroke. The upper left panel shows the representative MRI T2 sequence image (scale bar = 3 mm). The white dash line represents the primary stroke area. The red dotted line in the contralateral cortex represents the secondary, recurrent infarct. The lower left panel shows Fluoro Jade C (FJC) staining corresponding with the MRI (scale bar = 3 mm). The second column shows representative images of histological stainings (FJC, TUNEL, Iba-1) from control mice. The right column shows representative images from mice with a secondary lesion. FJC represents degenerative neurons (green), terminal deoxynuceotidyl transferase dUTP nick end labelling (TUNEL) represents apoptotic cells (red) and Iba-1 represents activated microglia (grey) (scale bar =50 µm). **(C)** Pie charts illustrate stroke recurrence rate 1 w after sham or stroke surgery (sham: n= 24, stroke: n= 40; red, with secondary lesion; grey, without secondary lesion). **(D)** Representative images of a thrombus found in the anterior cerebral artery (ACA). Ve = venules. * indicates the thrombus within the ACA (left scale bar = 3 mm; middle scale bar = 100 µm; right scale bar = 30 µm).

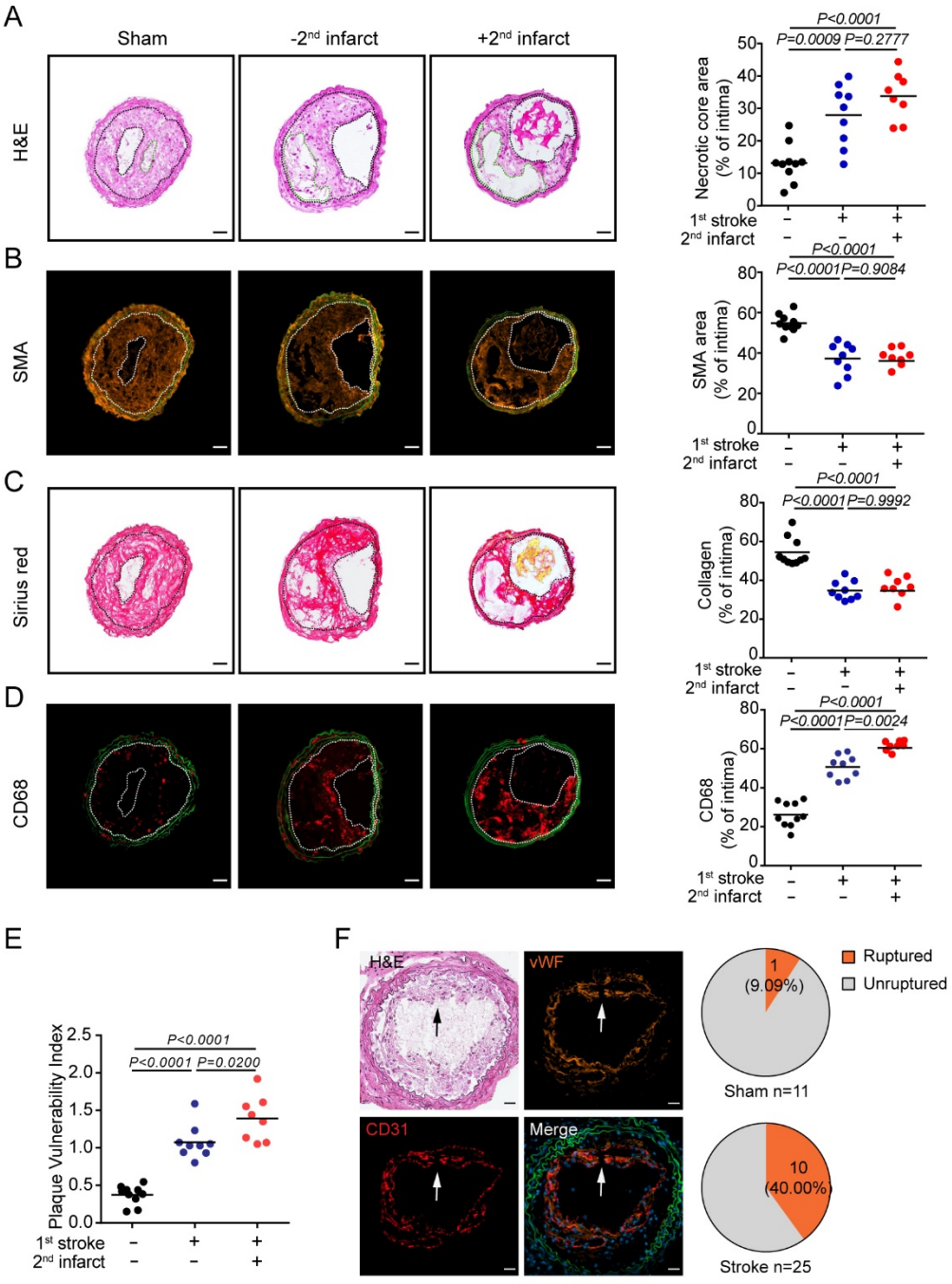

Figure 4.5 Stroke leads to atherosclerotic plaque rupture. (A) Representative microphotographs of CCA H&E staining (scale bar = 50 µm). Area between two black dotted lines represents intima. Green dotted lines represent necrotic cores. Necrotic core area was quantified as the percentage of total intima area (ANOVA, n = 8-10 per group). **(B)** Representative microphotographs of smooth muscle actin (SMA) immunofluorescence staining (scale bar = 50 µm). Area between two white dotted lines represent intima. SMA area was quantified as the percentage of total intima area (ANOVA, n = 8-10 per group). **(C)** Representative microphotographs of picro sirius red staining (scale bar = 50 µm). Collagen area was quantified as the percentage of total intima area. Area between two black dotted lines represent intima (ordinary one-way ANOVA test, n = 8 -10 per group). **(D)** Representative microphotographs of CD68 immunofluorescence staining

(scale bar = 50 µm). Images were segmented by thresholding to convert fluorescence signal into a binary image. Area between two white dotted lines represent intima. CD68 area was quantified as the percentage of total intima area (ordinary one-way ANOVA test, n = 8-10 per group). **(E)** Quantification of plaque vulnerability in CCA sections 1 w after sham or stroke surgery (black: sham; blue: stroke without secondary lesion; red: stroke with secondary lesion, ordinary one-way ANOVA test, n= 8 to 10 per group). **(F)** Representative microphotographs of ruptured plaque 1 w after stroke (left, scale bar = 50 µm). White arrows indicate a disrupted fibrous cap in lesion. The pie charts illustrate the proportion of mice with ruptured CCA plaques 1 w after sham or stroke surgery (orange: ruptured; grey: not ruptured; sham, n = 11; stroke, n = 25).

4.5 Ischemic stroke increases vascular inflammation

Following the evidence of increased macrophage content in the atherosclerotic CCA after stroke, we probed whether the stroke-induced plaque vulnerability was associated with vascular inflammation, and consequently, flow cytometry analysis of whole-CCA cell suspensions was performed. The analysis of CCA plaques revealed overall increased leukocyte ($CD45^+$) counts after stroke in comparison to sham surgery. More specifically, monocytes counts ($CD45^+CD11b^+$), in particular the number of inflammatory monocytes ($CD45^+CD11b^+Ly6C^{high}CCR2^+$), and macrophages ($CD45^+CD11b^+MHCII^+F4/80^+$) were significantly increased in atherosclerotic CCA plaques after stroke compared to sham (Fig. 4.6 A-B).

Next, we sought to investigate whether increased immune cellularity was due to either *de novo* invasion or local macrophage proliferation. To measure immune cells invasion in CCA plaque after stroke, *ApoE*$^{-/-}$ mice were intravenously injected by 3 µg CD45 antibody (leukocytes surface marker) conjugated with eF450 right before sham or stroke surgery. 24 h after surgery, to exclude the blood contamination, 3 µg CD45 antibody conjugated with APC Cy7 was intravenously injected 3 min before the mice were sacrificed (Fig. 4.6 C). Flow cytometry analysis of whole-CCA cell suspension indicated that stroke induced significant leukocytes infiltration in CCA plaque. Precisely, both $CD11b^+Ly6C^{high}$ and $CD11b^+CCR2^+$ population, known as pro-inflammatory monocytes, were significantly increased 24 h after stroke compared to sham (Fig. 4.6 D). With the

aim of examining local macrophage proliferation, CCA sections of 7 d after sham or stroke operated mice were labeled with macrophage marker (CD68) and proliferation marker (Ki67). Interestingly, local macrophage proliferation was observed significantly increased in stroke mice when compared to sham, and the local proliferation rate was associated with the occurrence of recurrent events (Fig. 4.6 E).

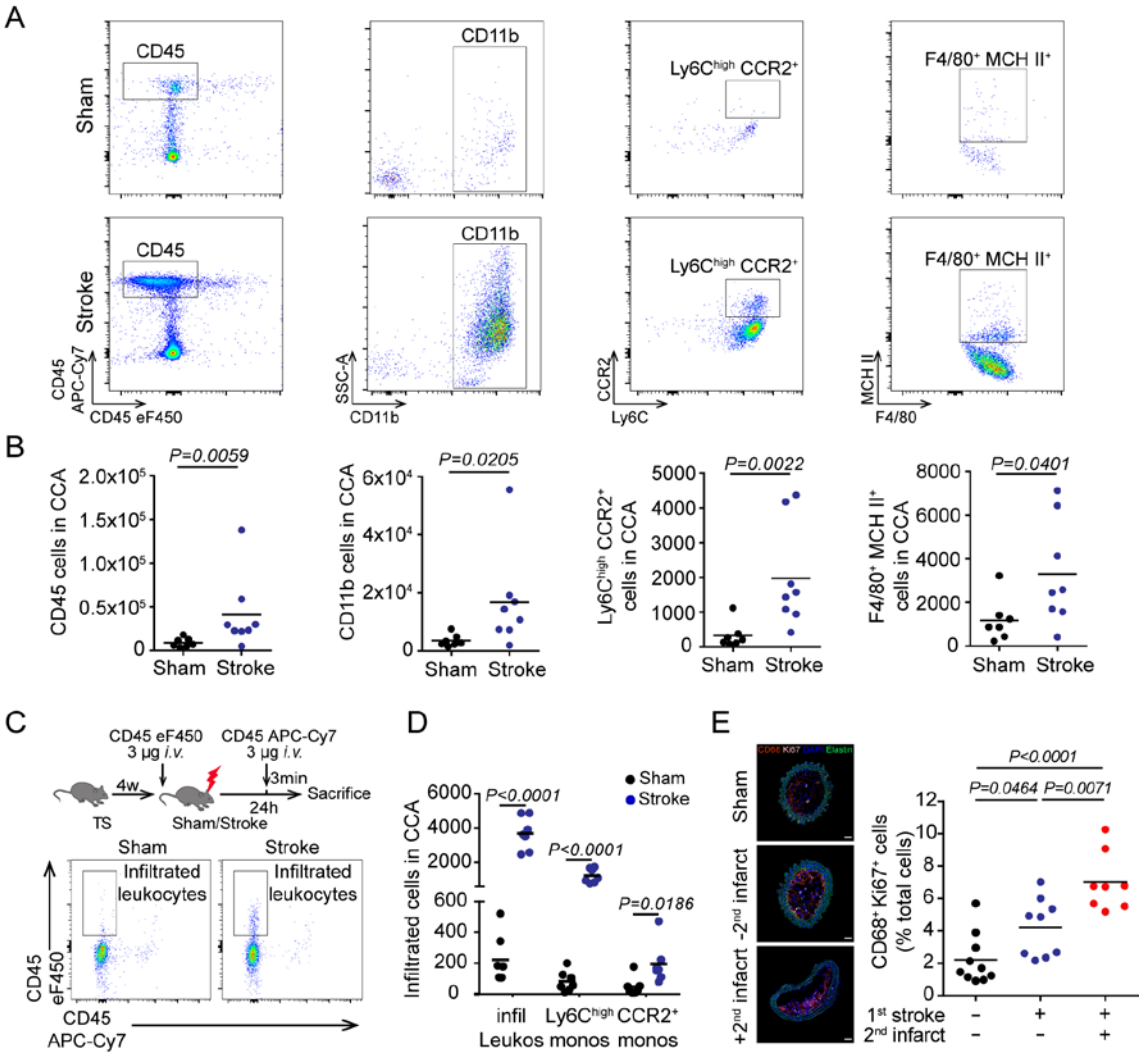

Figure 4.6 Post-stroke plaque vulnerability accompanied with vascular inflammation. (A) Representative gating strategy for flow cytometry analysis of whole CCA cell suspensions 24 h after sham or stroke surgery. (B) Flow cytometry analysis of CCA cell suspensions showing total leukocytes (CD45$^+$), monocytes (CD11b$^+$), pro-inflammatory subset (Ly6C^{high} CCR2$^+$) and macrophages (F4/80 MHCII$^+$) cell counts after experimental stroke compared to sham (U test, n = 7-8 per group). **(C)** Schematic illustration of experimental design for data shown in (D): HCD-fed *ApoE*$^{-/-}$ mice with TS received 3 µg anti-mouse CD45 eFluor 450 intravenously immediately before sham or stroke surgery. 24 h later these mice were intravenously injected with 3 µg anti-mouse CD45 APC-Cy7 3 min before sacrifice for exclusion of blood contamination in the FACS analysis. Representative gating strategy for infiltrated leukocytes (CD45 eFluor 450$^+$, CD45 APC-Cy7$^-$) in

CCA 24 h after sham or stroke surgery. **(D)** Quantification of infiltrated leukocyte counts for Ly6C^{high} monocytes and CCR2^{+} monocytes in CCA 24 h after sham or stroke surgery (black: sham; blue: stroke; multiple t-test, n = 7 per group). **(E)** Representative images of immunofluorescence staining for CD68 and Ki67 in CCA sections for detection of macrophage proliferation 1 w after sham or stroke with/without secondary lesion (left). Corresponding quantification of proliferating macrophages normalized to total cell count (right; black: sham; blue: stroke without secondary lesion; red: stroke with secondary lesion, ordinary one-way ANOVA, n = 8 to 10 per group).

4.6 Stroke leads to inflammasome activation in atherosclerotic plaque

It has been previously reported that the pro-inflammatory cytokine —interleukin (IL)-1β —was detected as the most abundantly upregulated cytokine in the circulation of mice after acute stroke[57]. IL-1β is mainly released by myeloid cells and is one of the main products of the inflammasome cascade[143]. The inflammasome contains multiple proteins, which can be triggered by a variety of signals, including microbial ligands and cholesterol crystals[143]. Upon sensing the signal, pattern recognition receptor assembles an ASC-caspase-1 inflammasome, which ultimately activates IL-1β[143]. Here, the increase of IL-1β concentration in mice serum 24 h after experimental stroke was confirmed by Enzyme Linked Immunosorbent Assay (ELISA) (Fig 4.7 A). Further analysis of the inflammatory milieu in the atherosclerotic plaque after stroke revealed a substantial increase in local IL-1β production, suggesting inflammasome involvement and active IL-1β secretion in atherosclerotic plaque after stroke (Fig. 4.7 B). The local inflammasome activation was then confirmed by western blot analyses of the inflammasome cascade including the hallmark proteins ASC, cleavage forms of caspase-1 and the preform of IL-1β (Fig. 4.7 C-G). Additionally, caspase-1 cleavage — the effector enzyme of the inflammasome — in the atherosclerotic plaque was independently verified by histological analysis showing an increased caspase-1 expression in CCA plaques after stroke (Fig. 4.7 H-I).

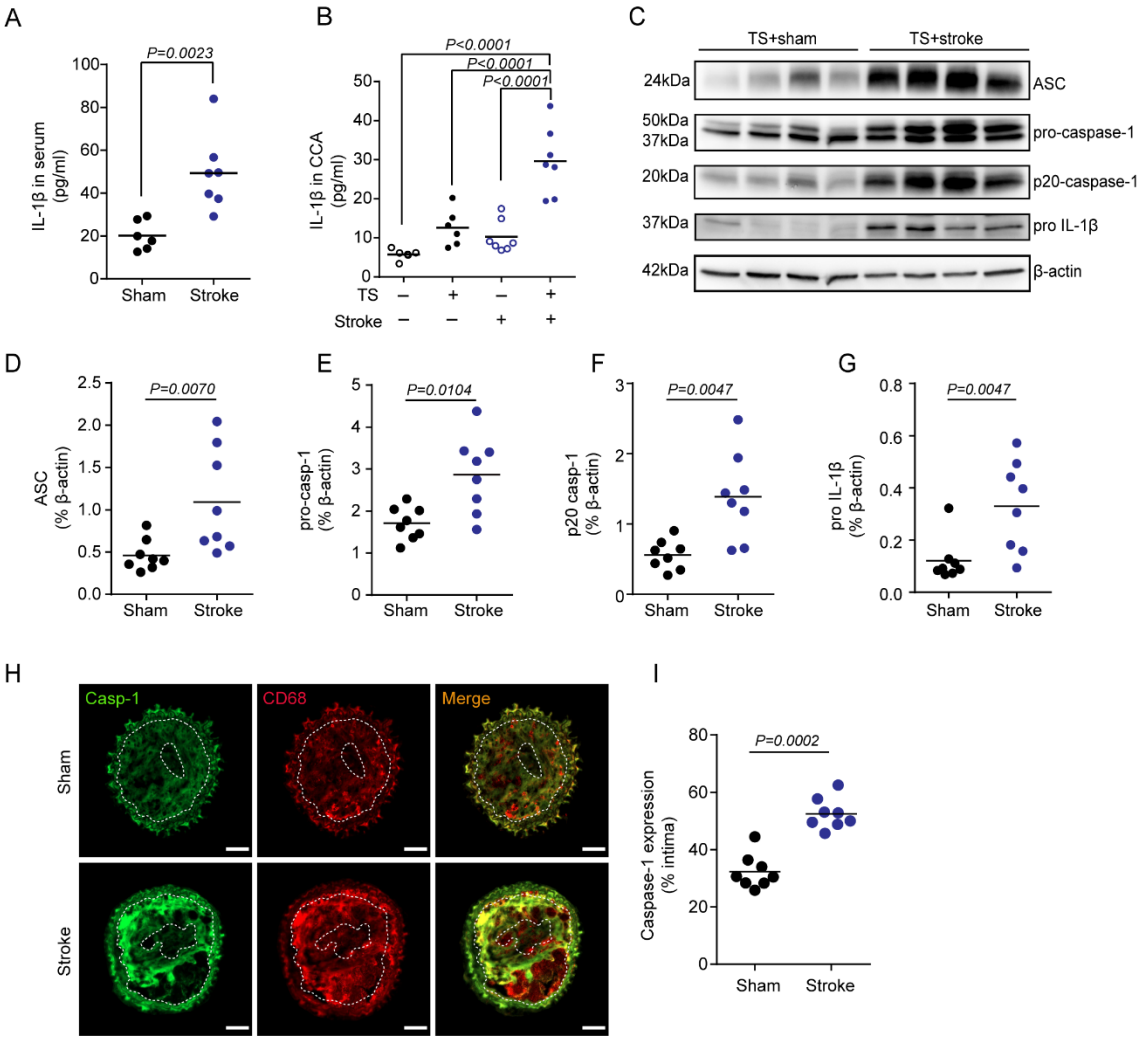

Figure 4.7 Post-stroke inflammasome activation within atherosclerotic plaques. (A) ELISA analysis of IL-1β concentrations in murine serum 24 h after sham or stroke surgery (U test, n = 6-7 per group). **(B)** ELISA analysis of IL-1β concentrations in murine CCA lysates 24 h after sham or stroke surgery (ANOVA, n= 6-7 per group). **(C)** Representative immunoblot of different proteins in inflammasome cascade from CCA lysates with TS 1 w after sham or stroke surgery. **(D-G)** Quantification of proteins in inflammasome cascade intensity normalized to β-actin (U test, n = 8 per group). **(H)** Representative immunofluorescence staining of caspase-1 (Casp-1) in CCA sections 1 w after sham or stroke surgery (scale bar = 50 µm). Images were segmented by thresholding to convert fluorescence signal into a binary image. Area between two white dotted lines represent intima. **(I)** Casp-1 expression was quantified as the percentage of total intima area (U test, n = 8 per group).

4.7 Pharmacological inflammasome inhibition attenuates plaque vulnerability as well as vascular inflammation

Since pronounced inflammasome activation was observed within atherosclerotic plaque after stroke, next, inflammasome activation was aimed to be blocked by a specific caspase-1 inhibitor (VX765). VX765 is a pro-drug which can be converted by plasma esterases into an active form, subsequently functions via covalent modification of the catalytic cysteine residue in the active site of caspase-1[144]. Thereby, it restrains caspase-1 activation and further antagonizes inflammasome assembling, as well as reduces the synthesis and release of downstream cytokines such as IL-1β and IL-18.

In order to block inflammasome activation after stroke, *ApoE*$^{-/-}$ mice were treated with VX765 at the dose of 100mg kg^{-1} 1 h before stroke surgery (Fig. 4.8 A). 7 d after surgery, immunofluorescent antibody staining of macrophages and cell proliferation indicated that pharmacological inflammasome blockage by VX765 prevented the proliferation of immune cells within the CCA plaque after stroke (Fig. 4.8 A). With the aim of tracking cell invasion to CCA plaques after VX765 treatment, circulating leukocytes were labeled by CD45 with eF450 conjugated antibody as previously described (see –'section'– 4.5) (Fig. 4.8 B). Flow cytometry analysis showed that VX765 treatment reduced leukocytes invasion, particularly inhibited the pro-inflammatory circulating monocytes (Fig. 4.8 C). The impact of inflammasome inhibition on atheroprogression after stroke was assessed by processing post-stroke CCA sections for histological analysis. A variety of key parameters were used to characterize plaque morphology, including necrotic core area, collagen content, macrophage content (CD68^{+} region), and smooth muscle cell content (SMA^{+} area). To evaluate plaque vulnerability, the vulnerability plaque index was calculated as shown previously (see –'section'– 4.2.2). Histological analysis suggested that inflammasome inhibition potently blocked the atheroprogression. Atherosclerotic plaques in mice treated with VX765 showed a tendency for a less necrotic core area (Fig. 4.8 D) and higher levels of SMA and collagen (Fig. 8 E, F). More strikingly, VX765 treatment

significantly reduced the macrophage content of atherosclerotic plaques and, overall, reduced the plaque vulnerability index after stroke to levels comparable to sham-operated mice, suggesting that the plaque is more stable (Fig. 4.8 G, H).

4.8 Post-stroke inflammasome activation within atherosclerotic plaques is DNA-dependent

Based on the previous observations, which specific inflammasome sensor mediates the effect of stroke on CCA plaque exacerbation needs to be further clarified. Here, two well-described inflammasome sensors AIM2 and NLRP3 in the context of atherosclerosis were considered[112, 123]. Moreover, it has been recently shown that stroke leads to systemic AIM2 inflammasome activation[57]. For pharmacological inhibition, specific inhibitors for NLRP3 (MCC-950)[145] and the AIM2 inflammasome (Calix[6]arene)[131] were used. Surprisingly, only the inhibition of the AIM2 but not of the NLRP3 inflammasome prevented inflammasome activation in the CCA plaque after stroke. This was seen in decreased CCA IL-1β levels and less pro- and cleaved caspase-1 in the Calix[6]arene-treated group (Fig. 4.9 A-C). Since dsDNA is the ligand of AIM2 inflammasome, the concentration of cell-free DNA in serum was analyzed. We observed that both total and dsDNA, not single-stranded DNA (ssDNA), were significantly increased in the blood 24 h after stroke (Fig. 4.9 D). The increase in circulating DNA levels suggests a broad release of cell-free DNA after stroke could be the mediator linking brain ischemia to the exacerbation of atherosclerotic plaque inflammation. To test whether cell-free DNA will induce plaque inflammation, mice with a CCA stenosis were challenged by intravenously injection of single bolus of cell-free DNA (5 µg per mouse). The DNA bolus was sufficient to detect elevated blood DNA levels in these mice (Fig. 4.9 E). Additionally, the DNA challenge led to plaque inflammasome activation, represented by increased CCA IL-1β levels (Fig. 4.9 F). Increased inflammasome activation was further confirmed via caspase-1 western blot, showing more pro- and cleaved caspase-1 after DNA challenge (Fig. 4.9 G, H). In

contrast, degradation of cell-free DNA after stroke by therapeutic administration of recombinant DNase I after stroke induction significantly reduced the plaque inflammasome activation. This was reflected by decreased caspase-1 cleavage and IL-1β secretion (Fig. 4.9 I, J). In summary, these data showed that the post-stroke AIM2 inflammasome activation in vulnerable atherosclerotic plaques by stroke-released DNA as the previously unrecognized cause of recurrent ischemic events due to inflammatory plaque rupture.

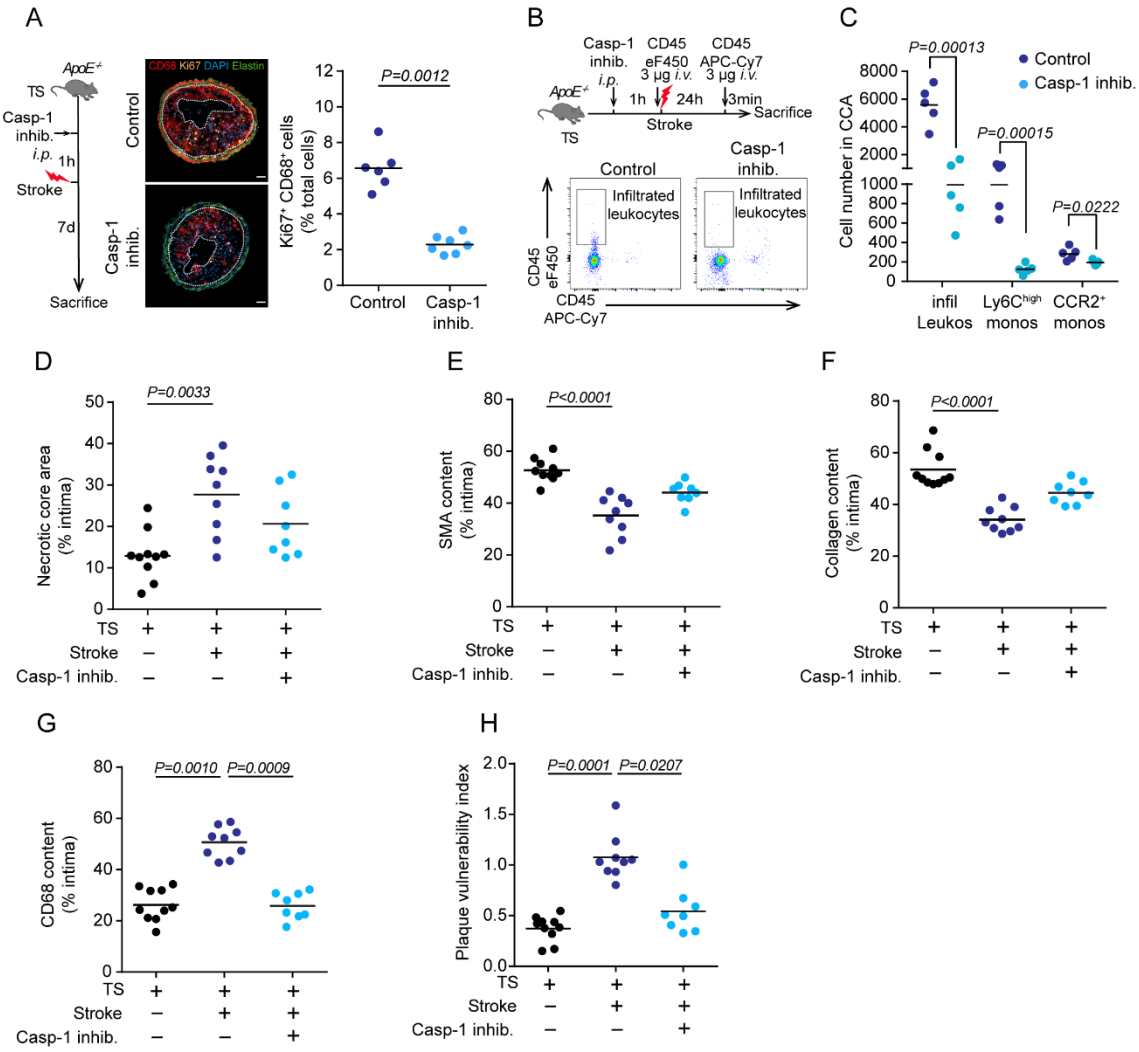

Figure 4.8 Post-stroke inflammasome inhibition attenuates vascular inflammation as well as plaque vulnerability. (A) Experimental design of post-stroke inflammasome inhibition (left panel): 4 w after TS surgery, *ApoE*$^{-/-}$ mice were intraperitoneally injected VX765 at the dose of 100mg kg^{-1} 1 h before stroke. Mice were sacrificed 7 d after stroke surgery. Representative images of immunofluorescence staining for the detection of macrophage proliferation (CD68^{+} Ki67^{+}) in CCA sections of control- or caspase-1 inhibitor (VX765)-treated mice 1 w after stroke (middle panel; scale bar = 50 µm). Corresponding quantification of proliferating macrophages normalized

to total cell counts (right panel; U test, n= 6-7 per group). **(B)** Schematic description of experimental design for data shown in (C): *ApoE*$^{-/-}$ mice with TS treated with VX765 1 h before stroke surgery. Immediately before stroke, mice received 3 µg anti-mouse CD45 eFluor 450 intravenously for circulating leukocytes labeling. 24 h later these mice were intravenously injected with 3 µg anti-mouse CD45 APC-Cy7 3 min before sacrifice for exclusion of blood contamination in the FACS analysis. Representative gating strategy for infiltrated leukocytes (CD45 eFluor 450^{+}, CD45 APC-Cy7^{-}) in control or VX765 treated CCA 24 h after stroke surgery. **(C)** Flow cytometry analysis of infiltrated leukocyte counts, corresponding to experimental paradigm in Fig. 4.8 B (dark blue: stroke control; light blue: stroke with caspase-1 inhibitor-treatment; t test, n=5 per group). **(D-G)** Quantification of necrotic core area, SMA, collagen and CD68 area 1 w after sham or stroke in the respective treatment groups (performed as shown in Fig. 4.5, ANOVA, n = 8-10 per group). **(H)** Quantification of plaque vulnerability of CCA sections in control or caspase-1 inhibitor-treated mice 1 week after stroke surgery (right, U test, n= 8 to 9 per group).

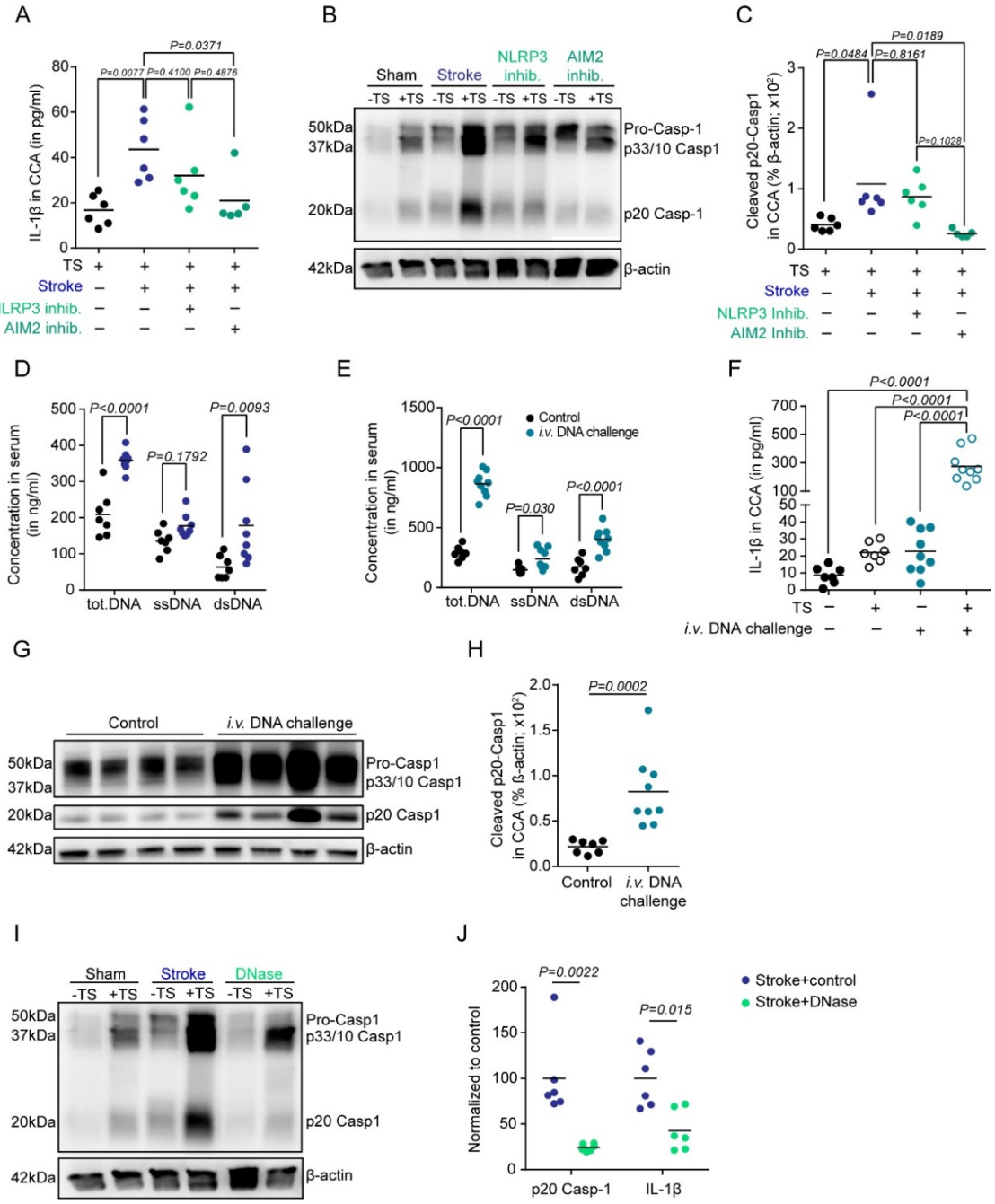

Figure 4.9 Post-stroke plaque inflammasome activation is cell-free DNA dependent. (A) ELISA analysis of IL-1β in CCA lysates from mice with tandem stenosis (TS), 24 hours after stroke in control-, NLRP3 inhibitor- (MCC-950) or AIM2 inhibitor- (4-sulfonic calix[6]arene) treated mice, and in sham operated mice (ANOVA, n = 5-6 per group). **(B)** Representative immunoblot micrograph of the different cleavage forms of caspase-1 (Casp-1) in CCA lysates 24 h after sham, stroke, stroke + NLRP3 inhibitor (MCC-950) or AIM2 inhibitor (4-sulfonic calix[6]arene) administration**. (C)** Corresponding immunoblot quantification of cleaved p20 Casp-1 intensity normalized to β-actin in CCA lysates with tandem stenosis (+TS) 24 h after sham, stroke, stroke + NLRP3 inhibitor or AIM2 inhibitor administration (black: sham; blue: stroke; light green: stroke + NLRP3 inhibitor; dark green: stroke+ AIM2 inhibitor; ordinary one-way ANOVA test, n= 5 to 6 per group). **(D)** Total cell-free DNA (tot.DNA), single-stranded DNA (ssDNA) and double-stranded DNA

(dsDNA) were measured in mice serum 24 h after sham or stroke surgery (black: sham; blue: stroke, U test, n= 7-8 per group). **(E)** Tot.DNA, ssDNA and dsDNA in mice serum were measured 24 h after control or *i.v.* DNA challenge (multiple t test, control, n = 7; DNA challenge, n = 9). **(F)** ELISA analysis for IL-1β in CCA lysates 24 hours after *i.v.* DNA challenge (black, control; blue, DNA challenge, ANOVA, n = 7-9 per group). **(G)** Representative immunoblot micrograph of the different cleavage forms of caspase-1 (Casp-1) in CCA lysates from HCD-fed *ApoE*$^{-/-}$ mice with TS surgery, 24 h after *i.v*. DNA challenge. **(H)** Corresponding quantification of cleaved p20 Casp-1 intensity normalized to β-actin in CCA lysates from HCD-fed *ApoE*$^{-/-}$ mice with TS surgery, 24 h after *i.v.* DNA challenge (U test, n = 7 to 9 per group). **(I)** HCD-fed *ApoE*$^{-/-}$ mice with TS surgery intravenously received 1000 U recombinant DNase (DNase) immediately before stroke. Mice were sacrificed 24 h after**.** Representative immunoblot micrograph of the different cleavage forms of caspase-1 (Casp-1) in CCA lysates 24 h after sham, stroke, stroke + DNase administration. **(J)** Cleaved p20 Casp-1 and IL-1β were quantified in CCA lysates by immunoblot (U test, n = 6). Data is shown as a ratio of the DNase treated group to the mean of the control group.

4.9 Stroke increases matrix metalloproteinase (MMP) activity within the atherosclerotic plaque

Previous findings revealed morphological features of atherosclerotic plaque destabilization after stroke, such as a necrotic core enlargement, increased plaque cellularity and thinned or ruptured fibrous cap. Moreover, also increased cellular inflammation within the atherosclerotic plaque—as observed here after stroke induction—is a conceivable factor that could lead to plaque rupture and secondary arterio-arterial embolism resulting in secondary infarctions. However, the interaction between local inflammation and plaque destabilization was so far not clarified in detail. Matrix metalloproteinases are able to degrade collagen and extracellular matrix (ECM) within atherosclerotic plaques[146]. Macrophages are the key source of MMPs secretion[147]. It has been shown that overproduction of MMPs by macrophages accelerate atherosclerotic plaque rupture and cause severe complications such as myocardial infarction and ischemic stroke[147]. Among different MMPs subforms, MMP2 and MMP9 have been shown to be important factors during atheroprogression[148]. A study discovered that upregulation of MMP2 and MMP9 expression correlate with atherosclerotic plaque vulnerability[149].

In order to detect MMP2/9 activity within the atherosclerotic plaque, CCA sections from sham or stroke operated mice were examined by *in situ* zymography. *In situ* zymography is used to reveal enzyme activity in tissue sections. Here, highly quenched, fluorescein-labeled gelatin was used as substrate. Upon proteolytic digestion, substrate yields bright, green fluorescence peptides which can be used to quantify MMP2/9 activity. *In situ* zymography of CCA plaque sections from stroke and sham operated mice with CCA stenosis discovered that stroke resulted in increased enzymatic activity of MMPs after stroke (Fig. 4.10 A). This was further validated by gel zymography for MMP2 and MMP9 subforms (Fig. 4.10 B, C).

To test whether soluble blood mediators are responsible to mediate this effect on MMP activity after stroke, bone-marrow derived macrophages (BMDM) were treated with serum obtained from mice 4 h after stroke or sham surgery (Fig. 4.10 D). BMDMs stimulated with serum from stroke mice resulted in massively increased active MMP2 and MMP9 secretion in comparison to sham serum treatment, both in total protein content (western blot) and enzymatic activity (zymography), suggesting a causative role of circulating factors after stroke on MMP expression and activation in the CCA plaque (Fig. 4.10 E-H). Since previous experiments demonstrated AIM2 inflammasome activation and IL-1β to be critical, the impact of IL-1β, here recombinant murine IL-1β, on MMP activity in BMDMs was tested. Quantitative real-time PCR detected indeed a dose-dependent effect of IL-1β on MMP 2&9 expression in BMDMs (Fig. 4.10 I,J).

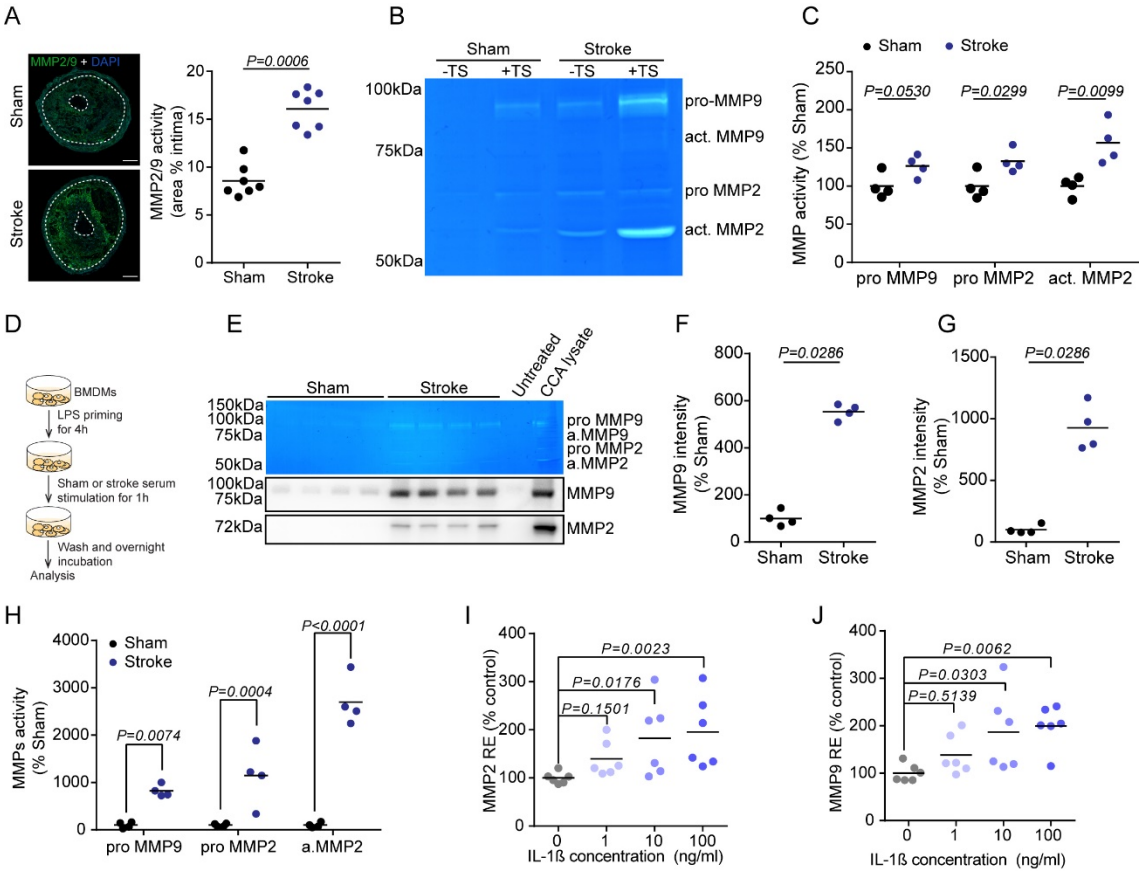

Figure 4.10 Stroke increases MMP activity within atherosclerotic plaques. (A) Representative images of in situ zymography on CCA sections for MMP2/9 activity 1 w after sham or stroke surgery revealing enzymatically active areas (left; scale bar = 50 µm). Quantification of MMP2/9 activity by enzymatically active area and normalized to the intima area (right; U test, n= 7 per group). **(B)** Representative images of gelatin zymography of CCA lysates for MMP activity in mice 1 week after sham or stroke surgery. The region of MMP activity appears as a clear band against dark blue background where the MMP has digested the gelatin substrate on the zymogram gel. **(C)** MMP activity shown in (B) was quantified as the gelatin digestion area 1 w after stroke surgery normalized to sham operated mice (multiple t test, n=4 per group). **(D)** Schematic experimental design: wild type (WT) bone marrow-derived macrophages (BMDMs) were stimulated with serum of mice after sham or stroke surgery, medium was then washed, and BMDMs cultured overnight in fresh medium. **(E)** Representative images of gelatin zymography (top) and immunoblot micrograph (bottom) of MMP9 and MMP2 in the culture medium. **(F, G)** Quantification of MMP9 and MMP2 intensity from immunoblot micrograph shown in (E) (normalized to sham stimulated, U test, n= 4 per group). **(H)** MMP activity shown in (E) was quantified as the gelatin digestion area in the stroke serum-stimulated medium normalized to sham serum-stimulated group (t test, n= 4 per group). **(I)** Relative expression (RE) of MMP2 expression in WT BMDMs after IL-1β stimulation was quantified as the percentage of the control group (H test, n= 6 per group). **(J)** Relative expression (RE) of MMP9 expression in WT BMDMs after IL-1β stimulation in increasing dose, data is presented as relative expression to control group (H test, n= 6 per group).

4.10 Stroke initiates the intrinsic coagulation cascade activation

While MMP-mediated degradation of the plaque extracellular matrix most probably contributes to plaque destabilization[150], the formation of the actual thrombus on the ruptured plaque is dependent on activation of the coagulation cascade, specifically by the contact activation pathway, initiated by Factor XII (F.XII) when exposed to injured tissue surfaces[151]. Therefore, *en face* staining of the whole CCA was performed and F.XII deposition on the luminal surface in the area of the CCA plaque was compared between stroke and sham operated mice. It showed a significant increase in F.XII deposition on the plaque surface after stroke (Fig. 4.11 A). The increase of activated F.XII (F.XIIa) was further confirmed by western blot analysis of whole CCA plaques (Fig. 4.11 B, C). Interestingly, an intravenous DNA challenge (as described before in –'section'– 4.8) fully mimicked the effect of stroke with significantly increased activated F.XII at the CCA plaque (Fig. 4.11 D, E). Taken together, these findings suggest that the AIM2 inflammasome activation and resulting IL-1β release after stroke lead to plaque destabilization and subsequently to atherothrombosis via activation of plaque-degrading MMPs and F.XII expression.

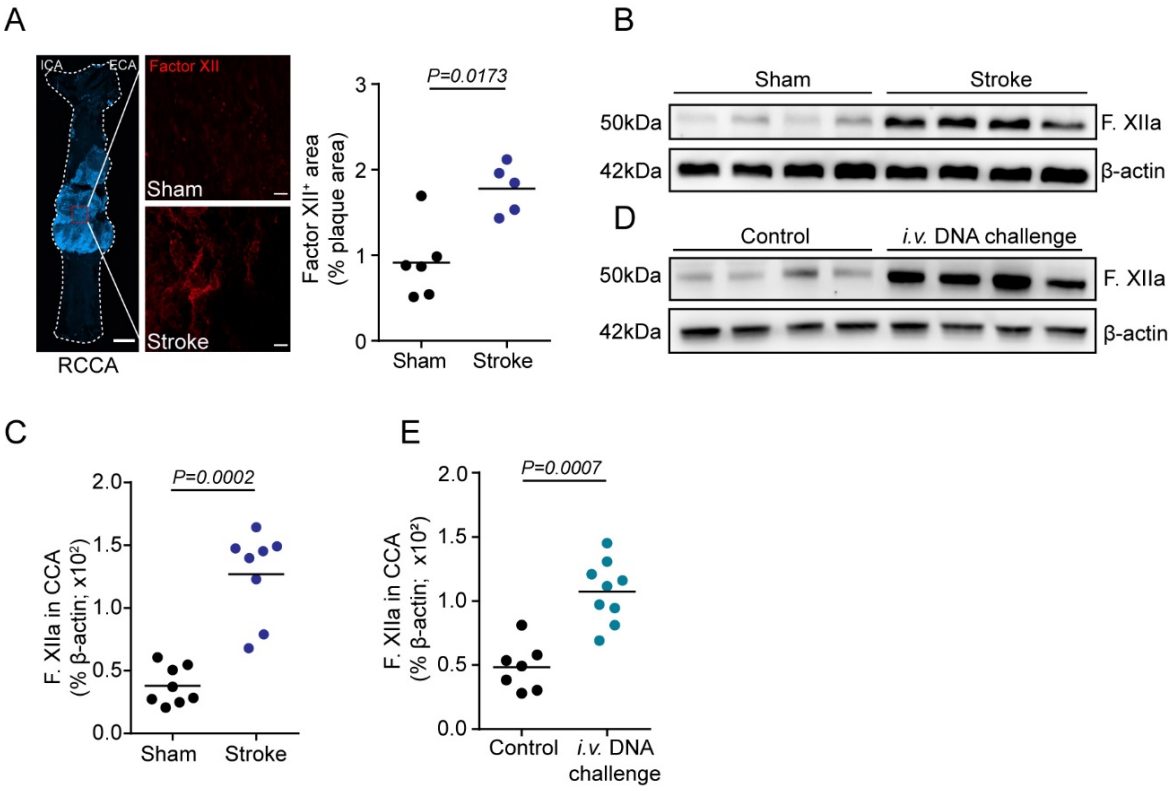

Figure 4.11 Stroke initiates intrinsic coagulation cascade activation. (A) Whole CCA *en face* immunofluorescence staining of Factor XII revealed intrinsic coagulation cascade activation on the CCA plaque 24 h after stroke but not sham surgery (left; overview scale bar = 500 µm, detailed images scale bar = 50 µm). Corresponding quantification of Factor XII^{+} area normalized to total plaque area (U test, n = 5 to 6 per group). All analyses were performed on CCA lysates in mice with stenotic CCA plaques after TS surgery in HFD fed *ApoE*$^{-/-}$ mice. **(B)** Representative immunoblot of activated Factor XII (F.XIIa) 1 w after stroke or sham surgery. **(C)** Quantification of activated FXII (F.XIIa) from immunoblot micrograph in (B) (U test, n= 8 per group). **(D)** Representative immunoblot micrograph of F.XIIa in CCA lysates 24 hours after *i.v*. DNA challenge. **(E)** Corresponding quantification of F.XIIa from immunoblot micrograph in (D) (U test, n = 7- 9 per group).

4.11 Inflammasome inhibition or cf-DNA neutralization reduces MMP activity and suppresses intrinsic coagulation cascade activation

Based on these observations, whether post-stroke MMP activity and F.XIIa deposition can be dampened by pharmacologically targeting inflammasome was further evaluated. With the aim of detecting MMP2/9 activity within the atherosclerotic plaque, post-stroke

CCA sections from control or caspase-1 inhibitor treated mice were assessed by *in situ* zymography. *In vivo* inflammasome inhibition using the caspase-1 inhibitor VX765 significantly reduced plaque MMP activity (Fig. 4.12 A). In addition, *en face* staining of the whole atherosclerotic CCA showed a significant reduction in F.XII deposition on the plaque surface after inflammasome inhibition (Fig. 4.12 B). Reduced level of activated F.XII in mice treated by inflammasome inhibitor was further confirmed by western blot analysis of whole CCA (Fig. 4.12 C, D). As the level of cell-free DNA increased in the blood after stroke, we then neutralized the cell-free DNA by treating the mice with DNase. Similarly, *i.v.* DNase treatment significantly reduced MMP activity and F.XIIa deposition (Fig. 4.12 E, F).

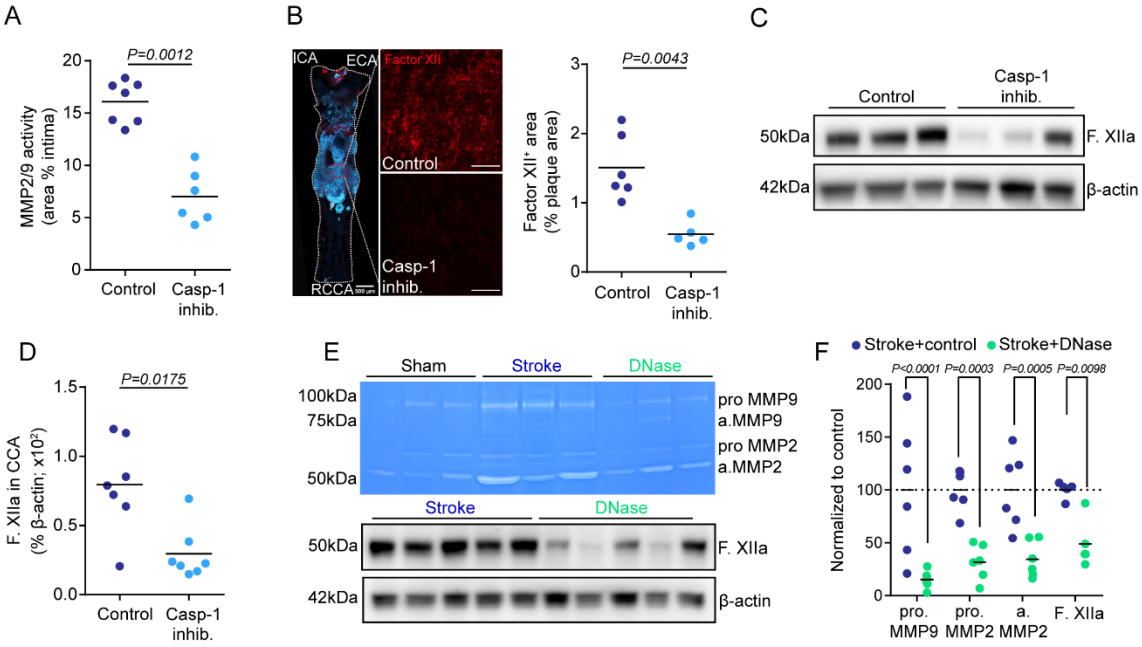

Figure 4.12 Inflammasome inhibition or cf-DNA neutralization dampens MMP activity and intrinsic coagulation cascade initiation. (A) Quantification of in situ zymography for MMP2/9 activity in CCA sections of control or caspase-1 inhibitor-treated mice 1 week after stroke (U test, n = 6 to 7 per group). **(B)** Whole CCA *en face* immunofluorescence staining of Factor XII in control or caspase-1 inhibitor-treated mice 1 w after stroke (left; overview scale bar = 500 µm, detailed images scale bar = 50 µm). Corresponding quantification of Factor XII intensity normalized to total plaque area (right; U test, n = 5 to 6 per group). **(C)** Representative immunoblot of the F.XIIa in CCA lysates 24 h after stroke in mice treated with control treatment or caspase-1 inhibition (VX765). **(D)** Corresponding quantification of F.XIIa intensity normalized to ß-actin in CCA lysates 1 w after stroke in control- or caspase-1 inhibitor- treated mice (U test, n = 7 per group). **(E)** Representative gelatin zymography of CCA lysates for MMP activity in mice 24 h after sham, stroke or stroke + DNase treatment (upper). Representative immunoblot of F.XIIa in +TS CCA

lysates 24 h after surgery (lower). **(F)** HCD-fed *ApoE*$^{-/-}$ mice with TS surgery intravenously received 1000 U recombinant DNase (DNase) prior to stroke, and 24 h after. ProMMP9, proMMP2, activated MMP2 (a.MMP2) and F.XIIa were quantified and normalized to control-treated mice after stroke (T test, n = 5-6 per group).

4.12 DNA-mediated inflammasome inhibition reduces early stroke recurrence

Finally, we investigated the possibility of using DNA-mediated inflammasome inhibition to prevent recurrent events. Therefore, mice with CCA stenosis were treated with caspase-1 inhibitor VX765 or recombinant DNase I as used in the above-described experiments, and the occurrence of secondary ischemic lesions was analyzed in the contralateral hemisphere to the primary, which was supplied by the stenotic CCA, 7 d after the primary stroke induction. Stroke recurrence was defined by brain MRI scan as well as histology analysis of brain sections for cell loss (FJC and TUNEL staining) (Fig. 4.13 A). Indeed, both caspase-1 inhibition and DNase I treatment reduced recurrence rate by 82% and 75%, respectively (Fig. 4.13 B). Notably, this therapeutic effect was consistently achieved in a large sample size of animals (stroke control, n=40; caspase-1 inhibition, n=37; DNase I, n=40; total sample size: 117 mice).

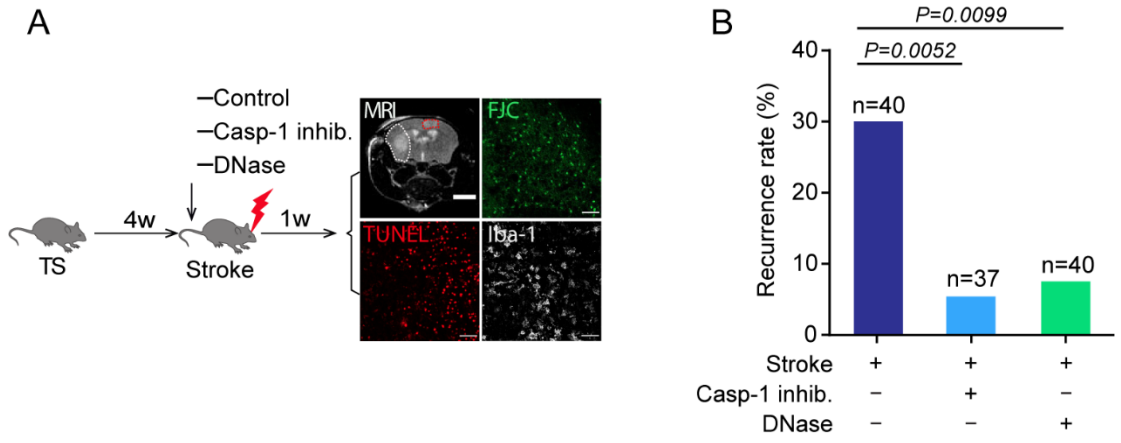

Figure 4.13 DNA-mediated inflammasome inhibition prevents recurrent events. (A) Schematic illustration of experimental design for therapeutic early recurrence prevention: HCD-fed *ApoE*$^{-/-}$ mice with TS received stroke surgery 4 w later. Control, caspase-1 inhibitor or DNase administration was compared for secondary lesion prevention. Secondary lesions were examined by MRI and histology (left). **(B)** Corresponding quantification of stroke recurrence rate in HCD-fed

ApoE$^{-/-}$ mice with TS 1 w after stroke surgery (right; chi-square test, control, n = 40, recurrence rate = 30%; stroke + caspase-1 inhibitor (VX765), n = 37, recurrence rate = 5.41%; stroke + DNase, n = 40, recurrence rather = 7.5%).

4.13 Plaque samples from stroke patients show higher level of vascular inflammation and MMP activity

To corroborate the translational relevance of the observed mechanism of post-stroke plaque rupture, we collected carotid endarterectomy samples from highly stenotic carotid artery plaques of asymptomatic patients and patients who are during the acute phase after ischemic stroke (Fig. 4.14 A). Carotid stenosis from stroke patients was defined as if cerebral ischemia occurred in the territory of the affected artery following standardized stroke diagnostics including cranial computed tomography (CT) and/or magnetic resonance (MR) imaging. Thirteen patients with stroke and seven patients with asymptomatic, high-grade carotid stenosis were recruited (detailed patients' information is provided in –'section'– 3.2.3). Flow cytometry analysis of the plaque material revealed a significant increase in monocyte counts in plaques from stroke patients as observed in the experimental model (Fig. 4.14 B), while blood monocyte and lymphocyte counts did not differ between groups (Fig. 4.14 C-E). Correspondingly, we found a significant increase in circulating cell-free DNA in blood of stroke compared to asymptomatic patients, as well as a substantial increase in inflammasome priming (pro-caspase-1 expression) and inflammasome activation (cleaved p20 isoform of caspase-1) (Fig. 4.14 F-I). Surprisingly, we detected a more than 10-fold increase in MMP9 activity by gel zymography of plaques from stroke in comparison to asymptomatic patients (Fig. 4.14 J, K). Finally, also the amount of plaque-associated F.XIIa was significantly increased in atherosclerotic plaques after stroke (Fig. 4.14 L, M). To sum up, the analysis of the human endarterectomy samples demonstrated that the DNA-mediated inflammasome activation, vascular inflammation, MMP activation and initiation of thrombus formation that were identified in the animal model were also observed in stroke patients.

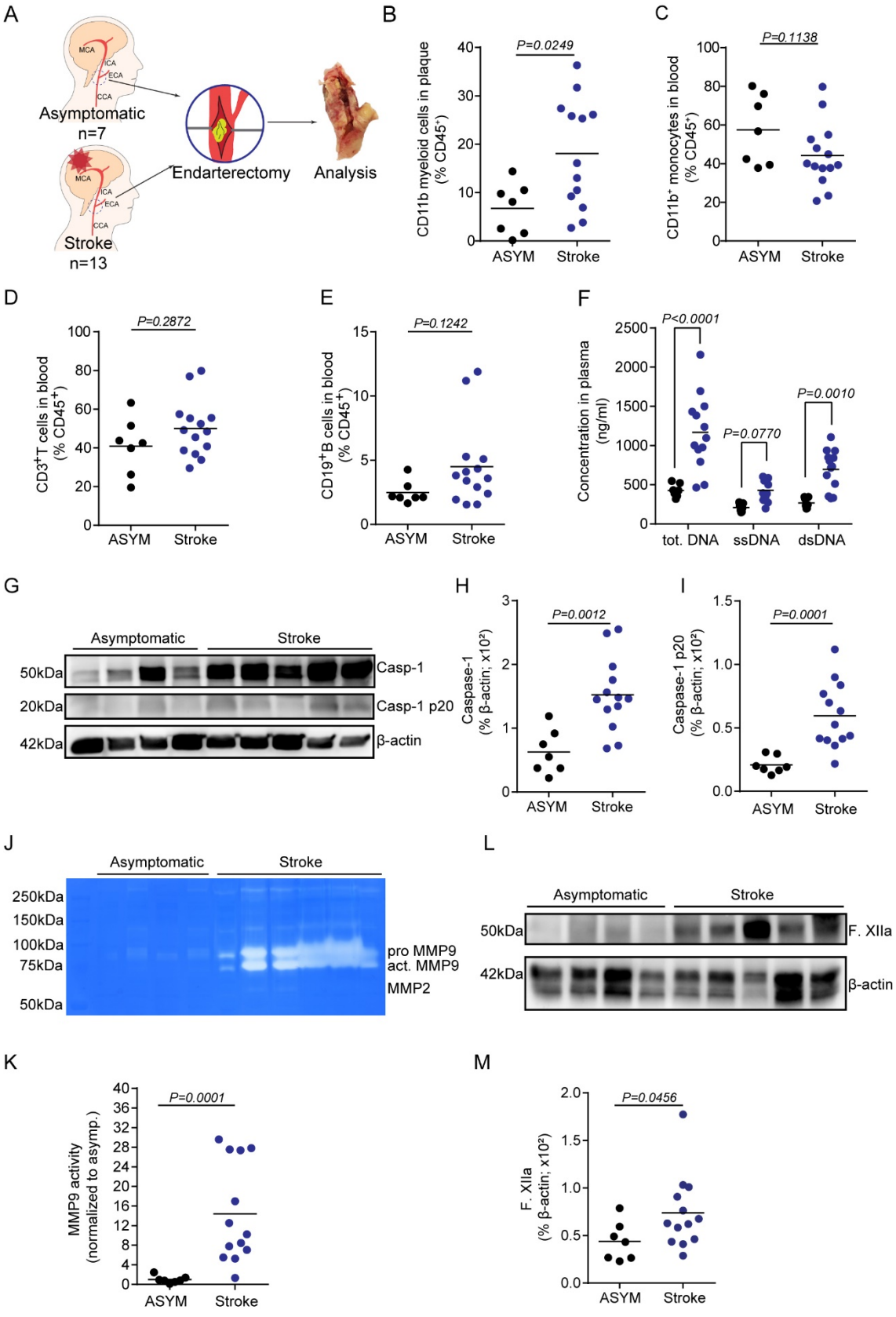

Figure 4.14 Plaque samples from stroke patients show exacerbated vascular inflammation as well as increased MMP activity. (A) Study layout illustrating collection of endarterectomy samples from 7 asymptomatic patients with internal carotid artery stenosis and from 13 stroke patients undergoing endarterectomy of the symptomatic carotid artery in the acute phase after

stroke. **(B)** Flow cytometry analysis of plaques showing the percentage of $CD11b^+$ myeloid cells out of total leukocytes ($CD45^+$). **(C-E)** Flow cytometry analysis of blood from asymptomatic patients or stroke patients showing the percentage of monocytes ($CD11b^+$), T cells ($CD3^+$) and B cells ($CD19^+$) out of total leukocytes ($CD45^+$) (U test, asymptomatic patients, n = 7; symptomatic patients, n = 13). **(F)** Quantification of total cell-free DNA (tot.DNA), single-stranded DNA (ssDNA) and double-stranded DNA (dsDNA) in plasma. **(G)** Representative immunoblot micrograph of the different cleavage forms of caspase-1 (Casp-1) in plaque lysates from asymptomatic or symptomatic patients and (**H, I**) the corresponding quantification of total Casp-1 and cleaved p20 Casp-1 intensity normalized to β-actin. **(J)** Representative image of gelatin zymography of plaque lysates from asymptomatic or symptomatic patients and (**K**) the corresponding quantification of MMP9 activity normalized to the activity in asymptomatic patients. (**L**) Representative immunoblot from asymptomatic and stroke patients for F.XIIa and (**M**) the corresponding quantification of F.XIIa intensity normalized to β-actin.

5. Discussion

5.1 Summary of results

Despite improvements of secondary prevention after stroke, early recurrent events remain a major challenge and impose global economic burden with an unmet need for efficient therapy. Patients with large artery atherosclerosis (LAA) have been shown to be at the greatest risk of suffering early recurrent stroke when compared to other stroke etiologies[14]. Early administration of aspirin has been recognized as a crucial intervention to prevent early stroke recurrence after TIA and minor stroke[152]. However, these studies did not evaluate the effect of aspirin for different stroke subtypes, thereby the effectiveness of early aspirin therapy in preventing early stroke recurrence in LAA patients needs to be carefully interpreted. Surgical atherosclerotic plaque removal (carotid endarterectomy) may prevent stroke recurrence, but is limited by a time window –surgery needs to be done less than 2 weeks after stroke onset[25]. These observations particularly emphasize the imperative need to investigate new therapeutic strategies to prevent early recurrent cardiovascular events.

In this study, an animal model of rupture-prone plaques of the carotid artery in combination with contralateral experimental stroke was developed to investigate the impact of ischemic stroke on atherosclerotic plaque rupture and subsequent recurrent events. Brain MRI scan and brain tissue histology analysis indicated that stroke induced recurrent ischemia in 30% *ApoE*$^{-/-}$ mice within the first week. Histology analysis of CCA identified that stroke increased macrophage amount and necrotic core area, as well as decreased smooth muscle cells and collagen content, which make the plaque more vulnerable. In addition, increased macrophage contents were due to not only increased local proliferation rate, but also higher number of pro-inflammatory monocytes recruitment. Further detailed experiments identified post-stroke inflammasome activation by cell-free DNA as initiator of an inflammatory cascade leading to atherosclerotic plaque degrada-

tion and thrombosis. Finally, *in vivo* neutralization of cell-free DNA or inhibition of downstream inflammasome activation is a highly efficient therapeutic approach to prevent early recurrent vascular events.

5.2 Clinical issues of recurrent stroke

Recurrent stroke is defined as a new stroke event occurring after the incident stroke[153]. Even with improved acute stroke management and intensive use of secondary prevention, population-based studies showed that approximately 30% of strokes are recurrent events which are more likely to be disabling than first strokes events[154]. Stroke recurrence rate remains debatable. The risk of recurrent stroke reaches a cumulative rate to 4.3% at 7 days[155], 4.9% to 12.9% at 90 days[156], 7.0% to 20.6% within the first year[22, 157,158], and from 16.2% to 35.5% over the first 5 years[22, 159]. As the risk of recurrent stroke differs from early to late stage after primary stroke, it is essential to determine the risk factors and clarify current clinical problems of treatments in each stage to establish optimal and effective therapeutic strategies for secondary stroke prevention.

5.2.1 Early recurrent stroke

Recurrent stroke that occurs within 90 days of a stroke onset are described as an early recurrent stroke[160]. Diverse etiologies and vascular mechanism underlying the subtype of stroke determines the symptoms, subsequent recovery and functional outcome. Therefore, a stroke subtype classification system according to The Trial of Org 10172 in Acute Stroke Treatment (TOAST) criteria has been widely used in clinic as well as research[10]. Large artery atherosclerosis (LAA) and cardioembolic (CE) stroke are the most frequently correlated with early recurrent stroke compared to the other subtypes[14, 161, 162]. However, previous investigations demonstrated that patients with minor stroke who have internal carotid artery stenosis had the highest risk of recurrent ischemic stroke within 90 days[14, 163], which indicates that LAA is an independent risk factor for early stroke recurrence.

A variety of treatments have been applied to reduce the residual cardiovascular risk including antiplatelet therapy, anticoagulant therapy, cholesterol lowering statin therapy, carotid endarterectomy, their combinations or other therapies[164, 165]. For patients with LAA, antiplatelet therapy alone might be not sufficient to prevent stroke recurrence[166]. Anticoagulant therapy has been identified to reduce stroke recurrence, pulmonary embolism, as well as deep vein thrombosis. However, its benefits were counteracted due to a high incidence of intracranial bleeding[167]. Consequently, anticoagulant therapy is not recommended in the early phase of acute ischemic stroke. Dual antiplatelet therapy has been suggested to be effective to lower stroke recurrence in several clinical studies[13, 23]. Nevertheless, these studies recruited all nonembolic ischemic stroke patients instead of LAA subtype only, thereby the efficiency of dual antiplatelet to prevent recurrent stroke for LAA patients needs to be carefully interpreted. The combination of aspirin and statin has been widely used in patients with LAA to prevent recurrent cardiovascular events. Both are effective in long-term progression of stroke comorbidities, but do not effectively target early recurrent cardiovascular events[22]. Carotid endarterectomy (CEA) is an other strategy to prevent recurrence, which has been performed for symptomatic patients with > 50% stenosis or asymptomatic with > 70%[168]. However, the optimal time window of CEA is controversial. It has been recommended that CEA needs to be performed within 2 weeks after stroke onset to reach its maximal benefit[25]. Paradoxically, CEA is associated with a high surgical risk in the first few days after stroke[169]. When CEA is performed within 14 days of stroke onset, the 30-day stroke and death rate is 7-fold higher than that of patients who undergo surgery after 14 days (7.1% vs 1.1%)[170].

5.2.2 Long term recurrent stroke

Risk factors of recurrent stroke in the chronic phase contain prevalent vascular risk factors (age, hypertension, diabetes, or smoking), embolic sources and causes (atrial fibrillation)[171-174]. Effective therapies established to prevent recurrent ischemic stroke long-term include antiplatelet therapy, anticoagulation and, cholesterol reduction. In addition,

anti-hypertensive medication has been proven to be associated with secondary stroke prevention[175].

Patients with ischemic stroke or TIA have been recommended to start antiplatelet therapy[176, 177]. As an agent for secondary stroke prevention, aspirin was found to be more effective than placebo in reducing any stroke by 17% (95% CI = 4%-28%) during long-term follow-up ranging from 1 to 6 years[177]. A dual antiplatelet therapy consists of aspirin and a P2Y12 inhibitor, such as clopidogrel. Dual antiplatelet therapy can effectively reduce recurrent stroke without increasing bleeding risk when initiated within 24 h after stroke onset and continued for a maximum of 90 days[178]. However, long-term use (more than 3 month) of aspirin combined with clopidogrel is not recommended, as it showed significant cumulative risk of bleeding[166, 179].

Anticoagulation therapy is highly recommended to patients with atrial fibrillation after ischemic stroke or TIA for secondary prevention[180, 181]. Nevertheless, the selection of an anticoagulant agent for patients need to be personalised based on renal and hepatic function, tolerability and other clinical characteristics[180].

Reducing low-density-lipoprotein cholesterol (LDL-C) concentration is the key component for the prevention of recurrent cardiovascular events. Clinical trials have been reported that statin therapy minimizes the stroke recurrence only in the group who achieved low LDL-C concentration (< 70 mg/dL) and low C-reactive protein (CRP, < 2 mg/L)[182, 183]. However, since statin also has an anti-inflammatory effect, it is difficult to clarify whether LDL-C reduction alone—in the absence of inflammation inhibition—was sufficient to lower recurrent stroke rates[182].

Apart from the preventions mentioned, blood-pressure lowering also effectively contributes to secondary prevention of stroke[175]. Irrespective of whether a patient had a prior history of hypertension, there was still a benefit, and a greater reduction in blood pressure was linked to a lower risk of a recurrent stroke[175]. However, in patients with severe

carotid stenosis, severe basilar or vertebral artery diseases, it is not advisable to drastically reduce blood pressure, as this could potentially lead to an increased risk of stroke[184]. According to the latest American Heart Association (AHA) guideline, a blood pressure of less than 130/80 mmHg is recommended for most patients to reduce the recurrent stroke risk and vascular events[185]. The effectiveness of medical treatment should be maximized by individualized medication regimens based on patient characteristics, pharmacological class, and patient preference[185].

5.3 Inflammatory risk after ischemic events

Immunological mechanisms have gained a wide attention in the context of current translational stroke research, and the intervention of neuroinflammatory pathways has been observed as a promising therapeutic strategy to reduce the pathophysiological consequences of brain ischemia[30-32]. However, stroke not only triggers local inflammatory response, but it also results in a profound systemic immune response[34]. Systemic post-stroke inflammation has been evaluated as an essential component in the acute and long-term prognosis of stroke patients[186, 187]. For instances, interleukin (IL)-6 or C-reactive protein levels that are elevated in the blood after stroke are correlated with a worse functional outcome and an increased mortality[186]. Consequently, targeting systemic inflammation after stroke has become a novel approach in translational research. Several clinical studies have been conducted aiming to modulate systemic inflammation to improve patients' functional disabilities, as well as prevent secondary comorbidities[188].

Cardiovascular comorbidities are the most common type after stroke, including atherosclerosis, arterial fibrillation, valvular heart disease and others[189, 190]. According to TOAST criteria, patients with LAA have the highest risk to suffer a recurrent stroke compared to other subtypes[14, 163]. Atherosclerosis is an established cardiovascular risk factor contributing to acute vascular events, including stroke[191]. There is solid evidence that inflammatory mechanisms play a key role both in the initiation and in development of

atherosclerosis in addition to lipid disturbances[192]. A number of steps in the pathophysiological process of atherosclerosis are mediated by inflammation, including the activation of endothelial cells[91, 93], the invasion of pro-inflammatory monocytes to the atherosclerotic lesion[95], the secretion of pro-inflammatory cytokines that further facilitate the infiltration of immune cells[96], the enrichment of macrophages and lipoprotein-containing foam cells, which further release more pro-inflammatory mediators[97, 98], and the apoptosis of macrophages and the formation of a necrotic plaque core[99, 101].

Early studies in mouse models of experimental myocardial infarction have already demonstrated that the systemic response after ischemic injury exacerbates chronic atherosclerosis[193]. More recently, there has been evidence that ischemic stroke aggregates atheroprogression[33]. Exacerbation of vascular inflammation has been observed to be related to the stroke-induced release of DAMP from the ischemic lesion. In the meantime, egress of monocytes from the bone marrow caused by sympathetic activation, thereby circulating alarmins from the ischemic lesion accelerated the activation and invasion of these monocytes into the atherosclerotic plaque[33, 61]. DAMP further enhance inflammation by activating more microglia and infiltrating leukocytes, thereby producing more pro-inflammatory cytokines[194]. These pro-inflammatory cytokines not modulate tissue damage, but they also contribute to peripheral immune response through their elevated levels in blood[57]. Both circulating and pro-inflammatory cytokines are known to accelerate the activation and invasion of circulating monocytes into the atherosclerotic plaques. For instance, IL-1β, one of the typical pro-inflammatory cytokines, has been reported to be involved in promoting leukocytes infiltration by upregulating the expression of leukocyte chemoattractant factors and adhesion molecules on endothelial cells from atherosclerotic aortas, increasing the supply of inflammatory leukocytes from bone marrow to the blood[118]. Indeed, anti- IL-1β treatment in atherosclerotic mice reduced total plaque volume and necrotic core size as well as vascular inflammation[118].

The CANTOS trial –testing the use of IL-1β-specific antibody (canakinumab) treatment in patients with previous myocardial infarction (MI) and evidence of inflammation (CRP

＞2 mg/L) –clearly highlighted the relevance of residual inflammatory risk and demonstrated the potential of anti-inflammatory therapies to prevent recurrent ischemic events[117]. These benefits were attributed to a lower systemic inflammatory response but did not interfere with other cardiovascular risk factors such as cholesterol or blood pressure levels. However, targeting this central cytokine of innate immune defense also significantly increased the risk of fatal infections[195]. Based on these findings, such immunomodulatory approaches should be used cautiously in patients with an increased susceptibility to infections, such as stroke patients.

Human pathological studies also support a strong correlation between plaque inflammation and clinical events, such as stroke. In the Oxford Plaque Study, carotid plaque samples from patients with symptomatic carotid stenosis were evaluated[196]. It showed that 66% of patients presented marked inflammation in the plaque from the ipsilateral carotid artery, whereas 64% showed other signs of plaque instability, including thin fibrous caps, large necrotic core, cap rupture or thrombus formation[196]. Furthermore, plaque inflammation may contribute to stroke recurrence. According to a previous study, endarterectomy was performed within 10 days in patients with ipsilateral carotid stenosis and TIA/ischemic stroke. Result showed that early stroke recurrence was associated with increased macrophage density and lymphocyte infiltration, decreased fibrous content, and cap rupture[197]. Interestingly, high macrophage content was the only independent factor of early stroke recurrence after age and degree of stenosis were ajusted[197]. There is, however, a lack of knowledge as to the specific immunological mechanisms by which stroke increases plaque inflammation and leads to destabilization, overall contributing to early stroke recurrence. Thus, this knowledge gap has prevented the development of more specific and consequently safer therapeutic approaches for stroke recurrence prevention.

5.4 Absent in melanoma 2 (AIM2) inflammasome

IL-1β is released mainly by myeloid cells and synthesized initially as a non-active precursor protein (pro IL-1β)[114]. The inflammasome, a multiple-protein complex located in the cytosol, can be activated by a variety of signals, such as microbial ligands, cholesterol crystals and monosodium urate crystals[114]. Once the inflammasome is assembled, caspase-1 –the effector enzyme in inflammasome cascade –can be activated, subsequently cleaving pro IL-1β into its active form[114]. Depending on the nature of pattern-recognition receptor (PRR) in response to pathogen-associated molecular patterns (PAMPs) or endogenous danger signals in the cytosol, inflammasomes can be differentiated as 4 main subtypes: nucleotide-binding oligomerization domain (NOD), leucine-rich repeat (LRR)-containing protein (NLR) family members including NLRP1, NLRP3 and NLRC4, as well as absent in melanoma 2 (AIM2)[143].

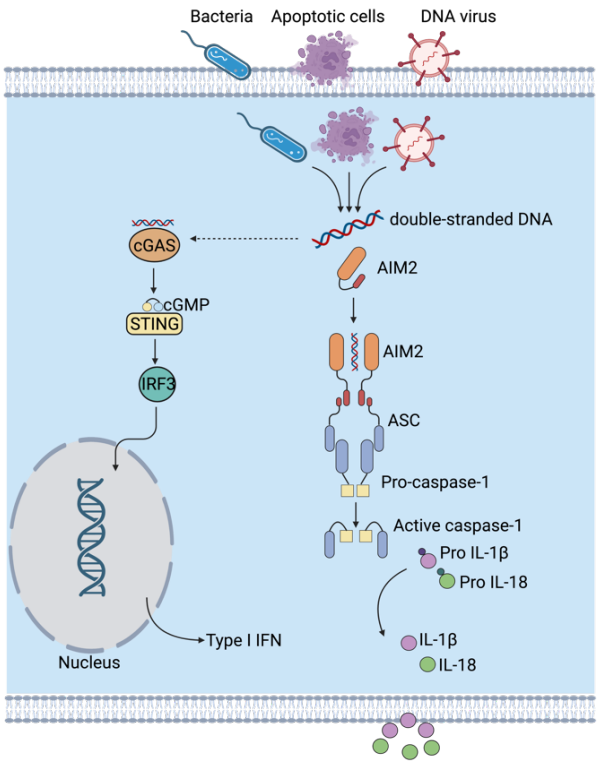

Figure 5.1 Schematic illustration of AIM2 inflammasome activation *(modified from Lugrin,J et al. 2018[121])*. Following infection with bacterial viral, double-stranded microbial DNA (dsDNA) is able to enter the cytosol where it can be identified by AIM2. Once sensing dsDNA, AIM2 initiates an ASC-caspase-1 inflammasome assembly, which consequently activates IL-1β and IL-18. cGAS also senses cytosolic dsDNA leading to the activation of STING-IRF3 pathway to synthesize type I IFN. In addition to self-extrinsic DNA, AIM2 also recognizes self-intrinsic DNA derived from apoptotic cells. AIM2 binding self-DNA and leading to inflammasome responses plays essential roles in autoimmunity.

The AIM2 inflammasome has been described to sense cytosolic double-stranded DNA (dsDNA) and is an essential defense mechanism against bacterial and virus infections[120]. AIM2 is a cytosolic receptor which can directly bind to dsDNA via the HIN domains[120]. Biochemical studies have shown that

at least 70 base pair (bp) of dsDNA is required for AIM2 inflammasome activation, while 200 bp of dsDNA enables the optimal AIM2 activation[198]. The AIM2-DNA binding initiates AIM2 inflammasome assembly, which induces ASC oligomerization and the downstream recruitment of pro-caspase-1 to the inflammasome complex leading to the cleavage of caspase-1, and further maturation of IL-1β and IL-18[121, 122]. As another cytosolic sensor for DNA, cGAS can also bind to DNA and consequently induce Type I interferons (IFNs) synthesis[199]. There is a complex interaction between AIM2 inflammasome and cGAS-STING-Type I IFNs pathway. AIM2 expression can be upregulated by cGAS-STING-Type I IFNs pathway[199]; conversely, caspase-1 activation by AIM2 inflammasome inhibit cGAS, thereby suppress type I IFN responses to cytosolic DNA[200]. Apart from sensing dsDNA from invaded pathogen, AIM2 also recognize self-DNA under several pathological conditions. Excessive accumulation of cholesterol in macrophages dampens mitochondrial respiration and membrane polarization, consequently mitochondrial DNA is spilled into the cytosol leading to AIM2 inflammasome activation[201]. In addition to cell-intrinsic DNA, extrinsic DNA can also be recognized by AIM2. Phagocytic cells including macrophages internalize cell-free DNA released due to cellular damage or apoptotic cells containing DNA[202]. Internalized DNA is first delivered to lysosomes, where it undergoes degradation by DNase. However, defective DNase activity leads to insufficient DNA degradation thus accumulation in the lysosome, which ultimately expels into the cytosol[202].

AIM2 plays critical role in various diseases including stroke, atherosclerosis, cancer, systemic lupus erythematosus[57, 109, 122, 123]. In previous study, it has been identified that ischemic stroke upregulates FasL expression on myeloid cells via AIM2 inflammasome activation in acute phase, which consequently binds to Fas on T cells and mediate T cells apoptosis[57]. Atherosclerotic mice showed increased expression of AIM2 within plaques in the chronic phase which colocalized with dsDNA[123]. Genetic deletion or therapeutic inhibition of AIM2 indeed decreased IL-1β and IL-18 release as well as stabilized atherosclerotic plaques in mice[123]. More recently, another study showed that increased

proliferation in clonal hematopoietic macrophages lead to AIM2 inflammasome activation, thus exacerbating atherosclerosis[109]. The results of these studies suggest that a comprehensive investigation of the role of the AIM2 inflammasome in the development of post-stroke atherosclerosis is necessary, which may provide a novel therapeutic strategy to prevent early recurrent stroke.

5.5 Immunotherapies targeting ischemic recurrence

Since the CANTOS trial has demonstrated that therapeutic targeting of the inflammatory response can be beneficial for cardiovascular outcomes in patients, immunotherapies targeting inflammation indicate a promising therapeutic approach to prevent ischemic recurrence. In addition to IL-1β, other anti-inflammatory therapies are also under investigation to reduce inflammation and prevent cardiovascular events. Colchicine is an oral therapeutic agent that decreases inflammation by inhibiting tubulin polymerization[203]. Early studies have reported that colchicine has broad cellular effects, comprising inhibition of monocytes and neutrophils motility and adhesion to endothelial cells[204], downregulation of TNF receptors on macrophages and endothelium[205]. The efficacy of colchicine to prevent adverse cardiovascular events has been investigated in patients with acute coronary syndrome (ACS)[206]. As found in a large randomized clinical trial, the administration of 0.5 mg twice daily of colchicine for ACS patients significantly reduced the risk of stroke and ischemic-driven revascularization, yet resulted in statistically significant increases in non-cardiovascular deaths in the colchicine group[206]. The effect and safety of colchicine to prevent recurrent cardiovascular events has also been evaluated in MI patients[207]. Colchicine significantly lowered the risk of cardiovascular death, MI, and stroke, although there was an increase of nonfatal pneumonia in the treatment group[207]. These clinical findings support the hypothesis that inflammatory pathways play a crucial role in the development of atherosclerosis, leading to strokes and other vascular events, and has demonstrated a promising therapeutic potential thus far. However, both cana-

kinumab and colchicine treatment brought significant side effects, which motivates further trials to investigate alternative anti-inflammatory approaches for the prevention of post-stroke comorbidities.

Advances in understanding of post-stroke pathogenesis have discovered several promising molecular therapeutic targets. Inflammasome activation has been observed in several post-stroke comorbidities including atherosclerosis. Selective inhibition of caspase-1 by VX765 administration showed reduction of atherosclerosis in mice[208]. However, clinical trials of caspase-1 inhibitors VX740 and VX765 in patients with psoriasis or epilepsy discovered drug-induced hepatotoxicity, indicating that drug design needs to be further improved[209].

The present study shows increased cell-free DNA (cfDNA) levels and local activation of the AIM2 inflammasome as the key mechanisms leading to plaque destabilization after stroke. Correspondingly, the use of recombinant DNase efficiently prevented plaque inflammation, destabilization and recurrent ischemic events. It is noteworthy that DNase treatment was not shown to have a direct immunosuppressive effect in various disease conditions, including cystic fibrosis and pleural infections[210-212]. In addition, DNase treatment might improve immunocompetence during secondary bacterial infections, as reduction of early inflammasome activation in response to tissue injury prevents subacute immunosuppression[57]. In this regard, the use of DNase is a promising candidate for future clinical development as a therapeutic approach in early secondary prevention.

References

1. Sacco RL, Kasner SE, Broderick JP, Caplan LR, Connors JJ, Culebras A, et al. An updated definition of stroke for the 21st century: A statement for healthcare professionals from the american heart association/american stroke association. *Stroke*. 2013;44:2064-2089
2. Virani SS, Alonso A, Aparicio HJ, Benjamin EJ, Bittencourt MS, Callaway CW, et al. Heart disease and stroke statistics-2021 update: A report from the american heart association. *Circulation*. 2021;143:e254-e743
3. Centers for Disease Control and Prevention NCfHS. National health and nutrition examination survey (nhanes) public use data files. April 1, 2020
4. Prevention CfDCa. Multiple cause of death, on cdc wonder online database. 2020
5. Writing Group M, Lloyd-Jones D, Adams RJ, Brown TM, Carnethon M, Dai S, et al. Heart disease and stroke statistics--2010 update: A report from the american heart association. *Circulation*. 2010;121:e46-e215
6. Collaborators GBDLRoS, Feigin VL, Nguyen G, Cercy K, Johnson CO, Alam T, et al. Global, regional, and country-specific lifetime risks of stroke, 1990 and 2016. *N Engl J Med*. 2018;379:2429-2437
7. Brown DL, Lisabeth LD, Roychoudhury C, Ye Y, Morgenstern LB. Recurrent stroke risk is higher than cardiac event risk after initial stroke/transient ischemic attack. *Stroke*. 2005;36:1285-1287
8. Johnston SC, Gress DR, Browner WS, Sidney S. Short-term prognosis after emergency department diagnosis of tia. *JAMA*. 2000;284:2901-2906
9. Chandratheva A, Mehta Z, Geraghty OC, Marquardt L, Rothwell PM, Oxford Vascular S. Population-based study of risk and predictors of stroke in the first few hours after a tia. *Neurology*. 2009;72:1941-1947
10. Adams HP, Jr., Bendixen BH, Kappelle LJ, Biller J, Love BB, Gordon DL, et al. Classification of subtype of acute ischemic stroke. Definitions for use in a multicenter clinical trial. Toast. Trial of org 10172 in acute stroke treatment. *Stroke*. 1993;24:35-41
11. Campbell BCV, Khatri P. Stroke. *Lancet*. 2020;396:129-142
12. Giles MF, Rothwell PM. Risk of stroke early after transient ischaemic attack: A systematic review and meta-analysis. *Lancet Neurol*. 2007;6:1063-1072
13. Wang Y, Wang Y, Zhao X, Liu L, Wang D, Wang C, et al. Clopidogrel with aspirin in acute minor stroke or transient ischemic attack. *N Engl J Med*. 2013;369:11-19
14. Lovett JK, Coull AJ, Rothwell PM. Early risk of recurrence by subtype of ischemic stroke in population-based incidence studies. *Neurology*. 2004;62:569-573
15. National Institute of Neurological D, Stroke rt PASSG. Tissue plasminogen activator for acute ischemic stroke. *N Engl J Med*. 1995;333:1581-1587
16. Jovin TG, Chamorro A, Cobo E, de Miquel MA, Molina CA, Rovira A, et al. Thrombectomy within 8 hours after symptom onset in ischemic stroke. *N Engl J Med*. 2015;372:2296-2306
17. Emberson J, Lees KR, Lyden P, Blackwell L, Albers G, Bluhmki E, et al. Effect of treatment delay, age, and stroke severity on the effects of intravenous thrombolysis with alteplase for acute ischaemic stroke: A meta-analysis of individual patient data from randomised trials. *Lancet*. 2014;384:1929-1935
18. Lansberg MG, Schrooten M, Bluhmki E, Thijs VN, Saver JL. Treatment time-specific number needed to treat estimates for tissue plasminogen activator therapy in acute stroke based on shifts over the entire range of the modified rankin scale. *Stroke*. 2009;40:2079-2084
19. Arhuidese I, Obeid T, Nejim B, Locham S, Hicks CW, Malas MB. Stenting versus endarterectomy after prior ipsilateral carotid endarterectomy. *J Vasc Surg*. 2017;65:1-11

20. Chamorro A, Dirnagl U, Urra X, Planas AM. Neuroprotection in acute stroke: Targeting excitotoxicity, oxidative and nitrosative stress, and inflammation. *Lancet Neurol*. 2016;15:869-881

21. O'Collins VE, Macleod MR, Donnan GA, Horky LL, van der Worp BH, Howells DW. 1,026 experimental treatments in acute stroke. *Ann Neurol*. 2006;59:467-477

22. Mohan KM, Wolfe CD, Rudd AG, Heuschmann PU, Kolominsky-Rabas PL, Grieve AP. Risk and cumulative risk of stroke recurrence: A systematic review and meta-analysis. *Stroke*. 2011;42:1489-1494

23. Johnston SC, Easton JD, Farrant M, Barsan W, Conwit RA, Elm JJ, et al. Clopidogrel and aspirin in acute ischemic stroke and high-risk tia. *N Engl J Med*. 2018;379:215-225

24. Rothwell PM, Eliasziw M, Gutnikov SA, Fox AJ, Taylor DW, Mayberg MR, et al. Analysis of pooled data from the randomised controlled trials of endarterectomy for symptomatic carotid stenosis. *Lancet*. 2003;361:107-116

25. Gladstone DJ, Oh J, Fang J, Lindsay P, Tu JV, Silver FL, et al. Urgency of carotid endarterectomy for secondary stroke prevention: Results from the registry of the canadian stroke network. *Stroke*. 2009;40:2776-2782

26. Yu F, Liu X, Yang Q, Fu Y, Fan D. In-hospital recurrence in a chinese large cohort with acute ischemic stroke. *Sci Rep*. 2019;9:14945

27. Kelly PJ, Murphy S, Coveney S, Purroy F, Lemmens R, Tsivgoulis G, et al. Anti-inflammatory approaches to ischaemic stroke prevention. *J Neurol Neurosurg Psychiatry*. 2018;89:211-218

28. Muhammad S, Barakat W, Stoyanov S, Murikinati S, Yang H, Tracey KJ, et al. The hmgb1 receptor rage mediates ischemic brain damage. *J Neurosci*. 2008;28:12023-12031

29. Liesz A, Suri-Payer E, Veltkamp C, Doerr H, Sommer C, Rivest S, et al. Regulatory t cells are key cerebroprotective immunomodulators in acute experimental stroke. *Nat Med*. 2009;15:192-199

30. Smith WS. Pathophysiology of focal cerebral ischemia: A therapeutic perspective. *J Vasc Interv Radiol*. 2004;15:S3-12

31. Yilmaz G, Granger DN. Leukocyte recruitment and ischemic brain injury. *Neuromolecular Med*. 2010;12:193-204

32. Endres M, Moro MA, Nolte CH, Dames C, Buckwalter MS, Meisel A. Immune pathways in etiology, acute phase, and chronic sequelae of ischemic stroke. *Circ Res*. 2022;130:1167-1186

33. Roth S, Singh V, Tiedt S, Schindler L, Huber G, Geerlof A, et al. Brain-released alarmins and stress response synergize in accelerating atherosclerosis progression after stroke. *Sci Transl Med*. 2018;10

34. Liesz A, Hagmann S, Zschoche C, Adamek J, Zhou W, Sun L, et al. The spectrum of systemic immune alterations after murine focal ischemia: Immunodepression versus immunomodulation. *Stroke*. 2009;40:2849-2858

35. Rubio-Ponce A, Hidalgo A, Ballesteros I. How to bridle a neutrophil. *Curr Opin Immunol*. 2021;68:41-47

36. Adrover JM, Del Fresno C, Crainiciuc G, Cuartero MI, Casanova-Acebes M, Weiss LA, et al. A neutrophil timer coordinates immune defense and vascular protection. *Immunity*. 2019;50:390-402 e310

37. Berchtold D, Priller J, Meisel C, Meisel A. Interaction of microglia with infiltrating immune cells in the different phases of stroke. *Brain Pathol*. 2020;30:1208-1218

38. Hermann DM, Kleinschnitz C, Gunzer M. Implications of polymorphonuclear neutrophils for ischemic stroke and intracerebral hemorrhage: Predictive value, pathophysiological consequences and utility as therapeutic target. *J Neuroimmunol*. 2018;321:138-143

39. Enzmann G, Kargaran S, Engelhardt B. Ischemia-reperfusion injury in stroke: Impact of the brain barriers and brain immune privilege on neutrophil function. *Ther Adv Neurol Disord*. 2018;11:1756286418794184

40. Pena-Martinez C, Duran-Laforet V, Garcia-Culebras A, Ostos F, Hernandez-Jimenez M, Bravo-Ferrer I, et al. Pharmacological modulation of neutrophil extracellular traps reverses thrombotic stroke tpa (tissue-type plasminogen activator) resistance. *Stroke*. 2019;50:3228-3237

41. Kang L, Yu H, Yang X, Zhu Y, Bai X, Wang R, et al. Neutrophil extracellular traps released by neutrophils impair revascularization and vascular remodeling after stroke. *Nat Commun*. 2020;11:2488

42. Garcia-Culebras A, Duran-Laforet V, Pena-Martinez C, Ballesteros I, Pradillo JM, Diaz-Guzman J, et al. Myeloid cells as therapeutic targets in neuroinflammation after stroke: Specific roles of neutrophils and neutrophil-platelet interactions. *J Cereb Blood Flow Metab*. 2018;38:2150-2164

43. Ginhoux F, Jung S. Monocytes and macrophages: Developmental pathways and tissue homeostasis. *Nat Rev Immunol*. 2014;14:392-404

44. Geissmann F, Jung S, Littman DR. Blood monocytes consist of two principal subsets with distinct migratory properties. *Immunity*. 2003;19:71-82

45. Jakubzick C, Gautier EL, Gibbings SL, Sojka DK, Schlitzer A, Johnson TE, et al. Minimal differentiation of classical monocytes as they survey steady-state tissues and transport antigen to lymph nodes. *Immunity*. 2013;39:599-610

46. Kratofil RM, Kubes P, Deniset JF. Monocyte conversion during inflammation and injury. *Arterioscler Thromb Vasc Biol*. 2017;37:35-42

47. Garcia-Bonilla L, Faraco G, Moore J, Murphy M, Racchumi G, Srinivasan J, et al. Spatio-temporal profile, phenotypic diversity, and fate of recruited monocytes into the post-ischemic brain. *J Neuroinflammation*. 2016;13:285

48. Dimitrijevic OB, Stamatovic SM, Keep RF, Andjelkovic AV. Absence of the chemokine receptor ccr2 protects against cerebral ischemia/reperfusion injury in mice. *Stroke*. 2007;38:1345-1353

49. Liu Q, Jin WN, Liu Y, Shi K, Sun H, Zhang F, et al. Brain ischemia suppresses immunity in the periphery and brain via different neurogenic innervations. *Immunity*. 2017;46:474-487

50. Romer C, Engel O, Winek K, Hochmeister S, Zhang T, Royl G, et al. Blocking stroke-induced immunodeficiency increases cns antigen-specific autoreactivity but does not worsen functional outcome after experimental stroke. *J Neurosci*. 2015;35:7777-7794

51. Haeusler KG, Schmidt WU, Fohring F, Meisel C, Helms T, Jungehulsing GJ, et al. Cellular immunodepression preceding infectious complications after acute ischemic stroke in humans. *Cerebrovasc Dis*. 2008;25:50-58

52. Klehmet J, Harms H, Richter M, Prass K, Volk HD, Dirnagl U, et al. Stroke-induced immunodepression and post-stroke infections: Lessons from the preventive antibacterial therapy in stroke trial. *Neuroscience*. 2009;158:1184-1193

53. Prass K, Meisel C, Hoflich C, Braun J, Halle E, Wolf T, et al. Stroke-induced immunodeficiency promotes spontaneous bacterial infections and is mediated by sympathetic activation reversal by poststroke t helper cell type 1-like immunostimulation. *J Exp Med*. 2003;198:725-736

54. Meisel C, Schwab JM, Prass K, Meisel A, Dirnagl U. Central nervous system injury-induced immune deficiency syndrome. *Nat Rev Neurosci*. 2005;6:775-786

55. Fu Y, Liu Q, Anrather J, Shi FD. Immune interventions in stroke. *Nat Rev Neurol*. 2015;11:524-535

56. Dirnagl U, Klehmet J, Braun JS, Harms H, Meisel C, Ziemssen T, et al. Stroke-induced immunodepression: Experimental evidence and clinical relevance. *Stroke*. 2007;38:770-773

57. Roth S, Cao J, Singh V, Tiedt S, Hundeshagen G, Li T, et al. Post-injury immunosuppression and secondary infections are caused by an aim2 inflammasome-driven signaling cascade. *Immunity*. 2021;54:648-659 e648

58. Vajpeyee A, Wijatmiko T, Vajpeyee M, Taywade O, Pandey S, Chauhan PS. Clinical usefulness of cell-free DNA as a prognostic marker in acute ischemic stroke. *Neurologist*. 2020;25:11-13

59. Tsai AS, Berry K, Beneyto MM, Gaudilliere D, Ganio EA, Culos A, et al. A year-long immune profile of the systemic response in acute stroke survivors. *Brain*. 2019;142:978-991

60. Schulze J, Zierath D, Tanzi P, Cain K, Shibata D, Dressel A, et al. Severe stroke induces long-lasting alterations of high-mobility group box 1. *Stroke*. 2013;44:246-248

61. Simats A, Liesz A. Systemic inflammation after stroke: Implications for post-stroke comorbidities. *EMBO Mol Med*. 2022;14:e16269

62. Moore KJ, Tabas I. Macrophages in the pathogenesis of atherosclerosis. *Cell*. 2011;145:341-355

63. Kwon GP, Schroeder JL, Amar MJ, Remaley AT, Balaban RS. Contribution of macromolecular structure to the retention of low-density lipoprotein at arterial branch points. *Circulation*. 2008;117:2919-2927

64. Organization WH. Cardiovascular diseases (cvds) fact sheet. 2021

65. Disease GBD, Injury I, Prevalence C. Global, regional, and national incidence, prevalence, and years lived with disability for 310 diseases and injuries, 1990-2015: A systematic analysis for the global burden of disease study 2015. *Lancet*. 2016;388:1545-1602

66. Chen M, Masaki T, Sawamura T. Lox-1, the receptor for oxidized low-density lipoprotein identified from endothelial cells: Implications in endothelial dysfunction and atherosclerosis. *Pharmacol Ther*. 2002;95:89-100

67. Moore KJ, Sheedy FJ, Fisher EA. Macrophages in atherosclerosis: A dynamic balance. *Nat Rev Immunol*. 2013;13:709-721

68. Tabas I, Bornfeldt KE. Macrophage phenotype and function in different stages of atherosclerosis. *Circ Res*. 2016;118:653-667

69. Libby P, Lichtman AH, Hansson GK. Immune effector mechanisms implicated in atherosclerosis: From mice to humans. *Immunity*. 2013;38:1092-1104

70. Ketelhuth DF, Hansson GK. Adaptive response of t and b cells in atherosclerosis. *Circ Res*. 2016;118:668-678

71. Nus M, Mallat Z. Immune-mediated mechanisms of atherosclerosis and implications for the clinic. *Expert Rev Clin Immunol*. 2016;12:1217-1237

72. Soehnlein O, Libby P. Targeting inflammation in atherosclerosis - from experimental insights to the clinic. *Nat Rev Drug Discov*. 2021;20:589-610

73. Bennett MR, Sinha S, Owens GK. Vascular smooth muscle cells in atherosclerosis. *Circ Res*. 2016;118:692-702

74. Libby P, Hansson GK. Inflammation and immunity in diseases of the arterial tree: Players and layers. *Circ Res*. 2015;116:307-311

75. Geng YJ, Libby P. Evidence for apoptosis in advanced human atheroma. Colocalization with interleukin-1 beta-converting enzyme. *Am J Pathol*. 1995;147:251-266

76. Clarke MC, Talib S, Figg NL, Bennett MR. Vascular smooth muscle cell apoptosis induces interleukin-1-directed inflammation: Effects of hyperlipidemia-mediated inhibition of phagocytosis. *Circ Res*. 2010;106:363-372

77. Tabas I, Garcia-Cardena G, Owens GK. Recent insights into the cellular biology of atherosclerosis. *J Cell Biol*. 2015;209:13-22

78. Yurdagul A, Jr., Doran AC, Cai B, Fredman G, Tabas IA. Mechanisms and consequences of defective efferocytosis in atherosclerosis. *Front Cardiovasc Med*. 2017;4:86

79. Libby P. Mechanisms of acute coronary syndromes and their implications for therapy. *N Engl J Med*. 2013;368:2004-2013

80. Bentzon JF, Otsuka F, Virmani R, Falk E. Mechanisms of plaque formation and rupture. *Circ Res*. 2014;114:1852-1866

81. Heemskerk JW, Mattheij NJ, Cosemans JM. Platelet-based coagulation: Different populations, different functions. *J Thromb Haemost*. 2013;11:2-16

82. Kuijpers MJ, van der Meijden PE, Feijge MA, Mattheij NJ, May F, Govers-Riemslag J, et al. Factor xii regulates the pathological process of thrombus formation on ruptured plaques. *Arterioscler Thromb Vasc Biol*. 2014;34:1674-1680

83. Maas C, Renne T. Coagulation factor xii in thrombosis and inflammation. *Blood*. 2018;131:1903-1909

84. Nickel KF, Long AT, Fuchs TA, Butler LM, Renne T. Factor xii as a therapeutic target in thromboembolic and inflammatory diseases. *Arterioscler Thromb Vasc Biol*. 2017;37:13-20

85. Renne T, Stavrou EX. Roles of factor xii in innate immunity. *Front Immunol*. 2019;10:2011

86. Hagedorn I, Schmidbauer S, Pleines I, Kleinschnitz C, Kronthaler U, Stoll G, et al. Factor xiia inhibitor recombinant human albumin infestin-4 abolishes occlusive arterial thrombus formation without affecting bleeding. *Circulation*. 2010;121:1510-1517

87. Larsson M, Rayzman V, Nolte MW, Nickel KF, Bjorkqvist J, Jamsa A, et al. A factor xiia inhibitory antibody provides thromboprotection in extracorporeal circulation without increasing bleeding risk. *Sci Transl Med*. 2014;6:222ra217

88. Chan NC, Weitz JI. Antithrombotic agents. *Circ Res*. 2019;124:426-436

89. Bickmann JK, Baglin T, Meijers JCM, Renne T. Novel targets for anticoagulants lacking bleeding risk. *Curr Opin Hematol*. 2017;24:419-426

90. Basatemur GL, Jorgensen HF, Clarke MCH, Bennett MR, Mallat Z. Vascular smooth muscle cells in atherosclerosis. *Nat Rev Cardiol*. 2019;16:727-744

91. Quinn MT, Parthasarathy S, Fong LG, Steinberg D. Oxidatively modified low density lipoproteins: A potential role in recruitment and retention of monocyte/macrophages during atherogenesis. *Proc Natl Acad Sci U S A*. 1987;84:2995-2998

92. Combadiere C, Potteaux S, Rodero M, Simon T, Pezard A, Esposito B, et al. Combined inhibition of ccl2, cx3cr1, and ccr5 abrogates ly6c(hi) and ly6c(lo) monocytosis and almost abolishes atherosclerosis in hypercholesterolemic mice. *Circulation*. 2008;117:1649-1657

93. Fiuza C, Bustin M, Talwar S, Tropea M, Gerstenberger E, Shelhamer JH, et al. Inflammation-promoting activity of hmgb1 on human microvascular endothelial cells. *Blood*. 2003;101:2652-2660

94. Zhu Y, Liao HL, Lin JH, Verna L, Stemerman MB. Low-density lipoprotein augments interleukin-1-induced vascular adhesion molecule expression in human endothelial cells. *Atherosclerosis*. 1999;144:357-365

95. van Dinther-Janssen AC, Horst E, Koopman G, Newmann W, Scheper RJ, Meijer CJ, et al. The vla-4/vcam-1 pathway is involved in lymphocyte adhesion to endothelium in rheumatoid synovium. *J Immunol*. 1991;147:4207-4210

96. Hoeksema MA, Stoger JL, de Winther MP. Molecular pathways regulating macrophage polarization: Implications for atherosclerosis. *Curr Atheroscler Rep*. 2012;14:254-263

97. Collot-Teixeira S, Martin J, McDermott-Roe C, Poston R, McGregor JL. Cd36 and macrophages in atherosclerosis. *Cardiovasc Res*. 2007;75:468-477

98. Jessup W, Gelissen IC, Gaus K, Kritharides L. Roles of atp binding cassette transporters a1 and g1, scavenger receptor bi and membrane lipid domains in cholesterol export from macrophages. *Curr Opin Lipidol*. 2006;17:247-257

99. Depuydt MAC, Prange KHM, Slenders L, Ord T, Elbersen D, Boltjes A, et al. Microanatomy of the human atherosclerotic plaque by single-cell transcriptomics. *Circ Res*. 2020;127:1437-1455

100. Oorni K, Rajamaki K, Nguyen SD, Lahdesmaki K, Plihtari R, Lee-Rueckert M, et al. Acidification of the intimal fluid: The perfect storm for atherogenesis. *J Lipid Res*. 2015;56:203-214

101. Back M, Yurdagul A, Jr., Tabas I, Oorni K, Kovanen PT. Inflammation and its resolution in atherosclerosis: Mediators and therapeutic opportunities. *Nat Rev Cardiol*. 2019;16:389-406

102. Andres V, Pello OM, Silvestre-Roig C. Macrophage proliferation and apoptosis in atherosclerosis. *Curr Opin Lipidol*. 2012;23:429-438

103. Rajavashisth TB, Andalibi A, Territo MC, Berliner JA, Navab M, Fogelman AM, et al. Induction of endothelial cell expression of granulocyte and macrophage colony-stimulating factors by modified low-density lipoproteins. *Nature*. 1990;344:254-257

104. Shaposhnik Z, Wang X, Lusis AJ. Arterial colony stimulating factor-1 influences atherosclerotic lesions by regulating monocyte migration and apoptosis. *J Lipid Res*. 2010;51:1962-1970

105. Sinha SK, Miikeda A, Fouladian Z, Mehrabian M, Edillor C, Shih D, et al. Local m-csf (macrophage colony-stimulating factor) expression regulates macrophage proliferation and apoptosis in atherosclerosis. *Arterioscler Thromb Vasc Biol*. 2021;41:220-233

106. Heyde A, Rohde D, McAlpine CS, Zhang S, Hoyer FF, Gerold JM, et al. Increased stem cell proliferation in atherosclerosis accelerates clonal hematopoiesis. *Cell*. 2021;184:1348-1361 e1322

107. Jaiswal S, Natarajan P, Silver AJ, Gibson CJ, Bick AG, Shvartz E, et al. Clonal hematopoiesis and risk of atherosclerotic cardiovascular disease. *N Engl J Med*. 2017;377:111-121

108. Jung C, Evans MA, Walsh K. Genetics of age-related clonal hematopoiesis and atherosclerotic cardiovascular disease. *Curr Opin Cardiol*. 2020;35:219-225

109. Fidler TP, Xue C, Yalcinkaya M, Hardaway B, Abramowicz S, Xiao T, et al. The aim2 inflammasome exacerbates atherosclerosis in clonal haematopoiesis. *Nature*. 2021;592:296-301

110. De Nardo D, Latz E. Nlrp3 inflammasomes link inflammation and metabolic disease. *Trends Immunol*. 2011;32:373-379

111. Davis BK, Wen H, Ting JP. The inflammasome nlrs in immunity, inflammation, and associated diseases. *Annu Rev Immunol*. 2011;29:707-735

112. Duewell P, Kono H, Rayner KJ, Sirois CM, Vladimer G, Bauernfeind FG, et al. Nlrp3 inflammasomes are required for atherogenesis and activated by cholesterol crystals. *Nature*. 2010;464:1357-1361

113. Martinon F, Burns K, Tschopp J. The inflammasome: A molecular platform triggering activation of inflammatory caspases and processing of proil-beta. *Mol Cell*. 2002;10:417-426

114. Vanaja SK, Rathinam VA, Fitzgerald KA. Mechanisms of inflammasome activation: Recent advances and novel insights. *Trends Cell Biol*. 2015;25:308-315

115. Zheng F, Xing S, Gong Z, Xing Q. Nlrp3 inflammasomes show high expression in aorta of patients with atherosclerosis. *Heart Lung Circ*. 2013;22:746-750

116. Devlin CM, Kuriakose G, Hirsch E, Tabas I. Genetic alterations of il-1 receptor antagonist in mice affect plasma cholesterol level and foam cell lesion size. *Proc Natl Acad Sci U S A*. 2002;99:6280-6285

117. Ridker PM, Everett BM, Thuren T, MacFadyen JG, Chang WH, Ballantyne C, et al. Antiinflammatory therapy with canakinumab for atherosclerotic disease. *N Engl J Med*. 2017;377:1119-1131

118. Hettwer J, Hinterdobler J, Miritsch B, Deutsch MA, Li X, Mauersberger C, et al. Interleukin-1beta suppression dampens inflammatory leucocyte production and uptake in atherosclerosis. *Cardiovasc Res*. 2022;118:2778-2791

119. Borissoff JI, Joosen IA, Versteylen MO, Brill A, Fuchs TA, Savchenko AS, et al. Elevated levels of circulating DNA and chromatin are independently associated with severe coronary atherosclerosis and a prothrombotic state. *Arterioscler Thromb Vasc Biol*. 2013;33:2032-2040

120. Hornung V, Ablasser A, Charrel-Dennis M, Bauernfeind F, Horvath G, Caffrey DR, et al. Aim2 recognizes cytosolic dsdna and forms a caspase-1-activating inflammasome with asc. *Nature*. 2009;458:514-518

121. Lugrin J, Martinon F. The aim2 inflammasome: Sensor of pathogens and cellular perturbations. *Immunol Rev*. 2018;281:99-114

122. Pan J, Han L, Guo J, Wang X, Liu D, Tian J, et al. Aim2 accelerates the atherosclerotic plaque progressions in apoe-/- mice. *Biochem Biophys Res Commun*. 2018;498:487-494

123. Paulin N, Viola JR, Maas SL, de Jong R, Fernandes-Alnemri T, Weber C, et al. Double-strand DNA sensing aim2 inflammasome regulates atherosclerotic plaque vulnerability. *Circulation*. 2018;138:321-323

124. Finn AV, Nakano M, Narula J, Kolodgie FD, Virmani R. Concept of vulnerable/unstable plaque. *Arterioscler Thromb Vasc Biol*. 2010;30:1282-1292

125. Noonan J, Bobik A, Peter K. The tandem stenosis mouse model: Towards understanding, imaging, and preventing atherosclerotic plaque instability and rupture. *Br J Pharmacol*. 2022;179:979-997

126. Chen YC, Huang AL, Kyaw TS, Bobik A, Peter K. Atherosclerotic plaque rupture: Identifying the straw that breaks the camel's back. *Arterioscler Thromb Vasc Biol*. 2016;36:e63-72

127. Caro CG. Discovery of the role of wall shear in atherosclerosis. *Arterioscler Thromb Vasc Biol*. 2009;29:158-161

128. Slager CJ, Wentzel JJ, Gijsen FJ, Thury A, van der Wal AC, Schaar JA, et al. The role of shear stress in the destabilization of vulnerable plaques and related therapeutic implications. *Nat Clin Pract Cardiovasc Med*. 2005;2:456-464

129. Chen YC, Bui AV, Diesch J, Manasseh R, Hausding C, Rivera J, et al. A novel mouse model of atherosclerotic plaque instability for drug testing and mechanistic/therapeutic discoveries using gene and microrna expression profiling. *Circ Res*. 2013;113:252-265

130. Kilkenny C, Browne WJ, Cuthill IC, Emerson M, Altman DG. Improving bioscience research reporting: The arrive guidelines for reporting animal research. *PLoS Biol*. 2010;8:e1000412

131. Jack P. Green LYE-S, Stefan Roth, Jie Zhu, Jiayu Cao, Andrew G. Leach, Arthur Liesz, Sally Freeman, David Brough. Discovery of an aim2 inflammasome inhibitor for the treatment of DNA-driven inflammatory disease. *bioRxiv*. 2022

132. Cheng S, Mao X, Lin X, Wehn A, Hu S, Mamrak U, et al. Acid-ion sensing channel 1a deletion reduces chronic brain damage and neurological deficits after experimental traumatic brain injury. *J Neurotrauma*. 2021;38:1572-1584

133. Lattouf R, Younes R, Lutomski D, Naaman N, Godeau G, Senni K, et al. Picrosirius red staining: A useful tool to appraise collagen networks in normal and pathological tissues. *J Histochem Cytochem*. 2014;62:751-758

134. Silvestre-Roig C, Braster Q, Wichapong K, Lee EY, Teulon JM, Berrebeh N, et al. Externalized histone h4 orchestrates chronic inflammation by inducing lytic cell death. *Nature*. 2019;569:236-240

135. Butcher MJ, Herre M, Ley K, Galkina E. Flow cytometry analysis of immune cells within murine aortas. *J Vis Exp*. 2011

136. Winter C, Silvestre-Roig C, Ortega-Gomez A, Lemnitzer P, Poelman H, Schumski A, et al. Chrono-pharmacological targeting of the ccl2-ccr2 axis ameliorates atherosclerosis. *Cell Metab*. 2018;28:175-182 e175

137. Katsanos AH, Hart RG. New horizons in pharmacologic therapy for secondary stroke prevention. *JAMA Neurol*. 2020;77:1308-1317

138. Cheng C, Tempel D, van Haperen R, van der Baan A, Grosveld F, Daemen MJ, et al. Atherosclerotic lesion size and vulnerability are determined by patterns of fluid shear stress. *Circulation*. 2006;113:2744-2753

139. Chatzizisis YS, Baker AB, Sukhova GK, Koskinas KC, Papafaklis MI, Beigel R, et al. Augmented expression and activity of extracellular matrix-degrading enzymes in regions of low endothelial shear stress colocalize with coronary atheromata with thin fibrous caps in pigs. *Circulation*. 2011;123:621-630

140. Cheruvu PK, Finn AV, Gardner C, Caplan J, Goldstein J, Stone GW, et al. Frequency and distribution of thin-cap fibroatheroma and ruptured plaques in human coronary arteries: A pathologic study. *J Am Coll Cardiol*. 2007;50:940-949

141. Falk E, Nakano M, Bentzon JF, Finn AV, Virmani R. Update on acute coronary syndromes: The pathologists' view. *Eur Heart J*. 2013;34:719-728

142. Hatsukami TS, Ross R, Polissar NL, Yuan C. Visualization of fibrous cap thickness and rupture in human atherosclerotic carotid plaque in vivo with high-resolution magnetic resonance imaging. *Circulation*. 2000;102:959-964

143. Broz P, Dixit VM. Inflammasomes: Mechanism of assembly, regulation and signalling. *Nat Rev Immunol*. 2016;16:407-420

144. McKenzie BA, Mamik MK, Saito LB, Boghozian R, Monaco MC, Major EO, et al. Caspase-1 inhibition prevents glial inflammasome activation and pyroptosis in models of multiple sclerosis. *Proc Natl Acad Sci U S A*. 2018;115:E6065-E6074

145. Coll RC, Robertson AA, Chae JJ, Higgins SC, Munoz-Planillo R, Inserra MC, et al. A small-molecule inhibitor of the nlrp3 inflammasome for the treatment of inflammatory diseases. *Nat Med*. 2015;21:248-255

146. Nagase H, Visse R, Murphy G. Structure and function of matrix metalloproteinases and timps. *Cardiovasc Res*. 2006;69:562-573

147. Newby AC. Metalloproteinase expression in monocytes and macrophages and its relationship to atherosclerotic plaque instability. *Arterioscler Thromb Vasc Biol*. 2008;28:2108-2114

148. Wagsater D, Zhu C, Bjorkegren J, Skogsberg J, Eriksson P. Mmp-2 and mmp-9 are prominent matrix metalloproteinases during atherosclerosis development in the ldlr(-/-)apob(100/100) mouse. *Int J Mol Med*. 2011;28:247-253

149. Heo SH, Cho CH, Kim HO, Jo YH, Yoon KS, Lee JH, et al. Plaque rupture is a determinant of vascular events in carotid artery atherosclerotic disease: Involvement of matrix metalloproteinases 2 and 9. *J Clin Neurol*. 2011;7:69-76

150. Johnson JL, Baker AH, Oka K, Chan L, Newby AC, Jackson CL, et al. Suppression of atherosclerotic plaque progression and instability by tissue inhibitor of metalloproteinase-2: Involvement of macrophage migration and apoptosis. *Circulation*. 2006;113:2435-2444

151. Renne T, Schmaier AH, Nickel KF, Blomback M, Maas C. In vivo roles of factor xii. *Blood*. 2012;120:4296-4303

152. Rothwell PM, Algra A, Chen Z, Diener HC, Norrving B, Mehta Z. Effects of aspirin on risk and severity of early recurrent stroke after transient ischaemic attack and ischaemic stroke: Time-course analysis of randomised trials. *Lancet*. 2016;388:365-375

153. Han J, Mao W, Ni J, Wu Y, Liu J, Bai L, et al. Rate and determinants of recurrence at 1 year and 5 years after stroke in a low-income population in rural china. *Front Neurol*. 2020;11:2

154. Coull AJ, Rothwell PM. Underestimation of the early risk of recurrent stroke: Evidence of the need for a standard definition. *Stroke*. 2004;35:1925-1929

155. Grau AJ, Weimar C, Buggle F, Heinrich A, Goertler M, Neumaier S, et al. Risk factors, outcome, and treatment in subtypes of ischemic stroke: The german stroke data bank. *Stroke*. 2001;32:2559-2566

156. Wang Y, Xu J, Zhao X, Wang D, Wang C, Liu L, et al. Association of hypertension with stroke recurrence depends on ischemic stroke subtype. *Stroke*. 2013;44:1232-1237

157. Salgado AV, Ferro JM, Gouveia-Oliveira A. Long-term prognosis of first-ever lacunar strokes. A hospital-based study. *Stroke*. 1996;27:661-666

158. Xu G, Liu X, Wu W, Zhang R, Yin Q. Recurrence after ischemic stroke in chinese patients: Impact of uncontrolled modifiable risk factors. *Cerebrovasc Dis*. 2007;23:117-120

159. Mohan KM, Crichton SL, Grieve AP, Rudd AG, Wolfe CD, Heuschmann PU. Frequency and predictors for the risk of stroke recurrence up to 10 years after stroke: The south london stroke register. *J Neurol Neurosurg Psychiatry*. 2009;80:1012-1018

160. Arsava EM, Kim GM, Oliveira-Filho J, Gungor L, Noh HJ, Lordelo Mde J, et al. Prediction of early recurrence after acute ischemic stroke. *JAMA Neurol*. 2016;73:396-401

161. Kang K, Park TH, Kim N, Jang MU, Park SS, Park JM, et al. Recurrent stroke, myocardial infarction, and major vascular events during the first year after acute ischemic stroke: The multicenter prospective observational study about recurrence and its determinants after acute ischemic stroke i. *J Stroke Cerebrovasc Dis*. 2016;25:656-664

162. Modrego PJ, Mainar R, Turull L. Recurrence and survival after first-ever stroke in the area of bajo aragon, spain. A prospective cohort study. *J Neurol Sci*. 2004;224:49-55

163. Ois A, Gomis M, Rodriguez-Campello A, Cuadrado-Godia E, Jimenez-Conde J, Pont-Sunyer C, et al. Factors associated with a high risk of recurrence in patients with transient ischemic attack or minor stroke. *Stroke*. 2008;39:1717-1721

164. Cholesterol Treatment Trialists C, Baigent C, Blackwell L, Emberson J, Holland LE, Reith C, et al. Efficacy and safety of more intensive lowering of ldl cholesterol: A meta-analysis of data from 170,000 participants in 26 randomised trials. *Lancet*. 2010;376:1670-1681

165. Fihn SD, Gardin JM, Abrams J, Berra K, Blankenship JC, Dallas AP, et al. 2012 accf/aha/acp/aats/pcna/scai/sts guideline for the diagnosis and management of patients with stable ischemic heart disease: A report of the american college of cardiology foundation/american heart association task force on practice guidelines, and the american college of physicians, american association for thoracic surgery, preventive cardiovascular nurses association, society for cardiovascular angiography and interventions, and society of thoracic surgeons. *Circulation*. 2012;126:e354-471

166. Investigators SPS, Benavente OR, Hart RG, McClure LA, Szychowski JM, Coffey CS, et al. Effects of clopidogrel added to aspirin in patients with recent lacunar stroke. *N Engl J Med*. 2012;367:817-825

167. Sandercock PA, Counsell C, Kane EJ. Anticoagulants for acute ischaemic stroke. *Cochrane Database Syst Rev*. 2015;2015:CD000024

168. Ricotta JJ, Aburahma A, Ascher E, Eskandari M, Faries P, Lal BK, et al. Updated society for vascular surgery guidelines for management of extracranial carotid disease: Executive summary. *J Vasc Surg*. 2011;54:832-836

169. Stromberg S, Gelin J, Osterberg T, Bergstrom GM, Karlstrom L, Osterberg K, et al. Very urgent carotid endarterectomy confers increased procedural risk. *Stroke*. 2012;43:1331-1335

170. Huang Y, Gloviczki P, Duncan AA, Kalra M, Oderich GS, DeMartino RR, et al. Outcomes after early and delayed carotid endarterectomy in patients with symptomatic carotid artery stenosis. *J Vasc Surg*. 2018;67:1110-1119 e1111

171. Paul NL, Simoni M, Chandratheva A, Rothwell PM. Population-based study of capsular warning syndrome and prognosis after early recurrent tia. *Neurology*. 2012;79:1356-1362

172. Purroy F, Jimenez Caballero PE, Gorospe A, Torres MJ, Alvarez-Sabin J, Santamarina E, et al. Recurrent transient ischaemic attack and early risk of stroke: Data from the promapa study. *J Neurol Neurosurg Psychiatry*. 2013;84:596-603

173. Ois A, Cuadrado-Godia E, Rodriguez-Campello A, Giralt-Steinhauer E, Jimenez-Conde J, Lopez-Cuina M, et al. Relevance of stroke subtype in vascular risk prediction. *Neurology*. 2013;81:575-580

174. Charidimou A, Kakar P, Fox Z, Werring DJ. Cerebral microbleeds and recurrent stroke risk: Systematic review and meta-analysis of prospective ischemic stroke and transient ischemic attack cohorts. *Stroke*. 2013;44:995-1001

175. Rashid P, Leonardi-Bee J, Bath P. Blood pressure reduction and secondary prevention of stroke and other vascular events: A systematic review. *Stroke*. 2003;34:2741-2748

176. Algra A, van Gijn J. Cumulative meta-analysis of aspirin efficacy after cerebral ischaemia of arterial origin. *J Neurol Neurosurg Psychiatry*. 1999;66:255

177. Antithrombotic Trialists C, Baigent C, Blackwell L, Collins R, Emberson J, Godwin J, et al. Aspirin in the primary and secondary prevention of vascular disease: Collaborative meta-analysis of individual participant data from randomised trials. *Lancet*. 2009;373:1849-1860

178. Kernan WN, Ovbiagele B, Black HR, Bravata DM, Chimowitz MI, Ezekowitz MD, et al. Guidelines for the prevention of stroke in patients with stroke and transient ischemic attack: A guideline for healthcare professionals from the american heart association/american stroke association. *Stroke*. 2014;45:2160-2236

179. Lee M, Saver JL, Hong KS, Rao NM, Wu YL, Ovbiagele B. Risk-benefit profile of long-term dual- versus single-antiplatelet therapy among patients with ischemic stroke: A systematic review and meta-analysis. *Ann Intern Med*. 2013;159:463-470

180. Saxena R, Koudstaal PJ. Anticoagulants for preventing stroke in patients with nonrheumatic atrial fibrillation and a history of stroke or transient ischaemic attack. *Cochrane Database Syst Rev*. 2004:CD000185

181. Healey JS, Hart RG, Pogue J, Pfeffer MA, Hohnloser SH, De Caterina R, et al. Risks and benefits of oral anticoagulation compared with clopidogrel plus aspirin in patients with atrial fibrillation according to stroke risk: The atrial fibrillation clopidogrel trial with irbesartan for prevention of vascular events (active-w). *Stroke*. 2008;39:1482-1486

182. Ridker PM, Cannon CP, Morrow D, Rifai N, Rose LM, McCabe CH, et al. C-reactive protein levels and outcomes after statin therapy. *N Engl J Med*. 2005;352:20-28

183. Morrow DA, de Lemos JA, Sabatine MS, Wiviott SD, Blazing MA, Shui A, et al. Clinical relevance of c-reactive protein during follow-up of patients with acute coronary syndromes in the aggrastat-to-zocor trial. *Circulation*. 2006;114:281-288

184. Rothwell PM, Howard SC, Spence JD, Carotid Endarterectomy Trialists C. Relationship between blood pressure and stroke risk in patients with symptomatic carotid occlusive disease. *Stroke*. 2003;34:2583-2590

185. Kleindorfer DO, Towfighi A, Chaturvedi S, Cockroft KM, Gutierrez J, Lombardi-Hill D, et al. 2021 guideline for the prevention of stroke in patients with stroke and transient ischemic attack: A guideline from the american heart association/american stroke association. *Stroke*. 2021;52:e364-e467

186. Dziedzic T. Systemic inflammation as a therapeutic target in acute ischemic stroke. *Expert Rev Neurother*. 2015;15:523-531

187. Anrather J, Iadecola C. Inflammation and stroke: An overview. *Neurotherapeutics*. 2016;13:661-670

188. Iadecola C, Buckwalter MS, Anrather J. Immune responses to stroke: Mechanisms, modulation, and therapeutic potential. *J Clin Invest*. 2020;130:2777-2788

189. Kim W, Kim EJ. Heart failure as a risk factor for stroke. *J Stroke*. 2018;20:33-45

190. Chugh SS, Havmoeller R, Narayanan K, Singh D, Rienstra M, Benjamin EJ, et al. Worldwide epidemiology of atrial fibrillation: A global burden of disease 2010 study. *Circulation*. 2014;129:837-847

191. Parish S, Arnold M, Clarke R, Du H, Wan E, Kurmi O, et al. Assessment of the role of carotid atherosclerosis in the association between major cardiovascular risk factors and ischemic stroke subtypes. *JAMA Netw Open*. 2019;2:e194873

192. Geovanini GR, Libby P. Atherosclerosis and inflammation: Overview and updates. *Clin Sci (Lond)*. 2018;132:1243-1252

193. Dutta P, Courties G, Wei Y, Leuschner F, Gorbatov R, Robbins CS, et al. Myocardial infarction accelerates atherosclerosis. *Nature*. 2012;487:325-329

194. Doll DN, Barr TL, Simpkins JW. Cytokines: Their role in stroke and potential use as biomarkers and therapeutic targets. *Aging Dis*. 2014;5:294-306

195. Liberale L, Montecucco F, Schwarz L, Luscher TF, Camici GG. Inflammation and cardiovascular diseases: Lessons from seminal clinical trials. *Cardiovasc Res*. 2021;117:411-422

196. Redgrave JN, Gallagher P, Lovett JK, Rothwell PM. Critical cap thickness and rupture in symptomatic carotid plaques: The oxford plaque study. *Stroke*. 2008;39:1722-1729

197. Marnane M, Prendeville S, McDonnell C, Noone I, Barry M, Crowe M, et al. Plaque inflammation and unstable morphology are associated with early stroke recurrence in symptomatic carotid stenosis. *Stroke*. 2014;45:801-806

198. Jin T, Perry A, Jiang J, Smith P, Curry JA, Unterholzner L, et al. Structures of the hin domain:DNA complexes reveal ligand binding and activation mechanisms of the aim2 inflammasome and ifi16 receptor. *Immunity*. 2012;36:561-571

199. Brunette RL, Young JM, Whitley DG, Brodsky IE, Malik HS, Stetson DB. Extensive evolutionary and functional diversity among mammalian aim2-like receptors. *J Exp Med*. 2012;209:1969-1983

200. Banerjee I, Behl B, Mendonca M, Shrivastava G, Russo AJ, Menoret A, et al. Gasdermin d restrains type i interferon response to cytosolic DNA by disrupting ionic homeostasis. *Immunity*. 2018;49:413-426 e415

201. Dang EV, McDonald JG, Russell DW, Cyster JG. Oxysterol restraint of cholesterol synthesis prevents aim2 inflammasome activation. *Cell*. 2017;171:1057-1071 e1011

202. Monteith AJ, Kang S, Scott E, Hillman K, Rajfur Z, Jacobson K, et al. Defects in lysosomal maturation facilitate the activation of innate sensors in systemic lupus erythematosus. *Proc Natl Acad Sci U S A*. 2016;113:E2142-2151

203. Deftereos SG, Beerkens FJ, Shah B, Giannopoulos G, Vrachatis DA, Giotaki SG, et al. Colchicine in cardiovascular disease: In-depth review. *Circulation*. 2022;145:61-78

204. Klimecki WT, Futscher BW, Grogan TM, Dalton WS. P-glycoprotein expression and function in circulating blood cells from normal volunteers. *Blood*. 1994;83:2451-2458

205. Cronstein BN, Molad Y, Reibman J, Balakhane E, Levin RI, Weissmann G. Colchicine alters the quantitative and qualitative display of selectins on endothelial cells and neutrophils. *J Clin Invest*. 1995;96:994-1002

206. Tong DC, Quinn S, Nasis A, Hiew C, Roberts-Thomson P, Adams H, et al. Colchicine in patients with acute coronary syndrome: The australian cops randomized clinical trial. *Circulation*. 2020;142:1890-1900

207. Tardif JC, Kouz S, Waters DD, Bertrand OF, Diaz R, Maggioni AP, et al. Efficacy and safety of low-dose colchicine after myocardial infarction. *N Engl J Med*. 2019;381:2497-2505

208. Li Y, Niu X, Xu H, Li Q, Meng L, He M, et al. Vx-765 attenuates atherosclerosis in apoe deficient mice by modulating vsmcs pyroptosis. *Exp Cell Res*. 2020;389:111847

209. MacKenzie SH, Schipper JL, Clark AC. The potential for caspases in drug discovery. *Curr Opin Drug Discov Devel*. 2010;13:568-576

210. Yang C, Montgomery M. Dornase alfa for cystic fibrosis. *Cochrane Database Syst Rev*. 2021;3:CD001127

211. Davis JC, Jr., Manzi S, Yarboro C, Rairie J, McInnes I, Averthelyi D, et al. Recombinant human dnase i (rhdnase) in patients with lupus nephritis. *Lupus*. 1999;8:68-76

212. Rahman NM, Maskell NA, West A, Teoh R, Arnold A, Mackinlay C, et al. Intrapleural use of tissue plasminogen activator and dnase in pleural infection. *N Engl J Med*. 2011;365:518-526

Acknowledgements

In the first place, I would like to thank Prof. Dr. Arthur Liesz for providing me the opportunity to study my doctoral thesis in a wonderful group as well as for creating a working atmosphere that is truly enjoyable. Additionally, my sincere gratitude goes out to Prof. Dr. Arthur Liesz for his continuous support, both in life and research. Apart from being an excellent supervisor to me during my doctoral studies, he is also a perfect mentor in my career development and life plans. It was such a pleasure to work with him because he paved the way for me to think independently, supported my ideas and allowed me to implement them the way I wanted. This project would not have been possible without his guidance and inspiration.

I would like to thank Prof. Dr. Martin Dichgans and Prof. Dr. Oliver Söhnlein for their constant support and critical input during my doctoral study. Thanks to Prof. Dr. Martin Dichgans for providing the good working environment and research resources at the ISD.

Special thanks to my colleague Dr. Stefan Roth for the advice and helpful discussions as well as for sharing his rich experimental experience and scientific knowledge. Especially, I would like to thank him for his close supervision as well as great contribution throughout my thesis. Thanks to Christina Fürle and Kerstin Thuß-Silczak for their great help in mouse breeding, research material ordering, tissue processing and histology analyzing. I would like to thank Dr. Gerrit Groß for providing human samples for this study. Moreover, I would like to acknowledge Dr. Ulrike Schillinger for her support in establishing the small-animal MRI analysis and Dr. Qihui Zhou for support with ultrasound analysis. Additionally, I would like to express my gratitude to all the past and present lab colleagues who have supported me in various aspects of science and have created a stimulating scientific environment. Thanks to Alessio Ricci, Olga Carofiglio, Sijia Zhang, Jie Zhu, Qilin Tang, Mengmeng Song, Hao Ji for their invaluable help and kind accompany throughout my study.

A special thanks goes out to the China Scholarship Council (CSC) for financially supporting me during the first four years of my doctoral study, and Prof. Dr. Arthur Liesz for funding me an additional year. Especially grateful for the assistance and guidance of Dr. Dongmei Zhang from the LMU International Office, along with the well-organized orientation and living assistance provided by the International Office.

Finally yet importantly, I am very much indebted to my family for their endless love and unconditional support. Specifically, I would like to express my deepest gratitude to my mother for her constant encouragement and counseling as well as the opportunity to start this whole academic journey.

Affidavit

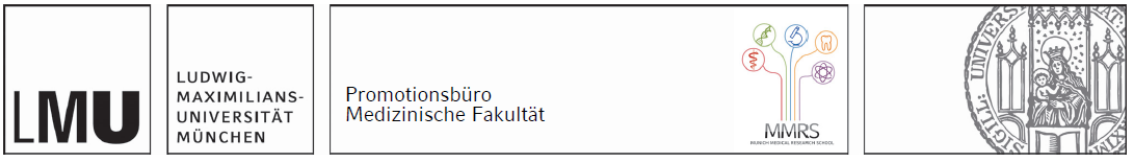

Affidavit

Cao, Jiayu
_____
Surname, first name

_____
Street

_____
Zip code, town, country

I hereby declare, that the submitted thesis entitled:

……

is my own work. I have only used the sources indicated and have not made unauthorised use of services of a third party. Where the work of others has been quoted or reproduced, the source is always given.

I further declare that the submitted thesis or parts thereof have not been presented as part of an examination degree to any other university.

Munich, 30.01.2023 Jiayu Cao

_____ _____
place, date Signature doctoral candidate

Confirmation of congruency

LMU LUDWIG-MAXIMILIANS-UNIVERSITÄT MÜNCHEN

Promotionsbüro
Medizinische Fakultät

MMRS

Confirmation of congruency between printed and electronic version of the doctoral thesis

Cao, Jiayu

Surname, first name

Street

Zip code, town, country

I hereby declare, that the submitted thesis entitled:

The impact of post-stroke sterile inflammation in atherosclerotic plaque rupture and recurrent stroke

……

is congruent with the printed version both in content and format.

Munich, 30.01.2023

place, date

Jiayu Cao

Signature doctoral candidate

List of publications

1. Stefan Roth, **Jiayu Cao**, Vikramjeet Singh, Steffen Tiedt, Gabriel Hundeshagen, Ting Li, Julia D. Boehme, Dhruv Chauhan, Jie Zhu, Alessio Ricci, Oliver Gorka, Yaw Asare, Jun Yang, Mary S. Lopez, Markus Rehberg, Dunja Bruder, Shengxiang Zhang, Olaf Groß, Martin Dichgans, Veit Hornung, and Arthur Liesz. Post-injury immunosuppression and secondary infections are caused by an AIM2 inflammasome-driven signaling cascade. *Immunity*. 2021
2. Jie Zhu, **Jiayu Cao**, Arthur Liesz, and Stefan Roth. A macrophage-T cell coculture model for severe tissue injury-induced T cell death. *STAR Protocols*. 2021
3. **Jiayu Cao**, Yong Lin, Yanfei Han, Shenghao Ding, Yilin Fan, Yaohua Pan, Bing Zhao, Qinhua Guo, Wenhua Sun, Jieqing Wan, Xiaoping Tong. Expression of nerve growth factor carried by pseudo lentivirus improves neuron survival and cognitive functional recovery of post-ischemia in rats. *CNS Neuroscience & Therapeutic*. 2018